Modeling Equilibrium Beach Profiles using a Theoretical Approach

by

Robert N. Meyer

Submitted to the Department of Civil and Environmental Engineering
in partial fulfillment of the requirements for the degree of

Master of Science in Civil and Environmental Engineering

at the

MASSACHUSETTS INSTITUTE OF TECHNOLOGY

March 1998

Author.....
Department of Civil and Environmental Engineering
March 27, 1998

Certified by.....
Ole S. Madsen
Professor, Civil and Environmental Engineering
Thesis Supervisor

Accepted by.....
Joseph Martin Sussman
Chairman, Departmental Committee on Graduate Studies

Modeling Equilibrium Beach Profiles using a Theoretically Approach

by

Robert N. Meyer

Submitted to the Department of Civil and Environmental Engineering
on March 27, 1998, in partial fulfillment of the
requirements for the degree of
Master of Science in Civil and Environmental Engineering

Abstract

Predicting equilibrium beach profiles (EBP) have been an ongoing effort since Bruun (1954) and Dean (1977) carried out extensive empirical studies of beach profiles. Although most efforts in predicting beach profiles are focused on empirical studies, recent models have been process-based. These models typically use the Energetics approach, a theory originally derived by Bagnold (1963) for open channel flow. It is felt that the use of this theory in a coastal environment is somewhat suspect. Hence, a traction model is preferred.

This thesis focuses on predicting EBP using a theoretical approach based on accepted empirical principles for bedload transport by waves. Madsen's (1991) theoretical derivation for bedload transport, based on the Meyer-Peter Muller empirical model, is rederived for a sloped bed. Nonlinear, normally incident, periodic waves are assumed and shoaling as well as wave orbital velocities are predicted using Cnoidal wave theory. Beach profiles are generated by adjusting the local bed slope so that at each depth the net sediment transport is zero. By comparing the results to the Inman et al. (1993) empirical study, this approach is shown to predict beach profile tendencies well outside the surf zone. Within the surf zone, wave heights are assumed to be proportional to the water depth and the model breaks down. In order to improve surf zone predictions, an undertow as well as suspended sediment transport are added to the model.

The present undertow model is in all essential details similar to existing undertow models, except for its treatment of the bottom boundary condition. In our model an assumed value of the average bottom shear stress is used in conjunction with the Grant-Madsen wave-current interaction model to predict the undertow velocities at the outer edge of the wave boundary layer. This bottom velocity is used as the bottom boundary condition necessary to solve for the undertow profile in the interior of the fluid following already established procedures. A valid solution is obtained when the assumed average bottom shear stress leads to a prediction of a zero net flow in the shorenormal direction. The solution compares favorably to detailed laboratory measurements of undertow velocity profiles by Cox and Kobayashi (1997).

Incorporating this undertow model along with suspended transport considerations in our existing equilibrium beach profile formulation improves our predictions within the surf zone. The generated EBP follow these trends: larger waves tend to erode the beach making the overall slope

gentler; beaches with coarser sediments tend to be steeper; and longer waves tend to cause beach accretion. There is a noticeable bar crest at the point of breaking. However, a comparison with Dean and Inman et al. empirical studies show some shortcomings of the modified model. It is felt that a swash zone model and a more accurate treatment of wave attenuation is warranted.

Thesis Supervisor: Ole S. Madsen
Title: Professor, Department of Civil and Environmental Engineering

Acknowledgements

This research was supported by the U.S. Army Research Office (AASERT) and NOAA's Sea Grant College Program.

I am especially thankful to have the opportunity to work with Ole Madsen on this project. Not only has he been an inspiration, but he has taken the time to help me through some of the more difficult stages of my adjustment at MIT.

And a special thanks to Nicole for being there....

Contents

LIST OF FIGURES **7**

LIST OF TABLES **10**

1 INTRODUCTION **12**

1.1 GENERAL REMARKS 12

1.2 HISTORY AND CURRENT THEORIES 13

1.2.1 Empirical Models *13*

1.2.2 The Energetics Approach *15*

1.3 THESIS ORGANIZATION 26

2 THEORY FOR BEDLOAD TRANSPORT **27**

2.1 DERIVATION OF BEDLOAD EQUATION 28

2.2 WAVE THEORY 33

2.2.1 Stokes Theory: *34*

2.2.2 Cnoidal Theory: *39*

2.2.3 Friction Factor Determination: *40*

2.3 THE MODEL 42

3 MODEL APPLICATION AND RESULTS **46**

3.1 CNOIDAL VS. STOKES THEORIES 47

3.2 THE ALGORITHM 48

3.3 RESULTS 50

3.4 DISCUSSION 58

3.4.1 Inman et al. Curve Fitting Methodology: *58*
3.4.2 Comparison of Theoretical Model to Inman et al. Curves: *60*
3.5 SUMMARY OF BEDLOAD MODEL 64

4 SUSPENDED LOAD AND THE UNDERTOW 67
4.1 SUSPENDED SEDIMENT DISTRIBUTION 68
4.2 THE UNDERTOW 72
4.2.1 General Remarks *72*
4.2.2 Theoretical Formulation *74*
4.3 VALIDATION OF MODEL 79
4.3.1 Sensitivity Analysis of Model *81*
4.3.2 Additional Comments and Comparisons *87*

5 MODIFIED MODEL FOR SURF ZONE APPLICATION 90
5.1 THE SUSPENDED SEDIMENT DISTRIBUTION 90
5.2 THE COMPLETE MODIFIED MODEL 91
5.3 RESULTS OF MODEL IN SURF ZONE 93
5.3.1 General Results *93*
5.3.2 Comparison with Empirical Curve-Fitting Lines *100*
5.3 MODEL LIMITATIONS AND SENSITIVITIES 106

6 CONCLUSION 110
6. 1 MODELLING ENERGY DISSIPATION 111
6.2 FURTHER REFINEMENTS 114

A. REFERENCES 116

B. SUSPENDED SEDIMENT OUTSIDE THE SURFZONE 122

List of Figures

Figure 1. Sediment Grain on Slope.....29

Figure 2. Modified Shield's Diagram taken from Madsen and Grant [1976].....32

Figure 3. Variation of beach profile with different sediment diameters.....52

Figure 4. Variation of beach profile with different sediment diameters shown with the best fit line superimposed.....53

Figure 5. Variation of beach profile with different deepwater wave heights.....54

Figure 6. Variation of beach profile with different deepwater wave heights with the best fit line superimposed over the modeled profile.....55

Figure 7. Variation of beach profile with different wave periods.....56

Figure 8. Variation of beach profile with different wave periods with the best fit line superimposed over the modeled profile.....57

Figure 9. Schematic diagram of Inman et al. curve fitting methodology.....59

Figure 10. Comparison of Inman et al. basic curve with proposed model.....61

Figure 11. Fall velocity as related to the sediment-fluid parameter, S_*.....70

Figure 12. A graphical representation of the undertow within the surf zone.....72

Figure 13. Force balance in the surf zone demonstrating the local imbalance of forces along the vertical.....73

Figure 14. Comparison of undertow model with data from Cox and Kobayashi.....82

Figure 15. Sensitivity test of undertow model to variations in shear stress.....83

Figure 16. Sensitivity test of undertow model to variations in the mean return flow 85

Figure 17. Sensitivity test of undertow model to variations in the way wave height is modeled.....86

Figure 18. Comparison of undertow model to data from Buhr-Hansen and Svendsen [1984] 88

Figure 19. Equilibrium beach profile modeled for both inside and outside the surf zone. This figure looks at the variation of the model for changes in sediment diameters 94

Figure 20. Equilibrium beach profile modeled for both inside and outside the surf zone. This figure looks at the variation of the model for changes in deep-water wave heights 97

Figure 21. Equilibrium beach profile modeled for both inside and outside the surf zone. This figure looks at the variation of the model for changes in wave period.....99

Figure 22. Variation of sediment scale parameter, A, with sediment size, d, and fall velocity, w_f [Dean, 1991].....101

Figure 23. Comparison with Dean's Curve-Fitting methodology, $h = Ax^{2/3}$ 102

Figure 24. Comparison of Model with Inman et al. Curve-Fitting Methodology, $h = Ax^m$ 104

Figure 25. Sensitivity of the equilibrium beach profile to $\overline{C}_R$ 107

Figure 26. Sensitivity of the equilibrium beach profile to u_{*1m} 109

Figure 27. Comparison of breaker model and "0.78" criterion to Horikawa and Kuo's laboratory dat for the 1/20, 1/30, 1/65, and 1/80 beach slope..... 112

Figure A1. Comparison between wave-induced suspended load with bedload and bedload alone..... 128

List of Tables

Table 1. Depths at which Cnoidal vs Stokes are valid. This table illustrates the approximate depths in which the Ursell Number is approximately 26 for varying wave heights and wave periods. For depth greater than those shown, stokes theory is considered valid. For depths less than those shown, Cnoidal theory is valid.....47

Table 2. Profiles with Sediment Variation, $H_o = 1m$, $T = 10\ s$. The parameters A and m are used in the profile equation $h = Ax^m$.....50

Table 3. Profiles with Deepwater Waveheight Variation, $d = 0.3\ mm$, T = 10 s. The parameters A and m are used in the profile equation $h = Ax^m$.....51

Table 4. Profiles with Wave Period Period Variation, $H_o = 1\ m$, $d = 0.3\ mm$. The parameters A and m are used in the profile equation $h = Ax^m$.....51

Table 5. Inman et al. Profiles with Seasonal Variation for the shorerise beach segment. Information concerning changes in wave climate between the seasons was minimal.....63

Table 6. Modeled Seasonal Variation. The wave conditions on the top row are assumed to approximate the winter months, whereas the bottom row parameters attempt to approximate ambient summer wave characteristics.....63

Table 7. This table is from Cox and Kobayashi, 1996. The x value is a vertical reference frame, H is the wave height measured, h is the mean still water depth, and Q_s is the return flow per unit width of the wave flume.....80

Table 8. Select measured numerical values of parameters from Buhr-Hansen and Svendsen [1984] experiments. The bed slope was 1/34 and the wave period was 2.2 sec.....87

Table A1. Comparison of Wave Induced Suspended Transport and Bedload transport at varying depths. The wave and sediment characteristics used to calculated these values were $H_o = 1\ m$, $T = 10\ s$, $d = 0.3\ mm$.....126

Chapter 1

1 Introduction

1.1 General Remarks

Understanding beach erosion is of utmost concern to many coastal engineers. Unfortunately, little is understood about how beaches are formed or destroyed. Certainly the simplest concept dealing with beach stability is the idea of equilibrium beach profiles (EBP). Equilibrium profiles are defined as having a local, time-averaged, cross-shore sediment transport of zero and a constant longshore transport.

Generally speaking, beach profiles are manifestations of forces generated by wave and current action, and since wave conditions and current speeds are rarely constant, beach profiles invariably change. Even "equilibrium beach profiles" are rarely in a constant state of equilibrium. Rather, "equilibrium beaches" are those beaches that exhibit stationary characteristics over a sufficient stretch of time. This thesis explores equilibrium beach profiles using a theoretical approach based on accepted empirical principles for bedload transport and suspended load transport induced by steady and unsteady flows over a sandy bed.

1.2 History and Current Theories

1.2.1 Empirical Models

The simplest and certainly the best known model concerning EBP is the Bruun/Dean model [Bruun, 1954; Dean, 1977]. Based on an extensive empirical analysis of beaches throughout the United States and abroad, it was found that the shape of beach profiles could generally be expressed in the form $h \propto x^m$. For the majority of the beaches sampled, m was approximately 2/3. This empirical relationship was further strengthened by theoretical arguments that proposed that beach profiles would adjust their shape to dissipate wave energy. Of the three mechanisms proposed by Dean, 1) wave energy dissipation per unit volume, 2) wave energy dissipation per unit surface area, and 3) uniform bottom shear stress due to oblique waves, only the first mechanism supported an exponential to the 2/3. Briefly, the derivation is outlined here.

$$\frac{\overline{D}}{h} = \varepsilon \tag{1.1}$$

where ε is a constant, $\overline{D}$ is the energy dissipation per unit bottom area, and h is the water depth. Since the energy dissipated is related to the energy flux, it follows then that for linear long waves,

$$\overline{D} = \frac{dE_f}{dx} = \frac{d(Ec)}{dx} \propto \frac{d(H^2\sqrt{h})}{dx} \tag{1.2}$$

Assuming that H is linearly related to water depth,

$$\varepsilon = \frac{\overline{D}}{h} \propto h^{1/2}\frac{dh}{dx} \tag{1.3}$$

With ε a constant, the equation can then be integrated resulting in

$$h \propto x^{2/3} \tag{1.4}$$

Therefore, by using an argument of energy dissipation per unit volume, it was concluded that EBPs could be expressed as $h = Ax^{2/3}$, in which A is a sediment scale parameter. It should be noted that the argument is limited to the surf zone.

Although it is unclear how energy dissipation per unit volume actually moves sediment, certainly the strongest aspect to this model is its simplicity. For blindfolded tests, as those carried out in New Zealand for example, this model for the most part succeeded at estimating the slope of the beach within the surf zone [Dean et al., 1993]. Because of its simplicity and general applicability, it has gained considerable recognition.

However, recent activity in the literature has begun to question this model. An exponential curvefitting model has been advocated as more accurate [Bodge, 1992; Komar and McDougal, 1994]. It has also been suggested to split the profile into two separate sections [Inman et al., 1993]. The main criticism cited by these various authors is that $h = Ax^{2/3}$ is insensitive to varying wave conditions. This feature was considered counterintuitive. Another limiting factor is that $h = Ax^{2/3}$ as a rough approximation is valid only within the breaker zone. Since energy dissipation per unit volume was evaluated only within the surf zone, those who approximate the entire beach using this model imply that sediment transport mechanisms are identical inside and outside the breaker region. This has yet to be established. In fact, Inman et al. [1993] propose that the mechanisms are different and that the use of a single curve-fitting model, therefore, may not be valid.

Inman et al. apply curve fitting models to numerous beaches throughout California, North Carolina, and the Nile Delta region. The profile is split into two sections, the

nearshore zone and the offshore zone, and analyzed separately. Although little theory is presented, the empirical data is extensively developed. Assuming the form $h = Ax^m$, it is proposed that the two separate shapes of the beach have an exponential $m \approx 2/5$ and that A is $O(1)$. Certainly, this method improves the fit of the EBP forms tested, but the methodology is too complicated with no clear way of applying it to engineering problems [Dean, 1994] . Moreover, there is little theoretical backing. However, the point raised by Inman et al. is a valid one: whether or not the theoretical argument for m = 2/3 is a justifiable one. If m was found to be closer to 2/5 than 2/3 under a more careful analysis of empirical data, then the theoretical argument of wave energy dissipation per unit volume needs to be rethought.

1.2.2 The Energetics Approach

The debate about the "best" curvefitting methodology is expected to continue. However, without understanding the physics behind the empirical relationships, little progress will be made in understanding the process of shore erosion. Hence, much of the new cross-shore profile models found in the literature today are indeed process-based. Sediment transport models are used in tandem with the cross-shore profiles, wave and current conditions, and sediment characteristics. The most popular process-based models are based on Energetics, first introduced by Bagnold [1963]. The Energetics approach is a sediment transport prediction method based on the idea that a portion of fluid energy is expended in maintaining a sediment transport load. This next section briefly outlines this approach.

There are two well known and widely used formulations for sediment transport using the Energetics approach. The first is the original formulation by Bagnold. A later variation of this equation was derived by Bailard [1981]. The expression given by both these authors for the total immersed weight cross-shore sediment transport rate based on the Energetics approach is simply

$$i_t = i_b + i_s \tag{1.5}$$

where i_b is the bedload transport rate and i_s is the suspended load. We will briefly outline the derivation of both these terms for both authors and discuss their applicability for sediment transport on beaches subject to oscillatory flow.

i) Derivation of Bedload, i_b.

Bagnold's expression for bedload was originally derived for open channel conditions for normal steady flow on a sloped bed. Positive x is considered to be parallel to the bed slope in the down-slope direction.

The force necessary to overcome frictional resistance and gravitational forces and keep sediment particles in motion on a sloped bed is:

$$F = [(\rho_s - \rho)]g\forall_b \cos\beta\left(\tan\phi - \frac{u_s}{|u_s|}\tan\beta\right) \tag{1.6}$$

where ρ_s is the sediment density, ρ is the fluid density, $\forall_b$ is the bedload volume per unit area, u_s is the sediment velocity and is positive down slope, β is the bed slope and is positive for increasing depths in the positive x direction, and ϕ is the internal angle of friction. The work done per unit time by the fluid on the sediment is then simply this

force multiplied by the sediment velocity, or $F|u_s|$. Bagnold defines the immersed sediment bedload transport rate as its immersed weight times its velocity:

$$i_b = [(\rho_s - \rho)]g\forall_s u_s . \tag{1.7}$$

Hence, the work expended per unit time can be written in terms of i_b:

$$F|u_s| = i_b \frac{u_s}{|u_s|}\left(\tan\phi - \frac{u_s}{|u_s|}\tan\beta\right)\cos\beta \tag{1.8}$$

Bagnold then makes the argument that since the rate of work ($F|u_s|$) is equal to some fraction of the total energy dissipated, it follows the cross-shore immersed weight sediment bedload transport rate is

$$\vec{i}_b = \frac{u_s}{|u_s|}\frac{\varepsilon_b\Omega}{\cos\beta\left(\tan\phi - \frac{u_s}{|u_s|}\tan\beta\right)} \tag{1.9}$$

where Ω is the energy dissipated and ε_b is the efficiency factor for the bedload. Ω is defined as

$$\Omega = \tau u_f = c_f \rho |u_f| u_f^{\,2} \tag{1.10}$$

where c_f is a friction factor coefficient and u_f is the depth averaged fluid velocity for open channel flow. For waves, u_f is the near-bottom fluid velocity and it is assumed that $u_s/|u_s| = u_f/|u_f|$. This derivation holds for a velocity going in either direction, such as under oscillatory flow.

Bailard uses Bagnold's derivation for bedload and his bedload formulation is therefore the same. However, Bagnold and Bailard differ in their expression for suspended load. We shall look at each derivation separately.

ii) Derivation of Suspended Load, i_s.

Bagnold maintained that the suspended sediment is supported by the stream fluid via turbulent diffusion. While suspended, sediment grains move both downstream with nearly the local fluid velocity and are falling downward toward the bed. In order for equilibrium to be maintained, Bagnold proposed that the center of mass of the suspended load must remain at a constant height above the bed.

Bagnold assumes steady normal flow on a sloped bed. The x-coordinate system is parallel to the bottom and is positive in the down-slope direction. The immersed weight is defined as

$$F = (\rho_s - \rho)\forall_s g \tag{1.11}$$

where $\forall_s$ is the total sediment volume per unit area.

In order for the sediment to remain parallel to the bottom as it moves downstream, Bagnold maintains that the sediment volume must lose potential energy at a rate equal to its immersed weight times the sediment's vertical velocity. But since the sediment is also settling at its fall velocity, work is required to keep it suspended. The rate of work necessary to counteract this settling is the immersed weight multiplied by the average sediment fall velocity. Hence, Bagnold argues that the total amount of work per unit time necessary to keep the sediment volume centroid parallel to the slope is the difference between these two quantities.

$$\textit{Rate of Work} = (\rho_s - \rho)\forall_s g(w - u_s \sin\beta) \tag{1.12}$$

where w is the sediment fall velocity and is positive in the direction of gravity, and u_s is positive downstream. With a suspended load defined as

$$i_s = [(\rho_s - \rho)]g\forall_s u_s \tag{1.13}$$

then (1.12) can be redefined in terms of i_s:

$$Rate\ of\ Work = i_s\left(\frac{w}{u_s} - \sin\beta\right) \tag{1.14}$$

As it was argued for the bedload component, Bagnold assumes that the rate of work required for (1.14) is equal to a fraction of the energy dissipated in the sediment-free free stream, $\varepsilon_s\Omega$. This then leaves us with the complete equation for suspended load:

$$i_s = \Omega\frac{\varepsilon_s}{(w/u_s - \sin\beta)} \tag{1.15}$$

The energy dissipated, Ω, is defined as it was for bedload, equation (1.10). ε_s is the efficiency factor for the suspended load. The sediment velocity is assumed to be the same as the fluid velocity.

For conditions when $\sin\beta > w/u_s$, (1.15) theoretically breaks down. A brief examination of (1.12) shows that for such conditions, in order to maintain the sediment centroid parallel to the bed slope, the rate of work required from the free stream is negative, so we would expect an increase in the free stream energy. This creates an inherent contradiction considering that Bagnold argues the exact opposite, that free-stream energy dissipation is necessary for sediment suspension. Since it is not possible to have an increase in energy by dissipating it, (1.15) makes no physical sense in this case. Even for $\sin\beta \rightarrow w/u_s$, unusual results are obtained. A cursory glance at (1.15) under these conditions shows that an infinite amount of suspended load is expected. Therefore, it is concluded that equation (1.15) should only be applied if $\sin\beta << w/u_s$.

That being said, it is clear that there are some problems with regards to the applicability of (1.15) in coastal environments. Along a coast, it is not unreasonable to

assume a typical sediment diameter of around 0.1 *mm* with a fall velocity of around 1 *cm/s*. If we assume that the offshore fluid velocity is around 1 *m/s*, again not an unreasonable assumption, the bed slope must be considerably *less* than $\tan\beta = 0.01$ in order for (1.15) to be valid. However, typical beach slopes in the surf zone are around $\tan\beta \cong 0.1$. Hence, Bagnold's formulation is not valid for typical coastal environments. In fact, one may even question the validity of the hypothesis itself.

The crux of the problem with Bagnold's formulation is that the power contribution from the suspended load to the free stream directly effects the suspended transport rate. Bailard attempts to address this problem.

Bailard [1981] assumes a normal steady flow in an open channel with a similar coordinate system to Bagnold's. He claims that a fraction of the total amount of energy in the stream dissipated is equal to the amount of energy necessary to keep the sediment suspended.

$$\Omega_{sed} = \varepsilon_s \Omega_{stream} \tag{1.16}$$

The amount of energy dissipated in the free stream is based on the rate of potential energy lost. For open channel flow, the amount of potential energy lost is simply

$$\Omega_{stream} = \rho_a g h u_s \sin\beta \tag{1.17}$$

where h is the water depth and ρ_a is the apparent density of the sediment ladened water and is defined as

$$\rho_a = (\rho_s - \rho)\frac{\forall_s}{h} + \rho \tag{1.18}$$

Using the same definition of suspended load as above (1.13), and inserting (1.18) into (1.17), the free stream's total energy dissipation is therefore:

For open channel flows, the energy dissipation for a sediment free stream is $\rho g h u_s \sin\beta$ and is equal to (1.10). Hence, (1.19) can be rewritten as

$$\Omega_{strean} = i_s \sin\beta + \Omega \tag{1.20}$$

where Ω is given by (1.10). The rate of work necessary to keep the sediment from falling is according to Baillard [1981] simply the immersed weight of the sediment times its fall velocity.

$$\Omega_{sed} = (\rho_s - \rho) g \forall_s w \tag{1.21}$$

Introducing (1.20) and (1.21) into (1.16) we derive Bailard's expression for the suspended load:

$$i_s = \Omega \frac{\varepsilon_s}{w/u_s - \varepsilon_s \sin\beta} \tag{1.22}$$

Considering that ε_s is of the order 0.01, this formulation makes more physical sense than Bagnold's. However, it is stressed that this equation was derived for normal steady flow in an open channel with the free stream flowing downstream. If one were to "convert" (1.22) into an equation that is applicable to oscillatory flow, the physical meaning of (1.22) would be lost. For example, if one were to derive (1.22) by assuming the velocity was moving upslope (ie. under a crest of a wave), one could not use the line of logic used by Bailard. According to Bailard then, energy would not be dissipated at a rate $\rho g h u_s \sin\beta$, but rather be produced at that rate. This of course does not make physical sense.

So even though the physical justification for using either Bagnold's or Bailard's suspended sediment transport rate for coastal environments is questionable, it is used

regardless. The coordinate system is redefined to be in accord with typical coastal problems. The bedload formulation (1.9) is changed such that the x-direction is horizontal and positive shore-wards. The negative sign in the denominator becomes positive. Equations (1.15) and (1.22) also are changed to reflect this the new coordinate system, and they are "generalized" for oscillatory flow. The velocity is positive in the onshore direction and β is positive for decreasing depths in the onshore direction. The total sediment transport rate along a sloped bed using Energetics is therefore

$$i_t = i_b + i_s = \Omega\left(\frac{\varepsilon_b}{\tan\phi} \frac{u_f}{|u_f|} \left(1 + \frac{u_f}{|u_f|} \frac{\tan\beta}{\tan\phi} \right)^{-1} + \frac{\varepsilon_s u_f}{w} \left(1 + \Gamma \tan\beta \frac{u_f}{w} \right)^{-1} \right) \tag{1.23}$$

where Bagnold assumes that $\Gamma = 1$, and Bailard assumes that $\Gamma = \varepsilon_s$. There are some slight geometric differences between (1.23) and that which was derived here. Let it be sufficient to note that (1.23) is the equation cited in the literature dealing with EBP (ie. Bowen [1980], Bailard [1981]) and hence we will just state it with out arguing the finer nuances of its derivation.

Equation (1.23) is further developed upon by Bowen [1980], Bailard and Inman [1981], and Bailard [1981] and applied directly to cross-shore sediment transport on beach profiles. Bowen assumes that $\Gamma = 1$ while Bailard uses his own formulation, $\Gamma = \varepsilon_s$. The expression for the cross-shore sediment transport equation as it pertains to equilibrium beaches is derived below.

One can Taylor expand (1.23) and only retain the leading order terms if it is assumed for the bedload contribution that $\tan\beta << \tan\phi$ and for the suspended load

contribution that $\Gamma \tan\beta << \frac{w}{u_f}$. After time-averaging, it can be shown that (1.23) is approximated as

$$\langle i_t \rangle = \rho c_f \frac{\varepsilon_b}{\tan\phi}\left[\left\langle |u_f|^2 u_f \right\rangle - \frac{\tan\beta}{\tan\phi}\left\langle |u_f|^3 \right\rangle\right] + \rho c_f \frac{\varepsilon_s}{w}\left[\left\langle |u_f|^3 u_f \right\rangle - \frac{\Gamma}{w}\tan\beta\left\langle |u_f|^5 \right\rangle\right] \tag{1.24}$$

It is not unrealistic to assume that $\tan\beta << \tan\phi$ if ϕ is to be taken to be around 30° to 50° and the bed slope to be less that 10°. However, the assumption $\Gamma \tan\beta << \frac{w}{u_f}$ is poor for $\Gamma = 1$. u_f is the time-varying velocity within the water column, and for shore-normal flows, this is simply the sum of the oscillatory flow and current flow

$$u_f = \tilde{u} + \bar{u}. \tag{1.25}$$

For nonlinear flows, we define the oscillatory velocity using the superposition of linear waves of varying harmonics:

$$\tilde{u} = u_m \cos\sigma t + u_{m2} \cos 2\sigma t + \ldots \tag{1.26}$$

where u_m is the maximum orbital velocity and σ is the radian frequency of the wave. By introducing (1.26), Bailard implicity states that $\langle \tilde{u}^n \rangle = 0$ when n is odd. Hence, by substituting (1.25) and (1.26) into (1.24), it is shown that

$$\langle i_t \rangle = \rho c_f u_m^3 \frac{\varepsilon_b}{\tan\varphi}\left(\chi_1 + \frac{3}{2}\delta_u - \frac{\tan\beta}{\tan\varphi}(u3)^*\right) + \rho c_f u_m^3 \frac{\varepsilon_s u_m}{w}\left(\chi_2 + 4\delta_u (u3)^* - \frac{u_m}{w}\Gamma \tan\beta (u5)^*\right) \tag{1.27}$$

where:

$\delta_u = \bar{u} / u_m$ is the dimensionless steady flow

$\chi_1 = \left\langle |\tilde{u}|^2 \tilde{u} \right\rangle / u_m^3$ is the first odd moment

$\chi_2 = \left\langle |\tilde{u}|^3 \tilde{u} \right\rangle / u_m^4$ is the second odd moment

(u3)* = $\left\langle |u_f|^3 \right\rangle / u_m^3$ is the third central even moment

(u5)* = $\left\langle |u_f|^5 \right\rangle / u_m^5$ is the fifth central even moment

Typical values for ε_b are of the order 0.2, ε_s is of the order 0.02, and c_f is of the order 0.01 [Bailard, 1981].

For equilibrium beaches $\langle i_t \rangle = 0$. Using Stokes second-order wave theory and Longuet-Higgin's [1953] bottom drift model, the odd moments and the dimensionless steady flow can be solved. The even moments are extrapolated from the figures presented in Bailard [1981] along with details of the methodology. Once these terms are plugged into (1.22), an explicit expression can be found for the beach slope at any depth given that the wave climate is known.

More sophisticated models have been recently developed. Southgate and Nairn [1993], for example, assume an offshore wave climate and then describe the localized wave and current climate by using linear theory to find refraction, shoaling, and by using theory presented by Battjes and Janssen [1973] to find wave energy dissipation. Once the localized wave-current climate is known, the volumetric transport rate using the immersed weight sediment transport is found [Nairn and Southgate, 1993]. Bailard's formulation is preferred over Bagnold's.

The main models that use this general approach are reviewed by Roelvink and Broker [1993]. These include the Nearshore Profile Model [Southgate and Nairn, 1993],

the UNIBEST model [Roelvink and Stive, 1993], and SEDITEL [Pechon, 1992]. Each of these numerical models use the Energetics model.

Use of the Energetic's approach has well known weaknesses. Some of the more obvious weaknesses have already been touched upon, such as whether or not there is any physical basis for applying the suspended sediment transport equation to coastal environments. Another obvious problem is that the constant and universal efficiency factors are hard to quantify and have been shown to fluctuate with varying hydrodynamic conditions [Nairn and Southgate, 1993]. Sensitivities to these parameters may retard efforts to derive a model that could predict beach evolution over significant time frames. In addition, more sophisticated models based on this approach are designed to describe the dynamic behavior of coastal profiles. According to Roelvink and Broker [1993], it is unclear as to whether these models could actually ever achieve an equilibrium beach profile for a barred beach with constant boundary conditions. In addition to the reasons just listed, there is also no threshold for sediment motion, limiting the use of the model to strong wave action, nor is there a use of coupled wave-current theory. Indeed there are waves and currents, but the same friction factor is applied to both. It is felt that the energetics approach is too limiting.

Use of a traction model, such as Madsen and Grant [1976], as the basis of a theoretical model to predict equilibrium beach profiles as well as predicting dynamic profile changes may be more advantageous than the Energetics approach for several reasons. First, there is no efficiency factor. Second, the mechanics of sediment transport based on a traction model makes it possible to incorporate wave-current interaction and a

sediment movement threshold. Lastly, the physical reasoning behind using the Energietics approach for coastal environments is questionable at best.

This thesis suggests the first steps of putting together such a model. Although the theory behind this model is relatively straight forward, the time variation of waves and the repetitive nature of the calculations make it necessary to use a computer to carry out the calculations iteratively. Both the theory and the rudiments of the computer algorithm are presented here.

1.3 Thesis Organization

The thesis is organized into two sections. The first section, chapters 2 and 3, deals with bedload transport alone. The second chapter develops a theoretical bedload model for sloping beds under both oscillatory and constant currents. Wave theories pertinent to shallow water are also discussed. In the third chapter, equilibrium beach profiles are generated using a computer algorithm based on the model developed in chapter 2. This model is then compared to existing field data. This data is taken from Inman et al. [1993].

The next section, chapters 4 and 5, further refines the bedload-based equilibrium beach profile model by adding suspended sediment transport within the surf zone. Chapter four discusses suspended load theory and the undertow current. A new theoretical model for predicting the structure of the undertow is presented and then used with the suspended sediment concentration to predict an off-shore suspended load. In chapter 5, the complete model is presented.

Chapter 2

2 Theory for Bedload Transport

In order for an equilibrium beach profile to exist, there must be a net sediment transport rate of zero everywhere. However, due to the increasing nonlinear nature of waves as they shoal, the wave peaks tend to become proportionally larger than the troughs (i.e. $|\eta_{max}|>|\eta_{min}|$). Since shear stress is related to bottom orbital velocity, which in turn is related to surface profile, it is deduced that the orbital velocity and associated shear stress under the crest are greater than the trough orbital velocity and shear stress. Since Meyer-Peter and Muller [1948] empirically relate bedload to the difference between critical and bottom shear stress, it follows that there would also be a net transport rate onshore. In order to offset this trend, a slope is introduced. Since a greater force is necessary to push a body up a slope than down, the increased effort should balance out the stronger shoreward shear stress.

Although heuristically, one can see why a slope is necessary to balance the onshore transport rate due to the nonlinear nature of the waves, it is also equally clear that transport mechanisms could include both suspended load and bedload. However, we maintain that suspended load outside the surf zone is relatively unimportant compared to

bedload and should be neglected altogether. The details of this argument are shown in Appendix A. So if bedload is the dominating transport mechanism outside the surf zone, a thorough investigation is warranted in which the immediate goal is to find an equilibrium beach slope at each depth such that there is no net transport.

This chapter rederives the conceptual mechanics-based model for bedload sediment transport process in steady and unsteady turbulent boundary layer flow as presented by Madsen [1991]. This model, which parallels the empirical sediment transport model proposed by Meyer-Peter and Muller, was derived for a non-sloping bed. Here, a slope is introduced into the original model presented by Madsen.

2.1 Derivation of Bedload Equation

Drawing on a wealth of empirical data, Meyer-Peter and Muller suggests that bedload transport is proportional to the shear stress raised to the 3/2 power. Madsen [1991] verifies this empirical relationship by theoretically deriving an expression for bedload transport on a flat bed. Following this derivation closely, one can modify Madsen's expression to solve for bedload on a sloping bed. Madsen proposes that:

$$NF_d = \tau_b - \tau_{cr} \tag{2.1}$$

where N is the number of grains moving per unit bottom area, F_d is the drag force acting on these moving grains, and the bottom and critical shear stresses are denoted by τ_b and τ_{cr}, respectively. Equation (2.1) can be rewritten as:

$$Nu_{s\infty}\forall_s = u_{s\infty}\forall_s \frac{(\tau_b - \tau_{cr})}{F_d} \tag{2.2}$$

to express bedload transport rate. The product $Nu_{s\infty}\forall_s$ represents the sediment volume transport per unit width perpendicular to the transport direction, with $u_{s\infty}$ being the terminal sediment grain velocity, and $\forall_s$ representing the sediment volume of a moving grain. The variables in (2.2) are derived for a sloped bed as follows.

For the drag force, F_d, a simple free body diagram of a sediment grain resting on a sloped bed is drawn (see figure 1).

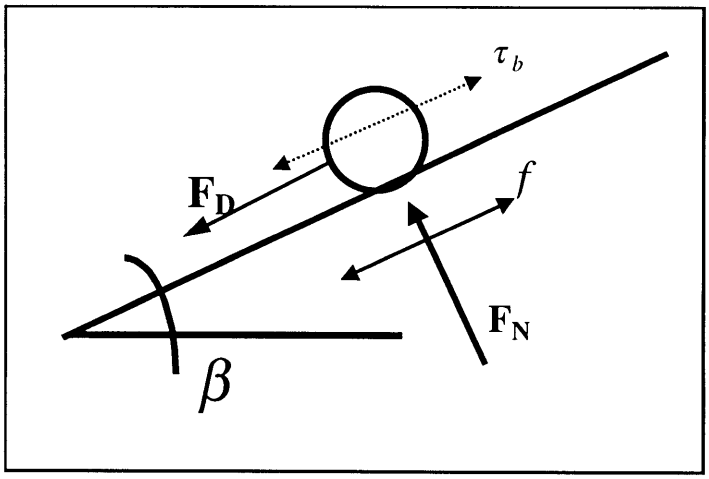

figure 1. Sediment Grain on Slope

The buoyant weight of the sediment is $(\rho_s - \rho)\forall_s g$. Therefore, the component parts of the free body diagram are:

$$\mathrm{F_N} = \text{ normal force} = (\rho_s - \rho)\forall_s g \cos\beta \tag{2.3}$$

$$f = \text{frictional force} = F_N \tan\phi \tag{2.4}$$

$$\mathrm{F_D} = \text{gravity force} = (\rho_s - \rho)\forall_s g \sin\beta \tag{2.5}$$

where ρ_s and ρ are the sediment and fluid densities, β is the beach slope angle, and ϕ is the internal angle of friction, either static (ϕ_s), or kinetic (ϕ_k). For steady state, the balancing forces are calculated. If the acting force is pushing upwards, the balancing or reacting force is:

$$F_{up} = (\rho_s - \rho)\forall_s g(\tan\phi\cos\beta + \sin\beta) \tag{2.6}$$

Likewise, if the force is pushing down, the reacting force is:

$$F_{down} = (\rho_s - \rho)\forall_s g(\tan\phi\cos\beta - \sin\beta) \tag{2.7}$$

Since wave action creates a shear stress that acts in both directions, the two equations are simplified into one:

$$F_d = (\rho_s - \rho)\forall_s g(\tan\phi\cos\beta \pm \sin\beta) \tag{2.8}$$

For the remainder of this report, these two equations will be combined into one, with a (+) sign signifying that the orbital velocity is in the shoreward direction (under the crest), a (-) sign indicating the seaward direction (under the trough).

Again following Madsen's derivation closely, it can be shown that the critical Shield's parameter associated with the initiation of motion on a sloped bed is:

$$\Psi_{cr} = \frac{u_{*cr}^2}{(s-1)gd} = 0.052(\tan\phi_s\cos\beta \pm \sin\beta) \tag{2.9}$$

where Ψ_{cr} is the critical Shield's parameter, u_* is the shear velocity, ϕ_s the internal angle of static friction, d the diameter of the sediment, s the specific weight of the grain, and g gravity. Since the shear stress is expressed as $u_* = \sqrt{\tau/\rho}$, the critical shear stress is simply:

$$\tau_{cr} = 0.052(s-1)\rho g d \tan\phi_s (\cos\beta \pm \frac{\sin\beta}{\tan\phi_s}) \tag{2.10}$$

For a flat horizontal bed, the critical shear stress is [Madsen, 1991],

$$\tau'_{cr} = 0.052(s-1)\rho g d \tan\phi_s \tag{2.11}$$

Therefore, the critical shear stress for a sloping bed can be written as

$$\tau_{cr} = \tau'_{cr} (\cos\beta \pm \frac{\sin\beta}{\tan\phi_s}) \tag{2.12}$$

where τ'_{cr} is given from (2.11).

The terminal sediment velocity, $u_{s\infty}$, is also found for a sloped bed. Madsen shows that the response time for a sediment accelerating from rest to terminal velocity is negligible such that $\overline{u}_s = u_{s\infty}$, and that the terminal velocity of the sediment is related to shear velocity

$$u_{s\infty} \cong 8(u_* - \alpha u_{*cr}) \tag{2.13}$$

where α, in the particular case of a sloped bed, is

$$\alpha^2 = \frac{\tan\phi_k \cos\beta \pm \sin\beta}{\tan\phi_s \cos\beta \pm \sin\beta} = \frac{\tan\phi_k \pm \tan\beta}{\tan\phi_s \pm \tan\beta} \tag{2.14}$$

Substituting equations (2.8) and (2.13) into equation (2.2), bedload is expressed as

$$q_{sb} = \frac{\pm 8(|\tau_b| - \tau_{cr})}{(s-1)\rho g \cos\beta(\tan\phi_k \pm \tan\beta)}(u_* - \alpha u_{*cr}) \tag{2.15}$$

The critical shear stress is found from equation (2.10) or from the generalized Shields diagram [Madsen and Grant, 1976] (figure 2). The values of 50° and 30° are used to

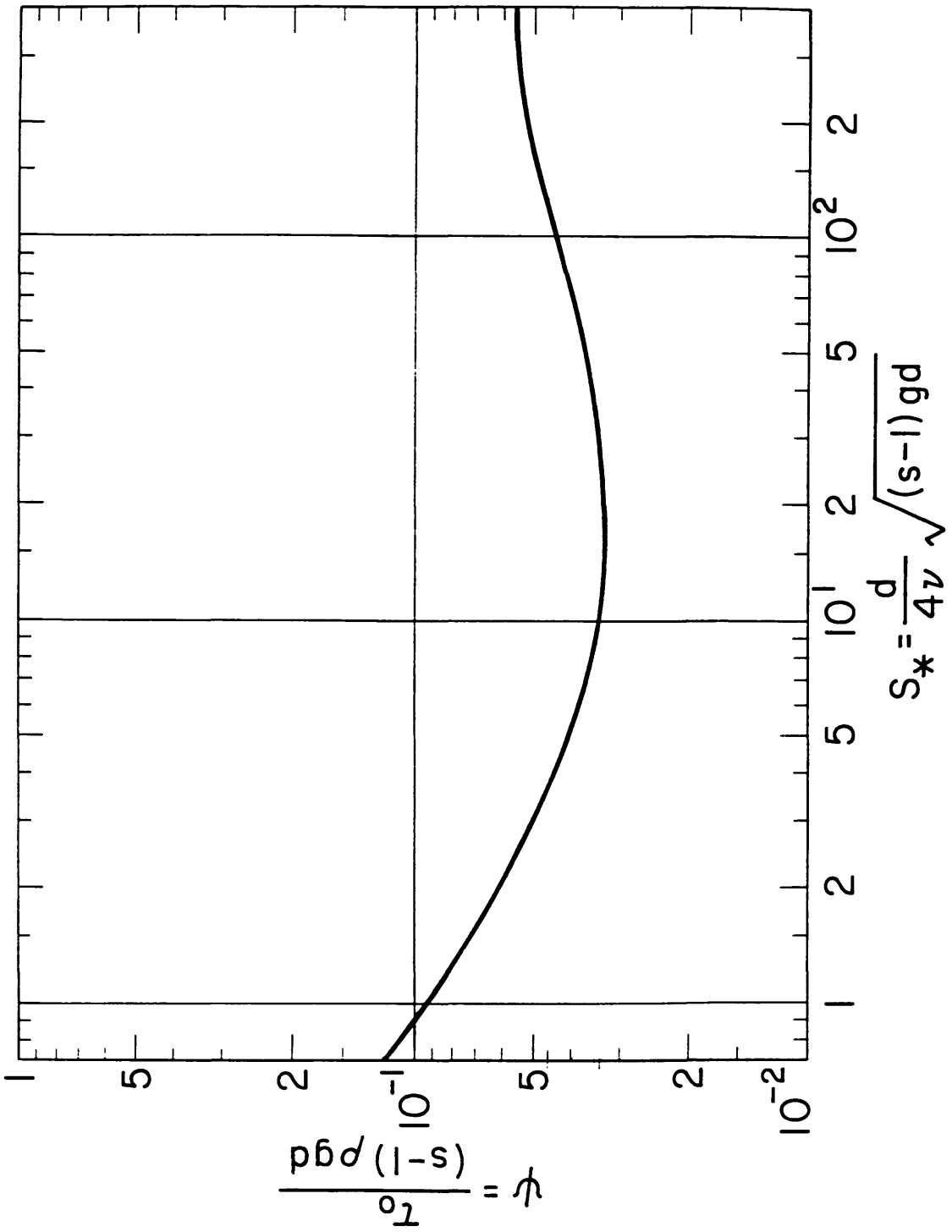

Figure 2. Modified Shield's Diagram taken from Madsen and Grant [1976].

approximate the angles of internal friction, ϕ_s and ϕ_k, respectively. These values are rooted in theoretical calculations and confirmed by experimental work. If $\Psi_{cr} = 0.052 \tan\phi_s$ for a flat bed (2.9) and typical values of critical Shield's parameter are $\Psi_{cr} \cong 0.06$ (figure 2), then $\phi_s \cong 50^o$. Moreover, the ratio

$$\alpha = \sqrt{\frac{\tan\phi_k}{\tan\phi_s}} \tag{2.16}$$

must satisfy the limits $0 < \alpha < 1$. By taking an average value of 1/2 or $\alpha = 1/\sqrt{2}$, it is not unreasonable to assume that $\phi_k \cong 30^o$. A comparison of sediment transport models with King [1991] gives a similar value of ϕ_k.

It should be noted at this point that the agreement of (2.15) with Meyer-Peter Muller is excellent for horizontal bottoms [Madsen, 1991]. It is this agreement that allows us to make the transition to a sloped bed with confidence. Moreover, theory outlined here also agrees with the slope effects predicted by the Energetics approach to bedload transport: a steeper slope reduces the onshore transport while increasing the offshore transport. So at least qualitatively, there is agreement with the Energetics approach.

2.2 Wave Theory

The generalized equation for bedload transport on a bottom slope is complete. However, the bottom shear stress, τ_b, needs to be evaluated. For wave motion over a surface it is known that $\tau_b \propto |u_b| u_b$ and $u_b \propto \eta$. Since τ_b is dependent on the phase of

the wave, one must accurately describe the time-variation of η, the surface profile. There are various theoretical approximations that describe η. As the wave shoals, it is expected that the waves become increasingly long. That is to say, the water depth, *h*, becomes much smaller than the characteristic horizontal wave length. This parameter, (*h/L*), helps define the shape of the wave as it shoals. Likewise, the amplitude of the wave relative to the water depth (*H/h*) also influences the characteristics of the wave as it shoals. An increasing wave amplitude/depth ratio increases the nonlinear nature of the wave. It appears that a combination of these two parameters $(H/h)(L/h)^2 \sim (HL^2/h^3)$ is critical in the way one describes the behavior of a wave in shallow water [Svendsen, 1974]. When this parameter, known as the Ursell number, U, is less than about 26, it is found that Stokes theory (linear or second order) is valid. For Ursell Numbers greater than about 26, Cnoidal theory is valid.

2.2.1 Stokes Theory:

Stokes theory is simply a superposition of differing harmonics. For a second order Stokes wave, the first and second harmonics are superimposed. So for U < 26, Stokes second order theory is used for which

$$\eta\ (t) = \eta_1 \cos\theta + \eta_2 \cos 2\theta \tag{2.17}$$

and,

$$u_b(t) = u_{1bm} \cos\theta + u_{2bm} \cos 2\theta \tag{2.18}$$

where θ is the phase of the wave, and $u_{1\,bm}$ and $u_{2\,bm}$ are the first and second harmonic maximum bottom orbital velocity given by

$$u_{1bm} = \frac{a\omega}{\sinh kh} \tag{2.19}$$

$$u_{2bm} = \frac{3}{4} ka \left(\frac{a\omega}{\sinh kh}\right) \frac{1}{\sinh^3 kh} \tag{2.20}$$

where k is the wave number, h the water depth, a the wave amplitude, and ω the wave radian frequency. The first and second harmonic bottom shear stress are now found.

By adopting the eddy viscosity model $\nu_t = \kappa u_{*1m} z$, where ν_t is the eddy viscosity, κ is von Karman's constant, u_{*1m} is based on the maximum first harmonic bottom shear, and z is the vertical distance from the bottom, the first harmonic shear stress is calculated using the principles laid out in Madsen [1994] for waves on a flat bottom surface. Simply stated

$$\tau_{1m} = \frac{1}{2} f_{1w} \rho u_{1bm}^2 . \tag{2.21}$$

The friction factor, f_{1w}, relating the bottom orbital velocity to the shear stress, is found as proposed by Madsen [1994] and the derivation is briefly outlined as follows.

The "exact" solution to the turbulent boundary layer problem is given by

$$u_1 = \mathrm{Re}\left\{\left[1 - \frac{\ker 2\sqrt{\zeta} + ikei2\sqrt{\zeta}}{\ker 2\sqrt{\zeta_{o1}} + ikei2\sqrt{\zeta_{o1}}}\right] u_{1bm} e^{i\omega t}\right\} \tag{2.22}$$

where $\zeta = z/l$; $\zeta_{o1} = z_o/l$; $l = \kappa u_{*1m}/\omega$; $u_1 = u_{1b} = u_{1bm}\cos\omega t$ as $\zeta \to \infty$. $z_o = \frac{k_N}{30}$

and k_N is the equivalent Nikuradse sand grain roughness of the bottom. We also define the shear stress as

$$\tau_1 = \left[\rho \upsilon_t (\partial u_1/\partial z)\right]_{z\to 0} . \tag{2.23}$$

We take the partial derivative of (2.22) with respect to z and incorporate the integrand into (2.23). Assuming that ζ is small, *ker* and *kei* can be expressed as their asymptotic expansion:

$$\ker 2\sqrt{\zeta} + ikei2\sqrt{\zeta} \cong -\frac{1}{2}\ln\zeta - \gamma - i\frac{\pi}{4} \tag{2.24}$$

where γ is the Euler constant, so that the partial derivative of (2.22) is simply

$$\frac{\partial u_1}{\partial z} = \frac{1}{2z(\ker 2\sqrt{\zeta_o} + ikei2\sqrt{\zeta_o})} u_{1bm} e^{i\omega t} . \tag{2.25}$$

The first harmonic bottom shear is, once we introduce the proposed eddy viscosity model and rearrange the denominator,

$$\tau_1 = \rho \nu_t \frac{\partial u_1}{\partial z} = \frac{\rho\kappa u_{*1m}}{2\left[\left(\ker 2\sqrt{\zeta_{o1}}\right)^2 + \left(kei2\sqrt{\zeta_{o1}}\right)^2\right]^{\frac{1}{2}}} u_{1bm} e^{i\omega t-\theta} \tag{2.26}$$

where $\tan\theta = \left(\frac{kei2\sqrt{\zeta_{o1}}}{\ker 2\sqrt{\zeta_{o1}}}\right)$. By introducing (2.21) into (2.26) we write

$$\tau_1 = \frac{\rho\kappa\sqrt{f_{1w}/2}}{2\left[\left(\ker 2\sqrt{\zeta_{o1}}\right)^2 + \left(kei2\sqrt{\zeta_{o1}}\right)^2\right]^{\frac{1}{2}}} u_{1bm}^2 e^{i\omega t-\theta} \tag{2.27}$$

By considering the maximum amplitude of (2.27), and again introducing (2.21) into the left-hand side, it is clear that the friction factor can be solved as:

$$\frac{1}{\kappa}\sqrt{f_w/2} = \frac{1}{2}\left[\left(\ker 2\sqrt{\zeta_{o1}}\right)^2 + \left(kei 2\sqrt{\zeta_{o1}}\right)^2\right]^{-\frac{1}{2}} \tag{2.28}$$

As stated earlier, for small arguments, Kelvin functions can be approximated by their asymptotic expansion, which is a logarithmic function. Hence, for small values of ζ_{o1}, we introduce the definition of ζ_{o1}

$$\zeta_{o1} = z_o / l = \frac{z_o}{\kappa u_{*1m}/\omega} = \frac{z_o \omega}{\kappa u_{1bm}\sqrt{f_{1w}/2}} = \frac{k_N}{30 A_{bm}\kappa\sqrt{f_{1w}/2}}$$

into (2.28) and then approximate (2.28) as

$$\frac{1}{4\sqrt{f_w}} + \log_{10}\frac{1}{4\sqrt{f_w}} = \log_{10}\frac{A_{bm}}{k_N} - 0.17 \tag{2.29}$$

where A_{bm} is the maximum bottom excursion amplitude and is equal to u_{1bm}/ω. This equation, (2.29), can likewise be approximated by an explicit expression. These explicit formulas are used in the program and detailed later. Once the friction factor is known, then the first harmonic shear stress (2.21) can be solved.

We now solve the second harmonic friction factor and shear stress. The boundary layer shear stress for the second harmonic is defined as

$$\tau_2 = \rho \upsilon_t \frac{\partial u_2}{\partial z} = \rho \kappa u_{*1m} z \frac{\partial u_2}{\partial z} \tag{2.30}$$

and the exact solution to the turbulent boundary layer for the second harmonic velocity is similar to (2.22):

$$u_2 = \mathrm{Re}\left\{\left[1 - \frac{\ker 2\sqrt{\zeta} + ikei2\sqrt{\zeta}}{\ker 2\sqrt{\zeta_{o2}} + ikei2\sqrt{\zeta_{o2}}}\right] u_{2bm} e^{i2\omega t}\right\} \tag{2.31}$$

where we denote $l_2 = ku_{*1m}/2\omega$ and $\zeta_2 = z/l_2$ so that $l_2 = l_1/2$. Following the same procedure as we did for the first harmonic (equations (2.24) to (2.26)), we arrive at the following expression:

$$\tau_2 = \frac{\rho\kappa u_{*1m}}{2\left[\left(\ker 2\sqrt{\zeta_{o2}}\right)^2 + \left(kei2\sqrt{\zeta_{o2}}\right)^2\right]^{\frac{1}{2}}} u_{2bm} e^{i2\omega t-\theta} \tag{2.32}$$

The maximum value of (2.32) can be rewritten as

$$\tau_{2m} = \left(\frac{\rho\kappa u_{*1m} u_{1bm}}{2\left[\left(\ker 2\sqrt{\zeta_{o2}}\right)^2 + \left(kei2\sqrt{\zeta_{o2}}\right)^2\right]^{\frac{1}{2}}}\right)\left(\frac{u_{2bm}}{u_{1bm}}\right) \tag{2.33}$$

The first bracketed term in (2.33) is identical to the maximum of (2.26) except for the fact that $\zeta_{o2} = 2\zeta_{o1}$. Since this difference is essentially buried within a log term and not expected to be significant (again, we note that Kelvin functions with small arguments can be approximated with a log function), we can assume then that $f_{2w} \cong f_{1w}$ and therefore (2.33) can be approximated as

$$\tau_{2m} \cong (\tau_{1m})\left(\frac{u_{2bm}}{u_{1bm}}\right) \tag{2.34}$$

By substituting equation (2.19) and (2.20) into (2.34) we develop a direct relationship between the first and second harmonic maximum bottom shear stress:

$$\frac{\tau_{2m}}{\tau_{1m}} = \frac{3}{4}\frac{ak}{\sinh^3 kh} \tag{2.35}$$

Introducing these results into equation (2.18), we arrive at the following equation describing the time variation of the bottom shear:

$$\tau_b(t) = \tau_{1m}\cos\theta + \tau_{2m}\cos 2\theta \tag{2.36}$$

Hence, it then follows that the time varying bottom shear stress can be written as

$$\tau_b(t) = \frac{1}{2} f_{1w}\rho u_{1bm} u_b(t) \tag{2.37}$$

where $u_b(t)$ is given by (2.18). The form of expression (2.37) becomes important when Cnoidal theory is applied to the problem.

2.2.2 Cnoidal Theory:

For U > 26, Cnoidal wave theory is applied. The surface profile variation is

$$\eta = \eta_{\min} + H\, cn^2(\theta, m) \tag{2.38}$$

where cn^2 is the square of the Jacobian Elliptic cosine, $\eta_{\min}$ is the location of the trough below still water level, H is the wave height, m is the parameter associated with the Jacobian Elliptic function, and θ is the phase angle [Svendsen, 1974]. The time varying bottom orbital velocity is approximated as the depth averaged velocity

$$u_b(t) = c\left(\frac{\eta}{h+\eta}\right) \tag{2.39}$$

where h is the water depth, and c is the phase velocity defined as the wave length divided by the wave period. The wave length is a function of wave height, wave period, and water

depth. Using an analogous expression to (2.37), the time varying bottom orbital velocity is expressed as

$$\tau_b(t) = \frac{1}{2} f_{1w} \rho u_{1bm} u_b(t) \tag{2.40}$$

The "first harmonic" orbital velocity is defined

$$u_{1bm} = (u_{b\max} - u_{b\min})/2 \tag{2.41}$$

where

$$u_{b\max} = c\left(\frac{\eta_{\max}}{h+\eta_{\max}}\right) \tag{2.42}$$

and

$$u_{b\min} = c\left(\frac{\eta_{\min}}{h+\eta_{\min}}\right) \tag{2.43}$$

The analysis is complete. For both Cnoidal and Stokes theory, expressions for the bottom shear stress have been derived.

2.2.3 Friction Factor Determination:

Section 2.2.1 derived exact expressions for the friction factor. Here, we present the explicit equations used to approximate the friction factor. If one assumes rough turbulent flow, the wave friction factor is calculated from one of the following expressions from Madsen [1994]:

$$f_{1w} = \exp\{7.02(A_{bm}/k_N)^{-0.078} - 8.82\} \quad \text{for} \quad 0.2 < (A_{bm}/k_N) < 100 \tag{2.44}$$

$$f_{1w} = \exp\{5.61(A_{bm}/k_N)^{-0.109} - 7.30\} \quad \text{for} \quad 10^2 < (A_{bm}/k_N) < 10^4 \tag{2.45}$$

$$f_{1w} = \exp\{5.50(A_{bm}/k_N)^{-0.120} - 7.02\} \quad \text{for} \quad 10^3 < (A_{bm}/k_N) < 10^6 \tag{2.46}$$

where k_N is the Nikuradse roughness factor and is approximated by the diameter of the sand grain. A_{bm} is the excursion amplitude and is estimated to be

$$A_{bm} = \frac{u_{1bm}}{\omega} \tag{2.47}$$

where u_{1bm} is found from either (2.19) or (2.41). For cases where it is valid, (2.46) is preferred over (2.45). For values of $(A_{bm}/k_N) > 10^6$, we revert back to solving the theoretical equation presented in section 2.2.1 (2.29).

The assumption of rough turbulent flow is checked. For values of $k_N u_{*1m}/\upsilon \leq 3.3$, ($\upsilon$ is the kinematic viscosity) the flow is smooth turbulent and the friction factor is recalculated.

$$f_{1w} = 0.25\exp\{7.02(\sqrt{RE/50})^{-0.078} - 8.82\} \quad \text{for} \quad 0.2 < \sqrt{RE/50} < 100 \tag{2.48}$$

$$f_{1w} = 0.25\exp\{5.61(\sqrt{RE/k_n})^{-0.109} - 7.30\} \quad \text{for} \quad 10^2 < \sqrt{RE/50} < 10^4 \tag{2.49}$$

$$f_{1w} = 0.25\exp\{5.50(\sqrt{RE/50})^{-0.120} - 7.02\} \quad \text{for} \quad 10^3 < \sqrt{RE/50} < 10^6 \tag{2.50}$$

where RE is the Reynolds number:

$$RE = u_{1bm}^2/\omega\upsilon \tag{2.51}$$

Equations (2.48) through (2.50) are variations of the equations (2.44) through (2.47). They are derived by realizing that the roughness for smooth turbulent flow is not based on

sediment characteristics but rather on the bottom shear velocity and viscosity of the water. Defining $k_N = 3.3\nu / u_{*1m}$ and inserting this definition into equation (2.29) it is possible to show after some algebraic manipulation that

$$\frac{1}{4\sqrt{4f_w}} + \log_{10}\frac{1}{4\sqrt{4f_w}} = \log_{10}\sqrt{\frac{RE}{50}} - 0.17 \tag{2.52}$$

So by analogy, for rough turbulent conditions if (2.29) can be approximated by equations (2.44) - (2.47), for smooth turbulent the above equation can be approximated by (2.48) - (2.50).

2.3 The Model

In order to make use of the transport model, the critical bottom shear stress on a flat bed, τ'_{cr} needs to be considered.

The critical shear stress is found by using the modified Shield's diagram, figure 2 [Madsen and Grant, 1976]. First, S_* is calculated by

$$S_* = \frac{d}{4\nu}\sqrt{(s-1)gd} \tag{2.53}$$

Ψ_{cr} is then estimated from figure 2. From this, τ'_{cr} is calculated (see (2.9)).

$$\tau'_{cr} = (s-1)\rho g d\Psi_{cr} \tag{2.54}$$

The analysis is complete. Equation (2.15) is expanded to its full form:

$$q_{sb} = \pm\left[\frac{8}{(s-1)\rho^{3/2} g\cos\beta}\right]\left[\frac{1}{\tan\phi_k \pm \tan\beta}\right]$$
$$\left[|\tau_b(t)| - \tau_{cr}^{'}(\cos\beta \pm \frac{\sin\beta}{\tan\phi_s})\right]\left[\sqrt{|\tau_b(t)|} - \alpha\sqrt{\tau_{cr}^{'}(\cos\beta \pm \frac{\sin\beta}{\tan\phi_s})}\right] \quad (2.55)$$

For any given depth, bed slope, and wave condition described by Stokes or Cnoidal theories, the bedload can be calculated from (2.55). Its application is simple. Recall that when the bottom orbital velocity is upslope (shorewards), then a (+) sign is used in place of the ($\pm$) sign, and when the orbital velocity is downslope (seaward), a (-) sign is used instead (see equation (2.8)). Therefore, for $\tau_b(t) > 0$, the (+) signs are used, and for $\tau_b(t) < 0$, the (-) signs are used. Also, for conditions such that $|\tau_b(t)| < \tau_{cr}$, then q_{sb}=0. Equation (2.54) calculates the critical shear stress for a flat bed. The time varying shear stress is calculated from equation (2.37) using Stokes or Cnoidal theory.

Shoaling of the wave is handled incrementally. The program starts at a depth in which Stokes theory is valid and at depths in which one would expect little sediment motion. From this point, the program attempts to find an angle, β, for which the net transport rate is zero. Once the equilibrium angle has been found, the program then decreases the depth by an arbitrary increment. This increment is constant and is used to continually decrease the water depth until the water depth is close to zero. Hence, at each depth, an equilibrium angle is obtained.

When Stokes theory is valid, linear theory is used to shoal the wave. While this shoaling process is relatively straight forward, cnoidal wave theory is somewhat more complex. For that reason, a simplified table of cnoidal wave parameters [Svendsen, 1974] was added to the program in order to facilitate shoaling of the wave for Ursell numbers

greater than 26. At each depth where cnoidal theory is valid, the program finds the wave length and height and the resulting Ursell number by using this table. The wave characteristics and bottom orbital velocities and shear stresses were calculated, and the excursion amplitude of the wave was estimated.

It is worth mentioning at this point how one goes about calculating the free surface for cnoidal waves. The Jacobian Elliptic cosine, cn, used in (2.38) is estimated from the *"Handbook of Mathematical Functions"* [Abramowitz and Stegun, ed. 1972]:

$$cn = \frac{1}{\cosh\theta} - 0.25m1(\sinh\theta\cosh\theta - \theta)\tanh\theta / \cosh\theta \tag{2.56}$$

where $m1$ is a parameter found from the table in Svendsen. Since the equation is only relevant for ranges 0-π, any phase greater than π is translated into its related phase, $\theta_a = (2\pi - \theta_{actual})$. Moreover, θ is scaled by K, another parameter from Svendsen, so θ is again further manipulated to account for differing K values: $\theta_{used} = K\theta_a/\pi$. Finally, we can calculate cn^2.

So starting with a phase angle $\theta = 0$, the free surface is calculated allowing us to calculate the bottom orbital velocity using (2.39). Next, the wave friction factor is calculated using the explicit equations as described in section 2.2.3. The bottom shear stress can now be calculated for any phase of the wave.

Once these parameters have been calculated for a given depth the iterative process of finding β in which $q_{sb,net} = 0$ begins. β is initially set to zero. The wave is then split up into differential parts so that the transport rate can be estimated for each phase of the wave period. The transport rate for each phase is calculated and then summed up to

produce a total transport rate. For conditions in which the net transport is onshore, the bed slope angle in increased, and vice versa.

Chapter 3

3 Model Application and Results

In order to find the average net transport over any given period of time, it is necessary to examine both the shoreward and seaward transport. By setting $\tau_b(t) = |\tau_b(t)|$, and looking at the transport in either direction separately, one arrives at the average transport rate over one period at any given depth.

$$q_{sb,net} = \sum q_{sb,shoreward} - \sum q_{sb,seaward} \tag{3.1}$$

In order for $\sum q_{sb,net} = 0$ at this depth and wave condition, there must exist an equilibrium slope that allows for a balancing of reacting forces. Using a simple computer algorithm, this angle can be calculated at each depth. From this information an equilibrium beach profile can then be pieced together.

This section briefly describes the computer algorithm used to carry out the equilibrium beach calculations. Some of this has already been discussed but will be reintroduced here for clarity.

3.1 Cnoidal vs. Stokes Theories

Calculating the depth at which the Ursell Number is approximately 26 (the point at which Stokes theory is replaced by Cnoidal theory), it becomes evident that Stokes theory, for the most part, is only valid at depths greater than 6 to 8 meters (table 1).

Table 1. Depths at which Cnoidal vs Stokes are valid. This table illustrates the approximate depths in which the Ursell Number is approximately 26 for varying wave heights and wave periods. For depth greater than those shown, Stokes theory is considered valid. For depths less than those shown, Cnoidal theory is valid

Wave Period	**Deepwater Wave Heights**		
	1.0 m	**1.5 m**	**2.0 m**
7 s	4.0 m	4.8 m	5.5 m
10 s	6.5 m	7.0 m	8.6 m
13 s	8.5 m	9.5 m	11.2 m

The majority of empirical data used to support $h = Ax^m$ was either confined to the surf zone (around 3 meters depth) or continued to slightly deeper depths just outside the surf zone. For this reason, it was decided not to include Stokes theory in the algorithm other than to determine at which depth $U = 26$. This simplified programming, and eradicated any discrepancy that may have arisen when theories were switched.

3.2 The Algorithm

Input values include kinetic angle of friction, static angle of friction, wave period (seconds), phase angle, diameter of sediment (d_{50}), and the deep water wave height. All length scales are in meters and all time scales in seconds.

The first step calculates the critical shear stress. The model simplifies the modified Shields diagram (figure 2) into four zones and calculates the critical shear stress by first calculating S_* using (2.53), estimating Shields critical parameter and then using (2.54). The deep water wave length is found using linear theory:

$$L_o = \frac{g}{2\pi} T^2 \tag{3.2}$$

The wave is then shoaled. Starting at a depth of 1/2 the deepwater wave length, the depth is decreased by an arbitrary increment. For Ursell Numbers < 26, linear theory is used to shoal the wave. Once the Ursell number is 26 or greater, Cnoidal theory is used. Shoaling using Cnoidal theory is simplified by using the table compiled by Svendsen [1974] . Once the switch is made from Stokes to Cnoidal, the equilibrium slope for which $\sum q_{sb,net} = 0$ is calculated at each depth until the wave breaks using the breaking criterion $H/h = 0.78$. After breaking, the program continues with Cnoidal theory except it assumes that the wave height is now given by a constant ratio of $H = 0.78h$.

At each depth the program determines an angle, β, for which the net transport rate is zero. This is accomplished by using nested iterative loops. Generally, this is done by setting β to zero and integrating the bedload transport rate over one wave period. If the

transport rate is onshore, then β is increased and vice versa. More specifically, the computer program breaks the wave period into an arbitrary number of discrete phases. Some experimentation was performed at this point to get the best resolution for the least amount of CPU used. Typical values ranged from 20 to 40 discrete phases per period and, therefore, 40 is used in all computations. The bottom orbital velocity at each phase is approximated by (2.39) by calculating the free surface at that phase (2.38). The shear stress is then calculated from (2.40) using equations (2.41) through (2.43).

The bottom shear stress is then used to calculate the "instantaneous" bedload transport. Equation (2.55) is used for this purpose. If $(\eta_{\min} + (\eta_{\max} - \eta_{\min})cn^2) > 0$, then the transport direction is shoreward. Otherwise, it is seaward. The appropriate signs in (2.55) are used. Motion occurs when

$$|\tau_b(t)| > \tau_{cr}^{'}(\cos\beta \pm \frac{\sin\beta}{\tan\phi_s}) \tag{3.3}$$

otherwise, it is assumed that no transport is taking place during that particular wave phase.

The transport rate is then calculated from the governing equation. The phase angle, θ, is then incrementally increased and the whole process repeated. θ is increased from 0 to 2π. The net transport is found by summing the component parts. If the net transport rate is onshore, β is increased. Otherwise it is decreased. Convergence is reached when the changes in the slope resulting from finding an absolute zero transport rate are imperceptible. The convergence criteria used was $\Delta\beta \leq 10^{-4}$.

Once β is found, it is translated into a segment of the beach profile. The "active" β is averaged with the β at one incremental depth greater to find the average

slope, $\overline{\beta}$, over the depth increment. The distance is calculated by dividing the depth increment by $\tan(\overline{\beta})$.

3.3 Results

A series of runs were made with a variety of combinations of wave heights, wave periods, and beach sediment diameter. Profiles were calculated and plotted. Each profile, from the point at which $U = 26$ to a depth close to zero, was subjected to a curve fitting of the form $h = Ax^m$, with the water level at the origin of the depth axis. Selected results are shown in Tables 2, 3 and 4. The actual profiles generated by the computer corresponding to the tables are shown in figure 3, 5, and 7, respectively. Each of these profiles are likewise compared to a profile using the best fit equation $h = Ax^m$ and are shown in separate figures (4, 6, 8) for clarity.

Table 2. Profiles with Sediment Variation, $H_o = 1m$, $T = 10\ s$. The parameters A and m are used in the profile equation $h = Ax^m$

Sediment Diameter	A	m
d = 0.1 mm	0.93	0.417
d = 0.5 mm	0.942	0.429
d = 1.0 mm	0.974	0.452

These results suggest that (1) as diameter of the sediment increases, the slope of the beach increases (table 2 and figure 3); (2) with increasing wave height there is a corresponding decrease in beach slope (table 3 and figure 5); and (3) longer waves give

Table 3. Profiles with Deepwater Waveheight Variation, $d = 0.3\ mm$, $T = 10\ s$. The parameters A and m are used in the profile equation $h = Ax^m$

Deepwater Wave Height	A	m
$H_o = 0.5$ m	0.860	0.47
$H_o = 1.0$ m	0.967	0.41
$H_o = 1.5$ m	1.4	0.30

rise to steeper slopes (table 4 and figure 7). In other words, higher waves acting on a slope previously formed by smaller waves will create a predominant offshore transport rate, thus eroding the beach. Likewise, longer waves on a shallower beach cause shoreward transport and will tend to build up the beach head. These results parallel documented trends [Dean, 1994].

Table 4. Profiles with Wave Period Period Variation, $H_o = 1\ m$, $d = 0.3\ mm$. The parameters A and m are used in the profile equation $h = Ax^m$

Wave Period	A	m
T = 7 s	0.86	0.31
T = 10 s	0.967	0.41
T = 13 s	1.14	0.46

It should be noted that there is no dramatic change of slope at the point of breaking, a change one would expect to find in nature. However, it should be pointed out that figure 5 shows a slight change in slope for the largest wave height (the solid line) right at the point of breaking (around 2.3 m depth of water), but it is hardly noticeable.

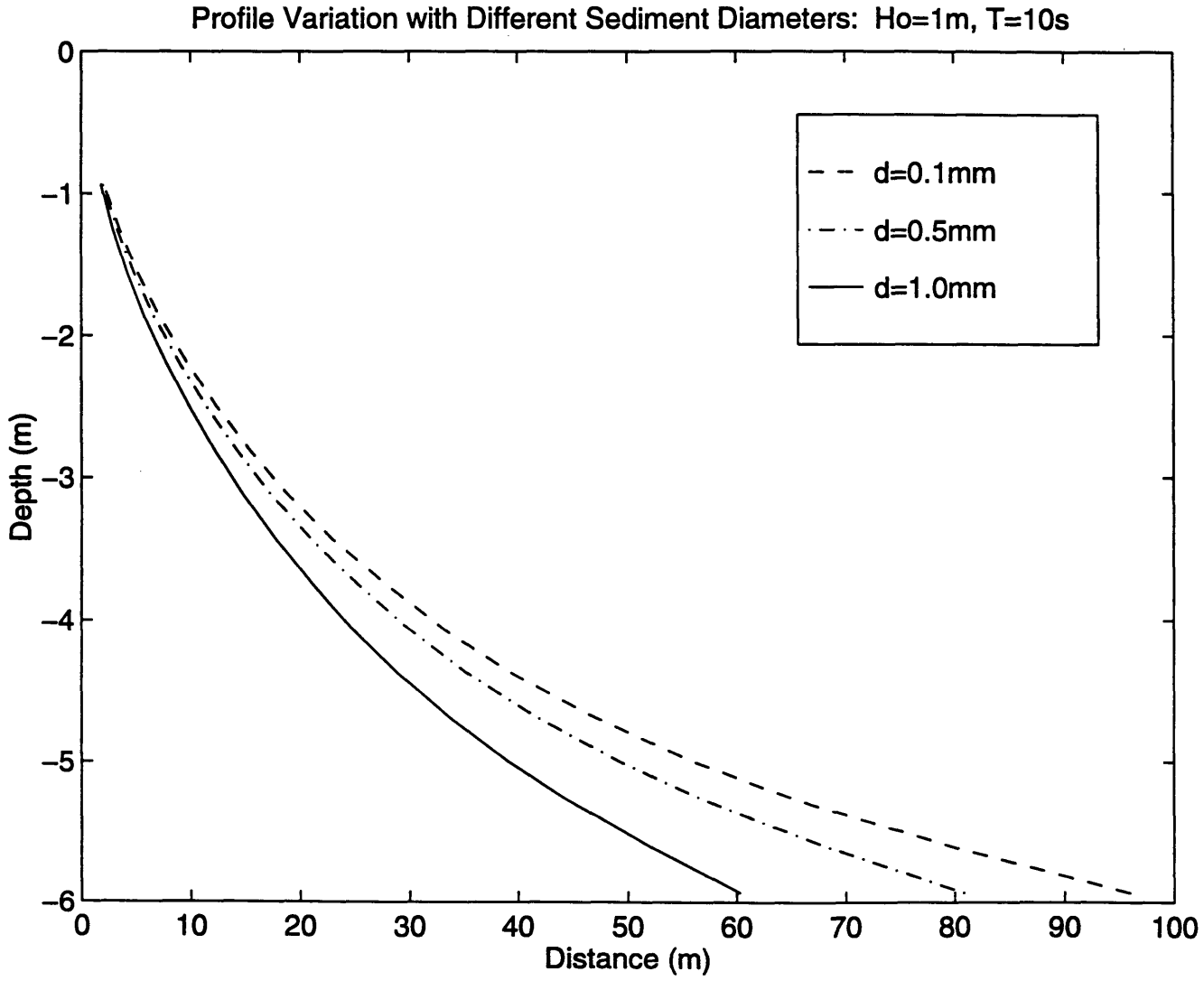

Figure 3. Variation of beach profile with different sediment diameters

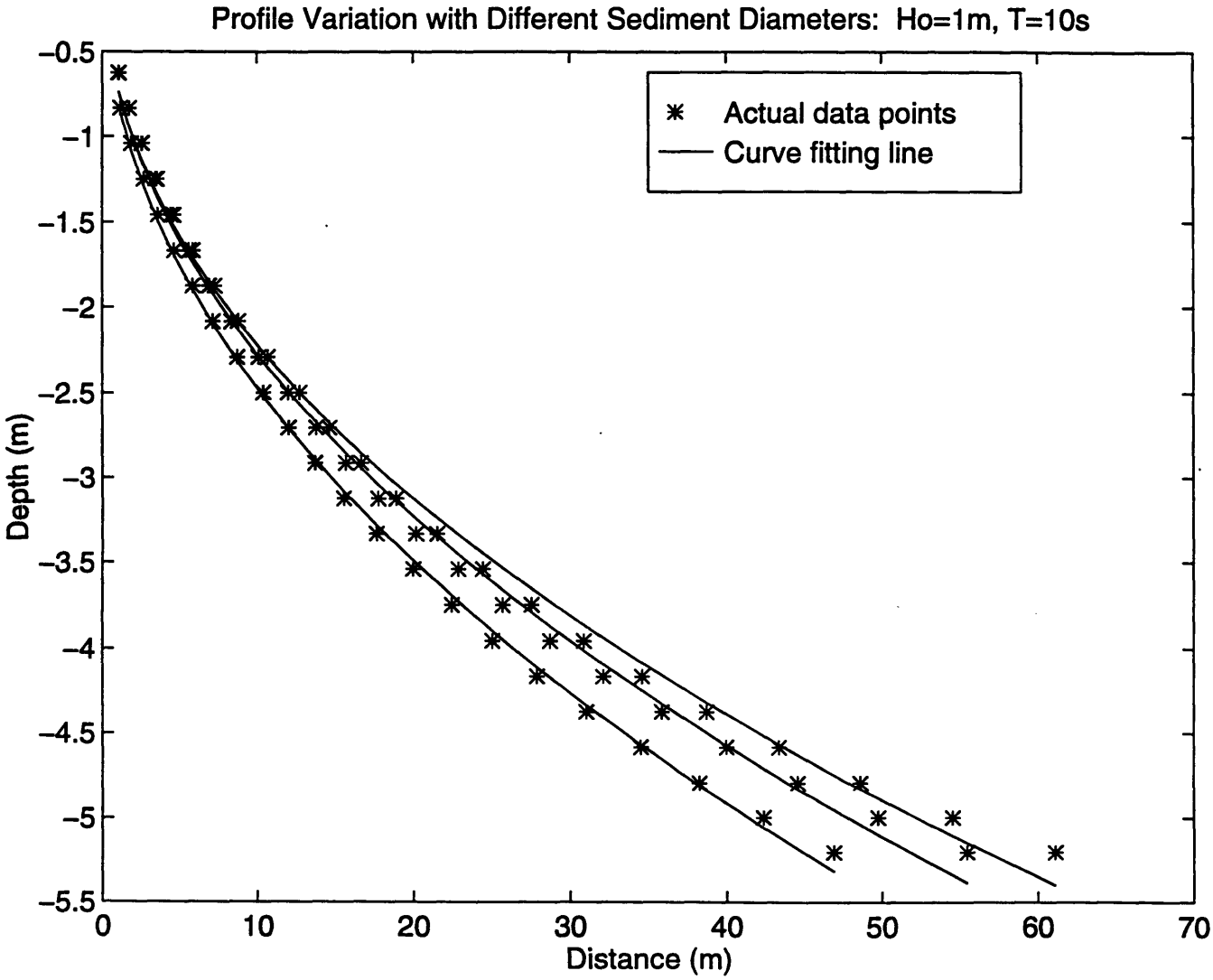

Figure 4. Variation of beach profile with different sediment diameters shown with the best fit line superimposed

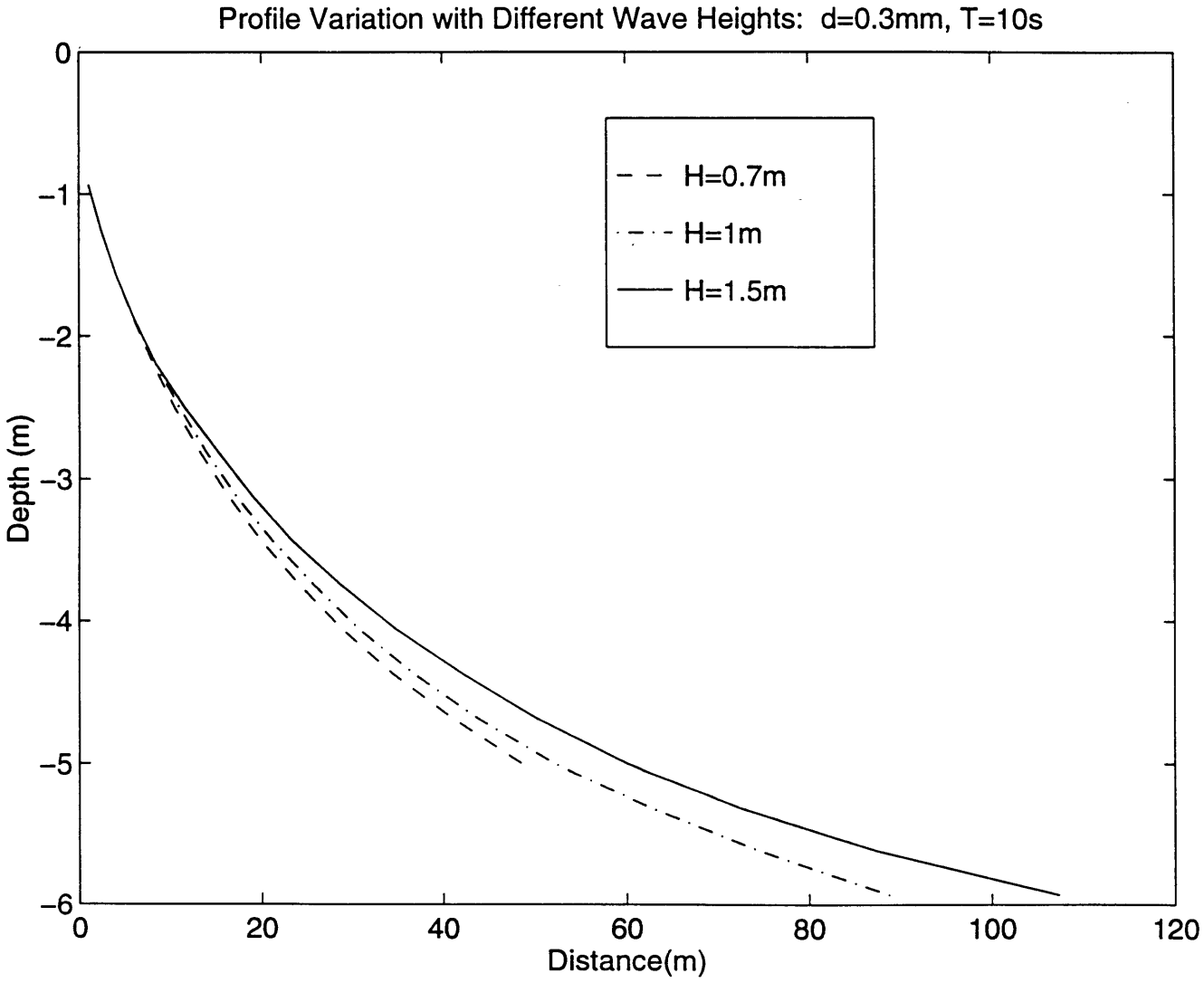

Figure 5. Variation of beach profile with different deepwater wave heights

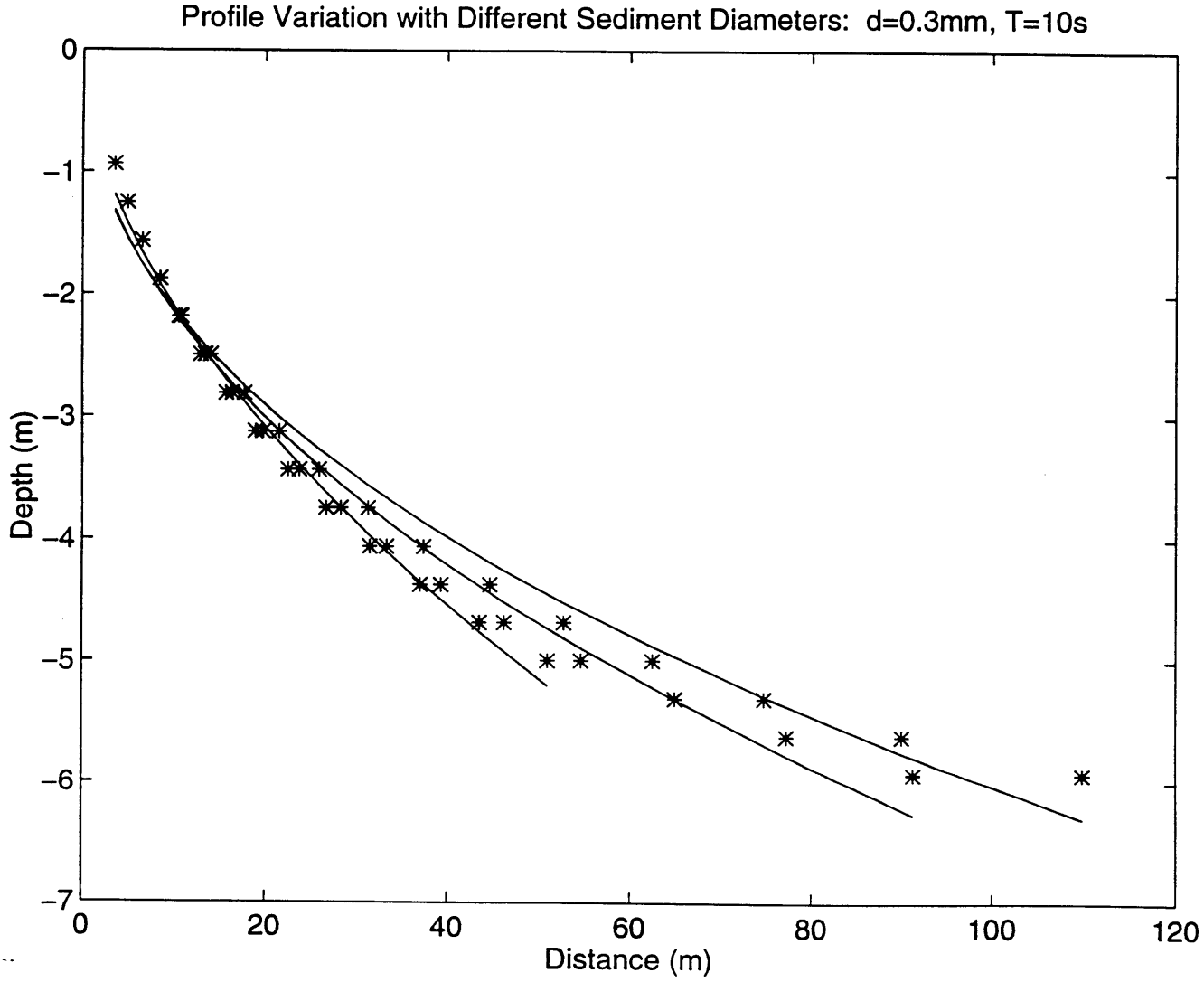

Figure 6. Variation of beach profile with different deepwater wave heights with the best fit line superimposed over the modeled profile

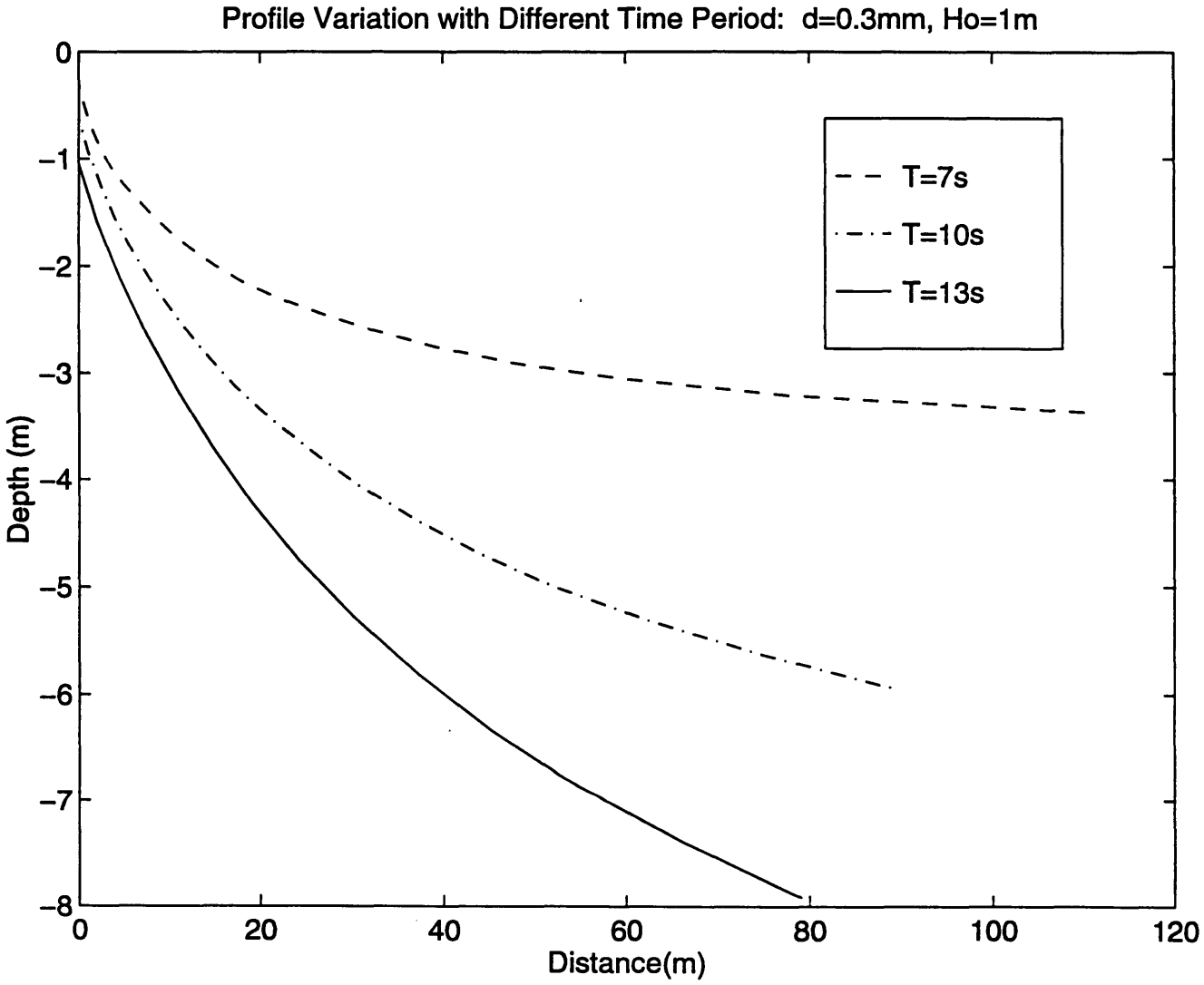

Figure 7. Variation of beach profile with different wave periods

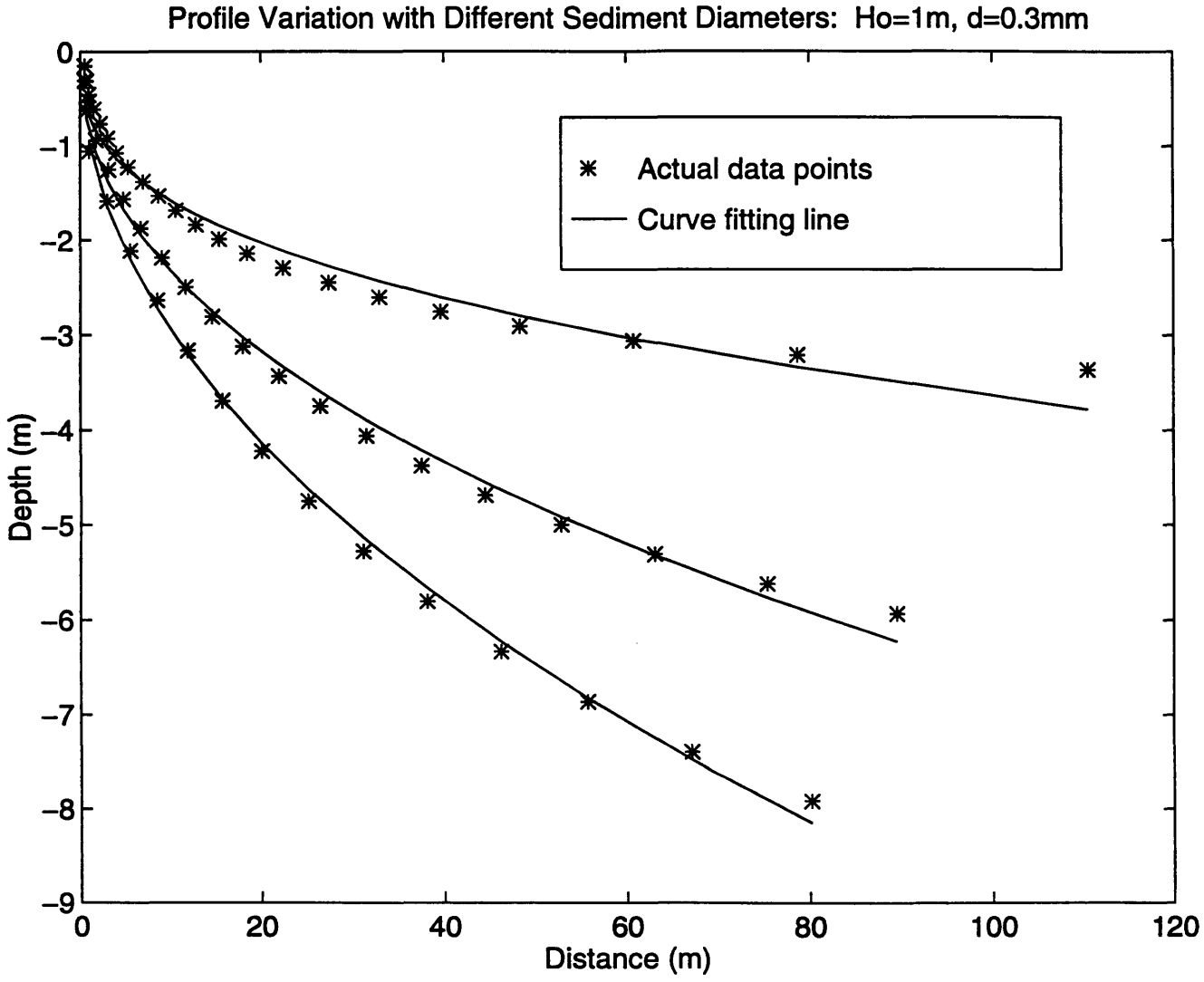

Figure 8. Variation of beach profile with different wave periods with the best fit line superimposed over the modeled profile.

Other profiles have the same subtle change in slope at the point of breaking but are even harder to notice. This is because the program terminates shortly after the point of breaking for smaller wave heights (a 1 meter high deep-water wave breaks in about 1.5 to 2 meters depth).

This brings up a point concerning some limitations of the model proposed. The program could not be run to depth of zero. As the depth approached around 50 cm, the nonlinear nature of the wave became so great that the bottom shear stress did not exceed critical under the trough of the wave and an equilibrium slope could not be found.

3.4 Discussion

Although the results do not seem to match $h = Ax^{2/3}$, there is a correlation to Inman et al.'s [1993] curvefitting results for the seaward segment.

3.4.1 Inman et al. Curve Fitting Methodology:

As previously mentioned, Inman et al. took data from three major locations (California, North Carolina, and the Nile delta), split all data profiles into two sections, the bar-berm component and the shorerise component, and applied a curvefitting model of the form $h \propto Ax^m$ to each section. The MSL was used as an origin for the shore-rise (or seaward) component whereas the berm crest was used as the origin for the surf zone. The curve fitting methodology is shown in figure 9.

It is found that the shorerise's average parameters are $A \cong 1.06$ and $m \cong 0.36$. The surf zone has average parameters of $A \cong 0.78$ and $m \cong 0.41$. The depth in which the switch

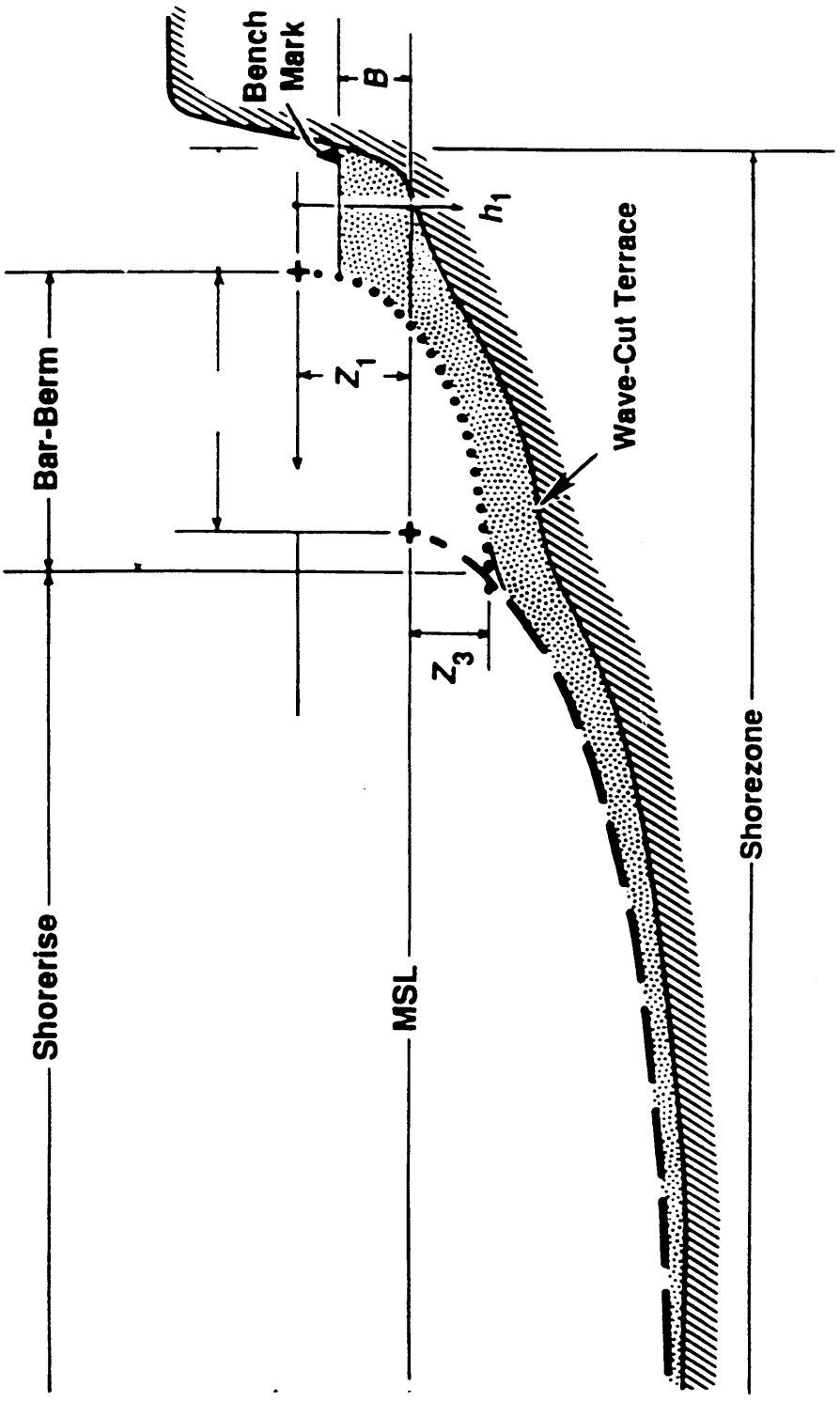

Figure 9. Schematic diagram of Inman et al. curve fitting methodology (from Inman et al., 1993)

is made, Z_3, is approximately 2 - 4 meters below MSL. This point is referred to as the breakpoint-bar to signify that it is the bar commonly at or near the breakpoint of the wave. Z_1 is approximately 3 - 4 meters. Other parameters in the definition sketch are irrelevant to this discussion.

3.4.2 Comparison of Theoretical Model to Inman et al. Curves:

The model suggested here produces similar results to Inman et al. with a 8 to 10 second wave and a deepwater height of approximately 1 to 1.5 meters for the shorerise component (see tables 3 and 4) . These similarities are illustrated in figure 10. Unfortunately, little information about the wave climate at each data site used in Inman et al.'s curvefitting procedures was reported. What is known is that there is considerable difference in wave climate between each of the three major areas. California's wave climate is characterized by near-breaking wave heights of $1 \le H_s(m) \le 6$ and peak spectral periods of $5 \le T_p(s) \le 20$; North Carolina, $1 \le H_s(m) \le 5$ and $5 \le T_p(s) \le 15$; and the Nile delta, $0.5 \le H_s(m) \le 3$ and $3 \le T_p(s) \le 8$ [Inman et al., 1993]. The average sediment size for all sites in 4 m depth is reported to be 0.1 mm to 0.3 mm. For deeper water, the sediment size is around 0.1 mm.

Data from Inman et al. show that the difference between the Nile and North Carolina profiles is significant. Averages for the North Carolina shorerise component is $A \cong 1.1$ and $m \cong 0.30$, but the Nile's shorerise parameters are $A \cong 0.43$ and $m \cong 0.48$. Assuming that the Nile is subjected to smaller waves with lower periods, it is seen that table 3 shows similar trends in beach parameters. In fact, assuming that the shores of

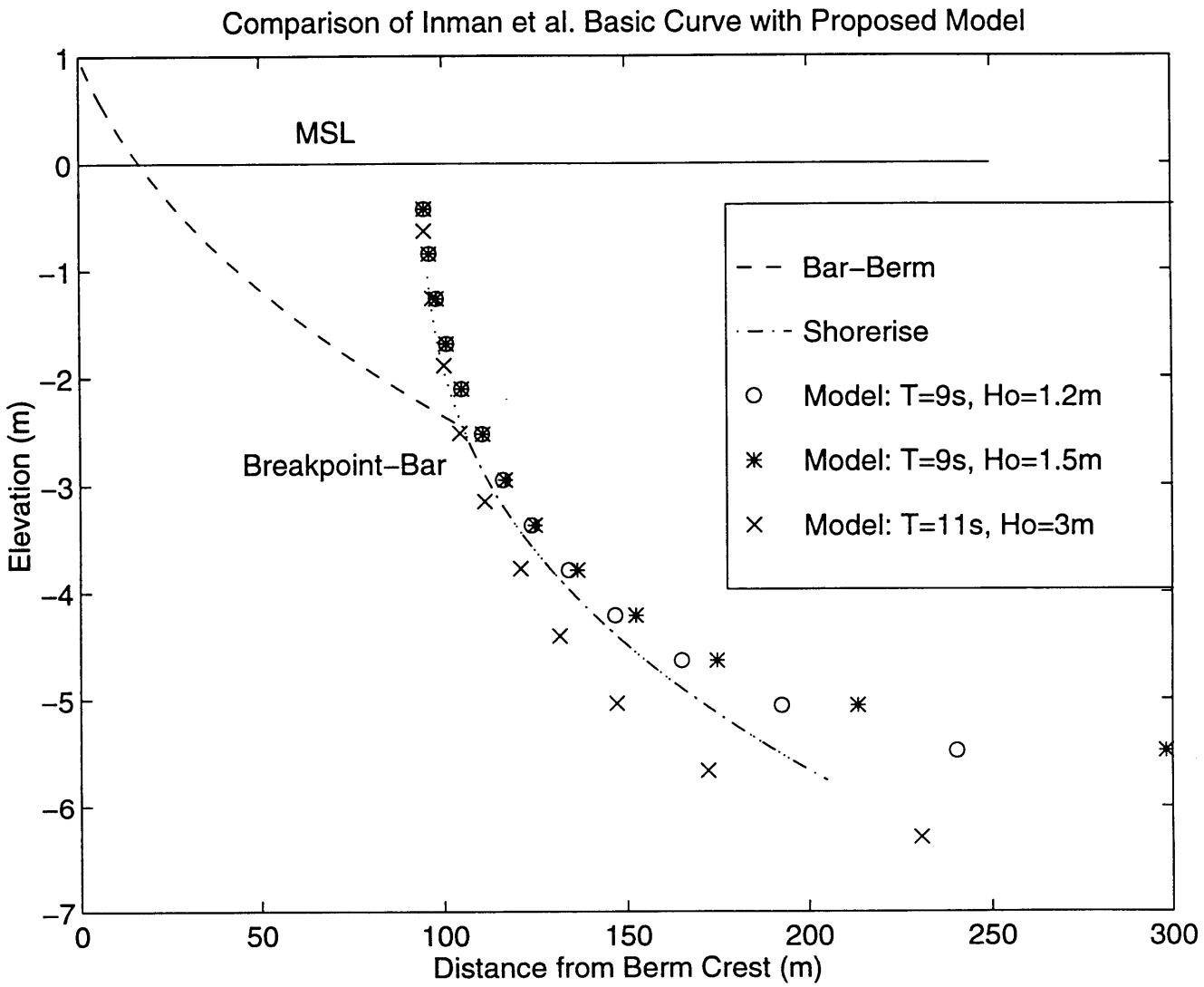

Figure 10. Comparison of Inman et al., 1993, basic curve with proposed model. The sediment diameter used was 0.2 *mm*.

North Carolina are subjected to waves with a significant deepwater height of 1.3 meters and peak spectral periods of 9 seconds and beaches with a sediment diameters of 0.2 *mm*, the model after being run with these particular wave characteristics indicates parameter values of $A \cong 1.1$ and $m \cong 0.33$. Although North Carolina may have typical sediment diameters less than or greater than 0.2 *mm* there is little change in profile due to variations of sediment size, as seen in figure 3. These results closely parallel the empirical data. Likewise, assuming that the Nile delta coast has a wave climate of significant deepwater heights of 0.4 meter and peak spectral periods of 6 seconds and a sediment diameter of 0.2*mm*, the parameter values found by the model after being run with these characteristics are $A \cong 0.57$ and $m \cong 0.46$ wave. Again, the results parallel those found in the field.

Inman et al. also propose that there are two main characteristic shapes: the summer profile and the winter profile, yet it is not explicitly stated what the change in the overall wave pattern is during seasonal changes. One could surmise that the winter brings strong local winds, and hence higher waves and perhaps slightly shorter wave periods. Table 5 illustrates findings from Inman et al. for seasonal variations. Table 6 proposes some typical winter conditions and their respective shapes based on the model presented here. It is assumed that the ambient wave condition would be much rougher in the winter than during the summer months and therefore to simulate this, it is assumed that the wave heights, but not necessarily the period, would be larger. It is assumed that the wave height is of the order 1.5 *m* for winter conditions, while for summer it is assumed that the wave height would be around 1.0 *m*. The period was kept constant at 10*s*.

Results from Table 5 and Table 6 indicate that the model captures general beach profile shifts with changing ambient wave characteristics. However, the model does not succeed at capturing the magnitude of change in the coefficient *A*. By studying the

Table 5. Inman et al. Profiles with Seasonal Variation for the shorerise beach segment. Information concerning changes in wave climate between the seasons was minimal. The sediment diameter was assumed to be d = 0.2 *mm*.

	A	**m**
Winter	1.52	0.31
Summer	0.73	0.42

Table 6. Modeled Seasonal Variation. The wave conditions on the top row are assumed to approximate the winter months, whereas the bottom row parameters attempt to approximate ambient summer wave characteristics. The sediment diameter was assumed to be d = 0.2 *mm*

	A	**m**
T=10s, H=1.5m	1.4	0.30
T=10s, H=1.0m	0.967	0.41

general trends of the model by perusing Tables 2 to 6, it is seen that shorter wave periods decrease the coefficient *A*, but slight increases in wave heights causes *A* to dramatically climb. The exponent *m*, on the other hand, decreases with increasing wave height, but increases for increasing wave period by approximately the same ratio. In order to better match results illustrated in Table 5, it would appear that wave heights for the winter should be increased while the proposed wave period for the summer should be decreased.

Increases in the wave height for winter months may be justifiable. However, it is unclear at this point whether or not the wave period for the summer is actually shorter than the wave period during winter months.

Too little is known of the sediment characteristics in any of individual profiles studied to permit comparison of sediment size with the changes in parameters noted here. The general trend noticed in figure 3 seems indicative of what is actually observed in the field [Inman et al., 1993; Swart, 1991]. Unfortunately, this is all that can be said at present about the impact of sediment size on profile variations.

3.5 Summary of Bedload Model

Using a simple theoretical model previously shown effective in applications for bedload transport over a flat bed under steady and unsteady currents, it is demonstrated that oscillatory flow generated by nonlinear wave action over a bed with a zero net transport rate creates a beach shape of the form $h = Ax^m$. It is assumed that the main mode of sediment transport is bedload and that there is only one shear generating force, that of wave action. Cnoidal theory is used to describe wave surface profiles and resultant orbital velocities. Bottom shear is related to the bottom orbital velocity squared multiplied by a resultant friction factor. Bedload is proportional to shear stress raised to the 3/2 power. At each depth, an equilibrium angle is calculated by adjusting the bed angle such that the time averaged bedload over one wave period is zero. Once the wave breaks, the theoretical approach changes only in the sense that wave height is dampened linearly with depth. By averaging adjacent angles over incremental depths, a beach shape is drawn. Profiles are generated from a depth in which the Ursell Number, denoted as $U = HL^2/h^3$,

equals 26 to a depth close to zero. Using best fit curves to describe theoretical beaches generated under varying wave conditions and sediment characteristics and, comparing these with empirical studies, indicate a strong correlation between empirical models used to describe the beach segment outside the breaker zone.

Inman et al. proposes that beach profiles are best described not by a single curve fitting model, but rather by two parabolic curves. It is claimed that transport mechanisms within the breaker zone (bar-berm) are different from the offshore (shorerise) segment. Results obtained here concur. It is seen that theoretical profiles match closely the shape of the offshore segment. Inman et al. reports that $A \approx O(1)$ and $m \approx 0.4$. Results obtained here suggest similar parameters. Variability in these parameters can be attributed to changes in wave conditions and sediment characteristics. Empirically, trends in the parameters indicate smaller m during winter, as well as steeper slopes with increasing grain diameter. Results obtained here parallel these findings.

Although the results match empirical data offshore, it is clear that once the wave breaks the model's effectiveness is severely limited. This is demonstrated quite distinctly in figure 10. The empirical curve fitting model for the shorerise beach segment, as suggested by Inman et al. is approximated very well by assuming some general wave conditions with a sediment diameter of 0.2 *mm* and then running these through the proposed model. However, Inman et al. suggests two separate curve fitting methodologies to account for the change in the hydrodynamics brought on by breaking. As figure 10 clearly illustrates, at the point of breaking our model does not radically change slopes to follow the bar-berm curvefitting component. In fact, our model does not deviate at all from the offshore curve-fitting line. Hence, we capture the key elements of the shore-rise

sediment transport processes and predict the equilibrium beach profile well for the region offshore of the breakerline, but fall far short within the surf zone.

It is suggested that adjustments are needed to account for changes in wave characteristics as well as the appearance of near-shore currents associated with breaking waves. In order to improve predictions within the surf zone, an undertow is added. This, coupled with increased turbulent kinetic energy and hence more suspended sediment, will cause greater offshore transport which will then presumably decrease the bed slope at the point of breaking. The next chapters further refines the model along these lines.

Chapter 4

4 Suspended Load and the Undertow

The surf zone, hydrodynamically, is quite different from the area outside the surf zone because of the breaking wave action. Not only will a strong undertow result in order to compensate the shoreward mass transport, but there will also be increased turbulence, increased near surface shear due to the roller affect, a significant amount of energy dissipation and hence a drop in wave height, and a transformation of wave form. The amount of energy dissipated, or the increased surface shear, is dependent on the type of breaking wave. This analysis assumes a roller-type breaker.

The increased turbulence in the surf zone generates the necessary energy to suspend a significant amount of sediment. Once suspended, the currents often associated with breaking waves (the undertow and longshore currents) can then transport the sediment more readily. Hence, suspended sediment within the surf zone becomes increasingly important, perhaps even dominating the bedload transport. It is therefore

imperative to include suspended transport into our model. For the purpose of modeling cross-shore suspended load, it is believed that the dominant features are wave-induced suspended sediment with an undertow current as the transport mechanism. Once the sediment concentration profile and the undertow velocity profile is found, the suspended load can be found by integrating the coupled suspended concentration and cross-shore velocity field:

$$q_{ss} = \int_{Z_R}^{\eta} (CU)dz \tag{4.1}$$

where Z_R is defined as the point near the bed below which, sediment transport is considered to be bedload, and above, sediment transport is considered to be suspended load. η is the free surface.

4.1 Suspended Sediment Distribution

The governing equation for the distribution of suspended sediment in the water column is the advective diffusion equation.

$$\frac{\partial c}{\partial t} - \frac{\partial}{\partial z}(w_f c) - \frac{\partial}{\partial z}\left(\nu_s \frac{\partial c}{\partial z}\right) = 0 \tag{4.2}$$

where w_f is the fall velocity, ν_s is the sediment diffusion coefficient and c is the volumetric concentration of suspended sediment. We assume a constant sediment size for which w_f is constant and where the sediment diffusion coefficient can be approximated by the turbulent eddy viscosity. Equation (4.2) is split into two equations, one for a constant

concentration, the other a time-varying, wave-associated concentration. This is accomplished by letting $c = \bar{c} + c_w$. The time-invariant concentration distribution is:

$$\frac{\partial}{\partial z}\left[(w_f \bar{c}) + \left(\nu_t \frac{\partial \bar{c}}{\partial z}\right)\right] = 0 \tag{4.3}$$

The sediment fall velocity, w_f, is simply estimated using the Grant-Madsen [1976] graph relating fall velocity and sediment-fluid parameter S_* (figure 11). The boundary conditions specified for this governing equations are as follows: 1) no sediment is transported through the surface, $c \to 0$ as $z \to \infty$, and 2) a reference concentration, $\overline{C}_R$, is specified at a reference height above the bottom, Z_R. The reference height is given as proportional to sediment diameter. Here we use the value of Z_R suggested by Madsen et al. [1993]:

$$Z_R = 7d \tag{4.4}$$

The reference concentration, theoretically, is considered to be proportional to the bedload. According to Einstien [1950], this can be expressed as

$$C_R \propto \frac{q_{sb}}{u_s Z_R} \tag{4.5}$$

where q_{sb} is the bedload and u_s is the sediment velocity. It has been shown in the second chapter (2.13) that $u_s = 8(u_* - \alpha u_{*cr})$, and from equation (2.15), stated here again,

$$q_{sb} = \frac{\pm 8(|\tau_b| - \tau_{cr})}{(s-1)\rho g \cos\beta(\tan\phi_k \pm \tan\beta)}(u_* - \alpha u_{*cr}) \tag{4.6}$$

we derive an expresion for C_R.

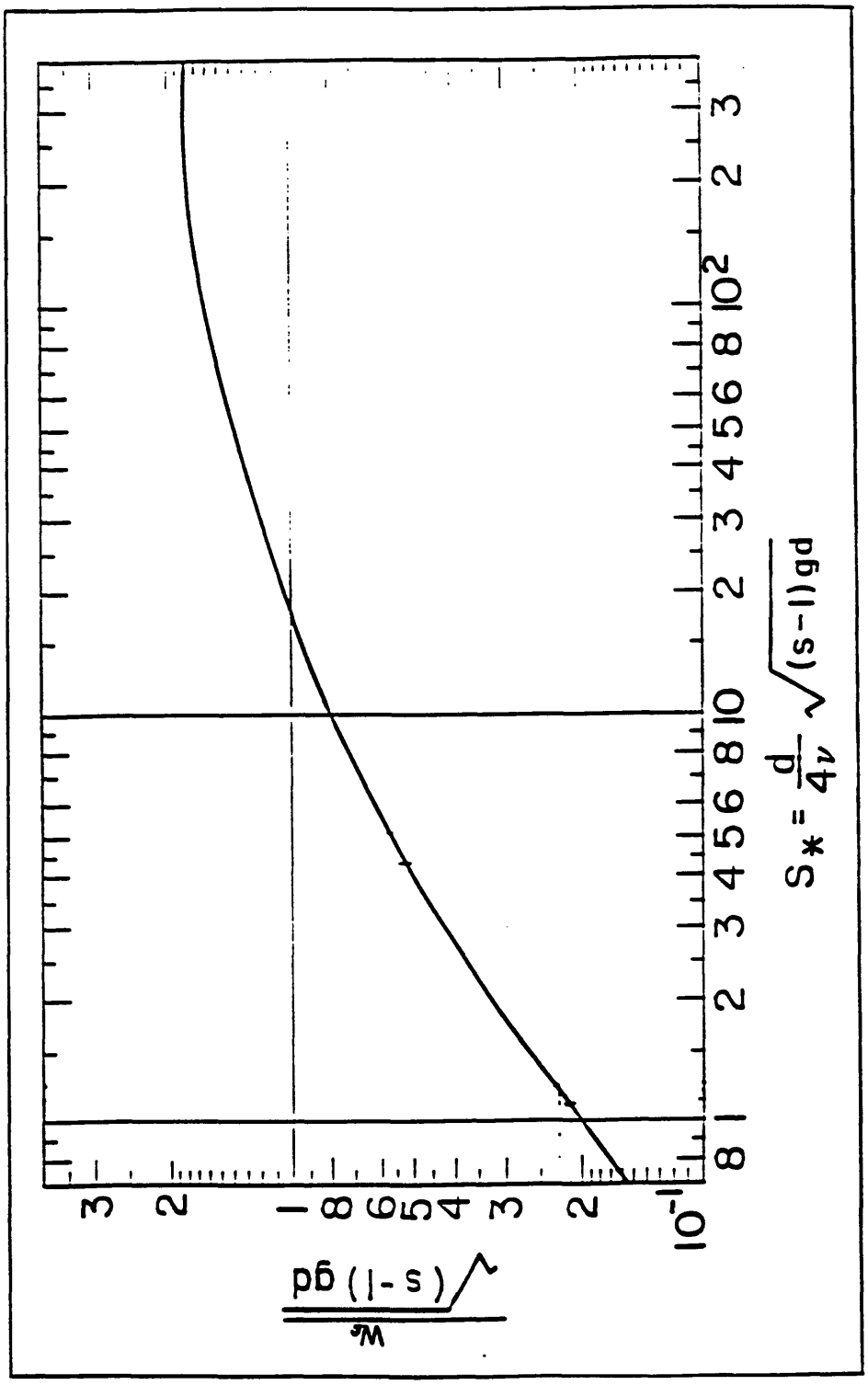

Figure 11. Fall velocity as related to the sediment-fluid parameter, S_*

$$C_R = \frac{\gamma(|\tau_b| - \tau_{cr})}{Z_R \rho g (s-1)(\tan\varphi_k \pm \tan\beta)} \tag{4.7}$$

where γ is the resuspension parameter and is set to $\gamma = 10^{-2}$ as detailed in Appendix A. The time-average reference concentration is then

$$\overline{C}_R = \frac{\overline{\gamma(|\tau_b(t)| - \tau_{cr})}}{Z_R \rho g (s-1)(\tan\varphi_k \pm \tan\beta)} \tag{4.8}$$

Equation (4.8) is calculated in much the same way bedload was calculated in section 2.3. A single wave period is broken down into discrete temporal phases. For each phase, the bottom shear stress is calculated using equation (2.40). The critical shear stress is calculated by (2.12). If $|\tau_t(t)| < \tau_{cr}$, then $C_R = 0$. Otherwise C_R is calculated using (4.7). Recall that for shoreward velocities, the positive sign in the denominator is used, while for seaward velocities, the negative sign is used. Note that while it is possible to get a negative (offshore) bedload transport, the reference concentration calculated by (4.7) is always positive. The reference concentrations calculated at each phase are then summed up and divided by the number of discrete phases specified. This is our calculated $\overline{C}_R$.

In order to solve the governing equation (4.3) more information is needed concerning the hydrodynamics within the surf zone, namely, the fluid eddy viscosity. Moreover, since we are looking for suspended sediment transport, a detailed description of the velocity field is also needed in order to solve equation (4.1).

4.2 The Undertow

The undertow is a phenomena that arises due to the local mismatch at each point in the water column between the radiation stress gradient and set-up induced pressure gradient. In order for a local balance to exist, a turbulent shear stress is introduced. This shear is generated by what is commonly known as the undertow.

4.2.1 General Remarks

Graphically, the undertow phenomenon is illustrated by figure 12. The depth integrated, time-averaged momentum equation is in balance. That is to say, the change in the radiation stress S_{xx} in the shore-normal direction is balanced by the setup gradient and bottom shear. However, a local imbalance exists. This is illustrated in figure 13. It is here that a local turbulent shear stress in the vertical must exist such that the horizontal

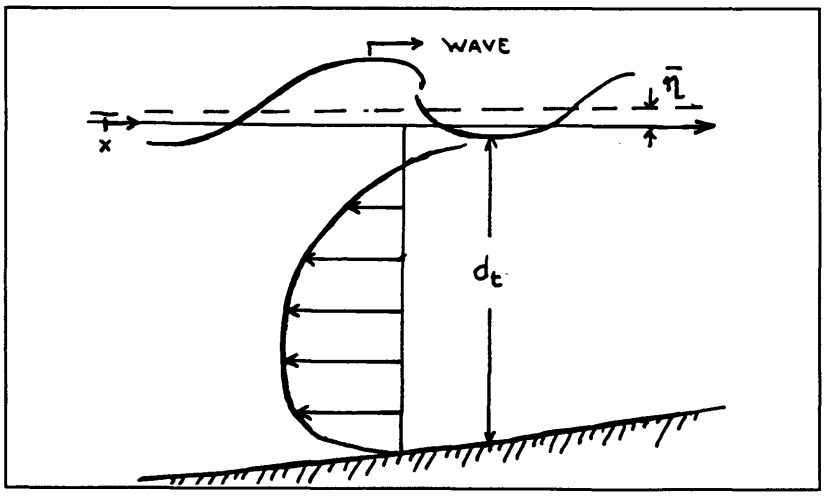

Figure 12. A graphical representation of the undertow within the surf zone.

time-averaged momemtum equation balances both over the depth and at each localized point in the vertical.

Many attempts have recently been made to come up with a simple analytical solution in order to predict the undertow. The present undertow model is in all essential details similar to existing undertow models, except for its treatment of the bottom boundary condition. This model assumes a value of the bottom boundary shear-stress which is then used in conjunction with the Grant-Madsen [1986] wave-current interaction model to predict the undertow velocity at the outer edge of the wave boundary layer. This bottom velocity is then used as the bottom boundary condition necessary to solve for the undertow profile in the interior of the fluid following established procedures. A valid

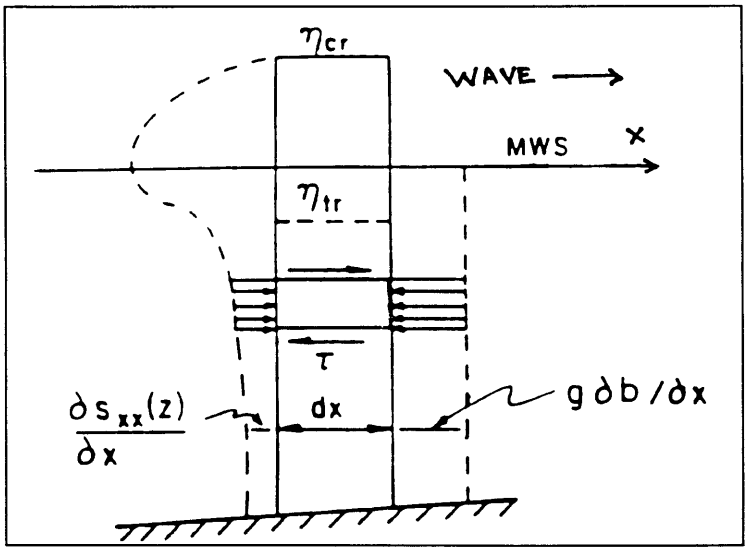

Figure 13. Force balance in the surf zone demonstrating the local imbalance of Forces along the vertical.

solution is obtained when the assumed average bottom shear stress leads to a prediction of zero net flow in the shore normal direction.

4.2.2 Theoretical Formulation

The time-averaged horizontal momentum equation as presented by Stive and Wind [1982] is

$$\frac{\partial}{\partial x}\overline{\left(\tilde{u}^2 - \tilde{w}^2\right)} + g\frac{\partial \overline{\eta}}{\partial x} + \frac{\partial \overline{uw}}{\partial z} = 0 \tag{4.9}$$

$\overline{uw}$ can be broken down to an organized wave component and a turbulent fluctuation component, $\overline{uw} = \overline{\tilde{u}\tilde{w}} + \overline{u'w'}$. Within in the surf zone, it is assumed that the organized wave motion is relatively small compared to the turbulent contributions, $\overline{\tilde{u}\tilde{w}} << \overline{u'w'}$. The dominant term is simply a turbulent Reynolds stress, and is related to a horizontal shear using an eddy viscosity concept:

$$\frac{\partial \overline{u'w'}}{\partial z} = -\frac{1}{\rho}\frac{\partial \overline{\tau}}{\partial z} \tag{4.10}$$

Since $\overline{\tau} = \rho \nu_t(z)\frac{\partial U}{\partial z}$, where $\nu_t(z)$ is the turbulent eddy viscosity, the horizontal time-averaged momentum equation can then be expanded to

$$\frac{\partial}{\partial x}\overline{\left(\tilde{u}^2 - \tilde{w}^2\right)} + g\frac{\partial \overline{\eta}}{\partial x} = \frac{\partial}{\partial z}\left(\nu_t(z)\frac{\partial U}{\partial z}\right) \tag{4.11}$$

It is observed that, generally, the local imbalance between the momentum flux and the setup is constant in the vertical at any particular depth in the surf zone [Stive and Wind, 1986]. Hence we can say that the term $\overline{\tilde{u}^2 - \tilde{w}^2} + g\overline{\eta}$ is only a function of x. We therefore simplify (4.11) by replacing these terms by a single variable, R:

$$\frac{\partial R}{\partial x} = \frac{\partial}{\partial z}\left(\nu_t(z)\frac{\partial U}{\partial z}\right) \tag{4.12}$$

(4.12) is only valid below the trough level, d_t. Integrating this equation with respect to z, we get

$$U(z) = \frac{\partial}{\partial x} R\int\frac{z}{\nu_t}dz + \psi'\int\frac{dz}{\nu_t} + \lambda \tag{4.13}$$

and since it has been proposed that $\nu_t(z)$ can be approximated fairly well as a constant in depth [Stive and Wind, 1986], the integrals in (4.13) can be solved to give:

$$U(y) = \frac{1}{2}\alpha y^2 + \psi y + \lambda \tag{4.14}$$

where $y = z+h$ (where h is the still water depth), ψ and λ are integration constants (note that $\psi' = \nu_t\psi$), and $\alpha = \frac{1}{\nu_t}\frac{dR}{dx}$ which includes the unknown setup term $\frac{\partial\overline{\eta}}{\partial x}$. This leaves us with three unknowns.

In order to solve for the two integration constants, ψ and λ, two boundary conditions must be specified. The first is that the volume of the return flow must equal the amount transported shorewards due to mass transport.

$$\overline{U}_m d_t = \int_0^{d_t} U(y)dy \tag{4.15}$$

where d_t is the height of the trough above bottom. $\overline{U}_m$ is the mean velocity of the return flow. By inserting (4.14) into (4.15), it can be shown that

$$\lambda = \overline{U}_m - \frac{1}{6}\alpha d_t^{\,2} - \frac{\psi}{2}d_t \tag{4.16}$$

The second boundary condition is satisfied by specifying a shear stress at the trough depth. If we differentiate (4.14) with respect to y and then multiply the result by the density and eddy viscosity, the result is

$$\rho\nu_t \frac{dU}{dy} = \rho\nu_t \alpha y + \rho\nu_t \psi \tag{4.17}$$

For $y = d_t$, the shear at the trough level, $\rho\nu_t \frac{dU}{dy} = \tau_{tr}$, is found.

$$\tau_{tr} = \rho\nu_t(\alpha d_t + \psi) \tag{4.18}$$

At $y = 0$, we know that $\tau = \tau_c$, the current bottom shear stress. Therefore, we can modify (4.18) to

$$\tau_{tr} = \rho\nu_t \alpha d_t + \tau_c \tag{4.19}$$

By using these three equations, (4.16), (4.18), and (4.19), and inserting them into (4.14), the general equation describing the undertow can be written in the following form:

$$U = \alpha\left(\frac{y^2}{2} - \frac{d_t^{\,2}}{6}\right) + \frac{\tau_c}{\rho\nu_t}\left(y - \frac{d_t}{2}\right) + \overline{U}_m \tag{4.20}$$

It is noted at this point that (4.20) is derived from the local force imbalances within the vertical plane of the water column. Equation (4.19), on the other hand, represents the total force balance within the water column. Both equations must be satisfied in order to have a comprehensive solution.

Unknown parameters in these two equation, ν_t, $\overline{U}_m$, τ_c, τ_{tr}, and α, are found using the relationships and methods outlined below.

The eddy viscosity is estimated from the empirical relationship given by Stive and Wind [1986]. The eddy viscosity is assumed to be constant over depth.

$$\nu_t = 10^{-2} ch \tag{4.21}$$

where c is the phase velocity. The average return velocity, $\overline{U}_m$, can be estimated from linear theory for long waves by calculating the mass transport rate, M:

$$\overline{U}_m = -\frac{M}{\rho h} = -\frac{1}{h}\int_0^{\eta} \overline{u}_L dz = -\frac{1}{8}\sqrt{gh}\left(\frac{H}{h}\right)^2 \tag{4.22}$$

However, it has been proposed that there will be an increase of mass transport within the surf zone due to the effects of the roller. In order to account for this extra mass associated with the rollers, Stive and Wind [1986] proposed an empirical equation to obtain the average return velocity.

$$\overline{U}_m \cong -\frac{1}{10}\sqrt{gh}\frac{H}{h} \tag{4.23}$$

This result corresponds closely to the solution for the linear net mass transport as derived above if we assume that $H = 0.8h$. Svendsen [1984] presents an alternative solution for the net return flow:

$$\overline{U}_m = -c\left(\frac{H}{h}\right)^2\left(B_o + \frac{A_r}{H^2}\frac{h}{L}\right) \tag{4.24}$$

where B_o is a shape factor, estimated to be 0.08 and A_r is the area of the roller estimated to be $0.9H^2$.

The trough shear can also be estimated using linear theory. The shear at the surface is simply the gradient of the time-averaged pressure in the shore-normal direction between the trough level and the free surface.

$$\tau_{tr} = -\frac{\partial}{\partial x}\overline{\int_0^{\eta} \rho g z dz} = -\frac{1}{2}\frac{\partial}{\partial x}\rho g\overline{\eta^2} = -\frac{1}{16}\rho g\frac{\partial H^2}{\partial x} \tag{4.25}$$

Again, because of the roller, it is expected that there will be a greater shear at the surface of the water than there would be if there was no breaking. A semi-empirical relationship is devised in order to accommodate this increase. This equation was proposed by Svendsen [Stive and Wind, 1986].

$$\tau_{tr} = -\left(\frac{1}{16} + \frac{A_r h}{H^2 L}\right)\rho g \frac{\partial H^2}{\partial x} \tag{4.26}$$

It is worth noting that the additional $\frac{A_r h}{H^2 L}$ term is an empirical correction factor added to account for the roller effect. A_r, again, is the area of the roller and is approximated by $0.9H^2$. Without this correction term, (4.26) is simply the expression found above using linear theory.

The last step in solving all unknown parameters entails the introduction of a boundary layer profile. We use a combined wave-current model [Grant-Madsen, 1986] to describe the boundary layer flow:

$$u(z) = \frac{1}{\kappa}\frac{{u_{*c}}^2}{u_{*m}} \ln\left(\frac{z}{z_o}\right) \tag{4.27}$$

where u_{*m} is the maximum combined wave-current shear velocity. Now we have all the necessary information to analytically and completely solve (4.20), the undertow current profile.

Our final solution methodology is as follows. We assume a current bottom shear, τ_c, and by using (4.26) we calculate α from (4.19). We can now solve (4.20) in its entirety by using our solution for α, our assumed value of τ_c, and the equations (4.21) and (4.23). We then solve the boundary layer flow (4.27). The boundary layer flow and the free stream flow (4.20) should have matching velocities at the boundary layer

thickness. If they do not then a new value of τ_c is assumed and the process is repeated. The thickness of the boundary layer is estimated from the following relationship:

$$\delta = \frac{\kappa u_{*_m}}{\omega}. \tag{4.28}$$

If $\tau_c << \tau_m$, then the maximum combined wave-current shear velocity can be approximated by the maximum wave shear velocity, ie. equation (2.21), and for most situations within the surf zone, this is a valid approximation.

4.3 Validation of Model

We have compared our theoretical profile to the experimental results presented by Cox and Kobayashi [1997]. Cox and Kobayashi measured both the free surface variaton as well as the vertical velocity distribution for the case of periodic waves (1.2 s period) spilling on a rough, impermeable, 1:35 slope where a single layer of sand was glued to the bottom. The median grain size, d_{50}, was reported to be approximately 0.10 cm. Velocities were measured at six stations, one outside the surf zone, one right at the point of breaking , one during the "transition" zone, and the other three within the inner surf zone. Unlike previous studies of the undertow, Cox and Kobayashi were able to capture detailed measurements of the instantaneous velocities and shear stresses in the bottom boundary layer of about 1 cm thickness under the breaking waves [Cox and Kobayashi, 1996]. Therefore, it was possible to obtain the mean undertow velocities, even within the boundary layer. The results of the free surface measurements are presented in table 7.

Cox and Kobayashi [1997] presented their own theoretical model and attempted to validate it with their measured results. However, they relied on a calibration coefficient

which they themselves showed to be highly sensitive. Moreover, they used measured values Q_s, H, and $\overline{\eta}$ (Table 7) in order to further increase the accuracy of their model. In our model, we use a minimal number of these measured values. Actual, the only values used, other than the bed slope and sediment diameter to scale roughness, is the average of the measured H normalized by water depth $\overline{h}$ and the time period of the waves. For example, the measured values of Q_s are ignored in favor of Stive and Wind's formulation for return flow, $\overline{U}_m$ (4.23). There is no calibration coefficient. The model is meant to be predictive and not rely on detailed information about the undertow in order to "predict" it.

Table 7. This table is from Cox and Kobayashi, 1997. The x value is a horizontal reference frame, H is the wave height measured, h is the mean still water depth, and Q_s is the return flow per unit width of the wave flume.

Station Number	X (cm)	H (cm)	$\overline{h}$ (cm)	$k\overline{h}$	$\overline{\eta}_{min}$ (cm)	$\overline{\eta}$ (cm)	Q_s (cm^2/s)
1	0	13.22	27.60	0.4982	-3.88	-0.30	-88
2	240	17.10	20.64	0.4265	-3.60	-0.44	-99
3	360	12.71	17.56	0.3917	-2.82	-0.05	-148
4	480	8.24	14.38	0.3529	-2.33	0.20	-114
5	600	7.08	11.51	0.3144	-1.60	0.75	-70
6	720	5.05	8.50	0.269	-0.82	1.13	-45

The procedure to calculate the wave height at the station depth is as follows. At station 2, breaking occurs. From the next set of points, stations 3 to 6, the ratio between H and $\overline{h}$ is calculated. The average is taken to be 0.62, and this value is then used to predict the wave height at any given depth, regardless of what the actual measured height was.

This assumption made certain calculations easier. Knowing the bed slope, one can analytically predict $\frac{dH^2}{dx}$ if one assumes that $H \propto h$ and therefore solve (4.26) in a relatively straight forward manner.

Since we are concerned mainly with the hydrodynamics within the surf zone, only the last four stations are used for comparative purposes. Figure 14 illustrates that the three inner surf zone stations are the most successful at predicting the structure of the flow field both within and outside the boundary layer. At the transition zone, the shear at the trough level seems to be overpredicted. One possible explanation for this is that the surf itself is not moving as a structured whole at this point in the breaking process, as suggested by Svendsen [1984]. Also, the assumption that the eddy viscosity is constant throughout depth may not be valid during the transition.

4.3.1 Sensitivity Analysis of Model

To see how changes in the near surface shear affect the structure of the velocity profile, a run was made using linear theory to calculate τ_{tr} and was compared to the semi-empirical equation (4.26) proposed by Svendsen [1984]. The results are shown in figure 15. This figure illustrates that indeed closer to the point of breaking, where presumably the surf has not structured itself sufficiently, linear theory without any correction factors does a better job at predicting the undertow structure.

The model's sensitivity to other parameters is also explored. Computer runs were performed with varying methods of calculating the average return velocity, $\overline{U}_m$. Figure 16

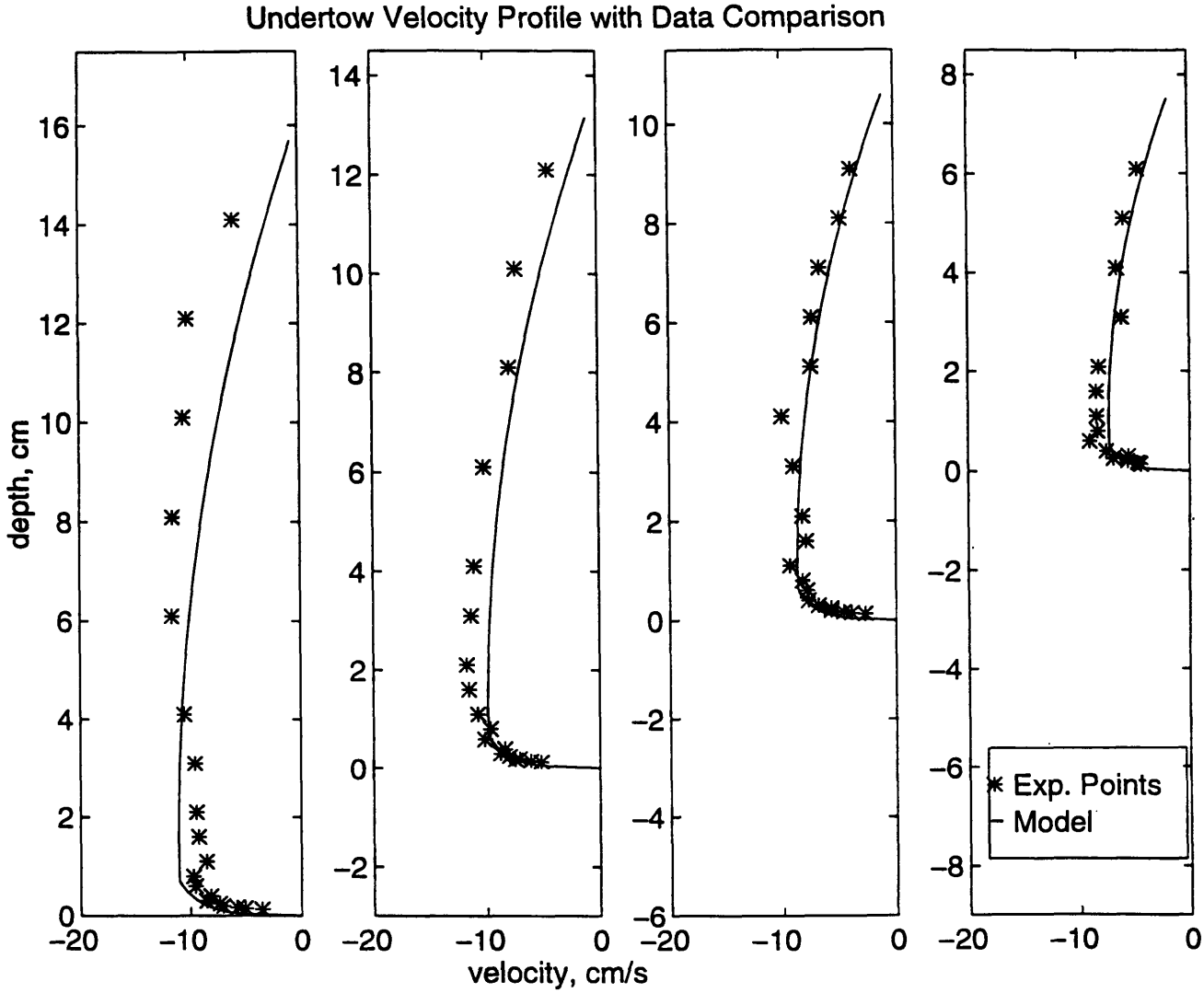

Figure 14. Comparison of undertow model with data from Cox and Kobayashi. (4.23) is used to predict $\overline{U}_m$, and (4.26) is used to predict τ_{tr}.

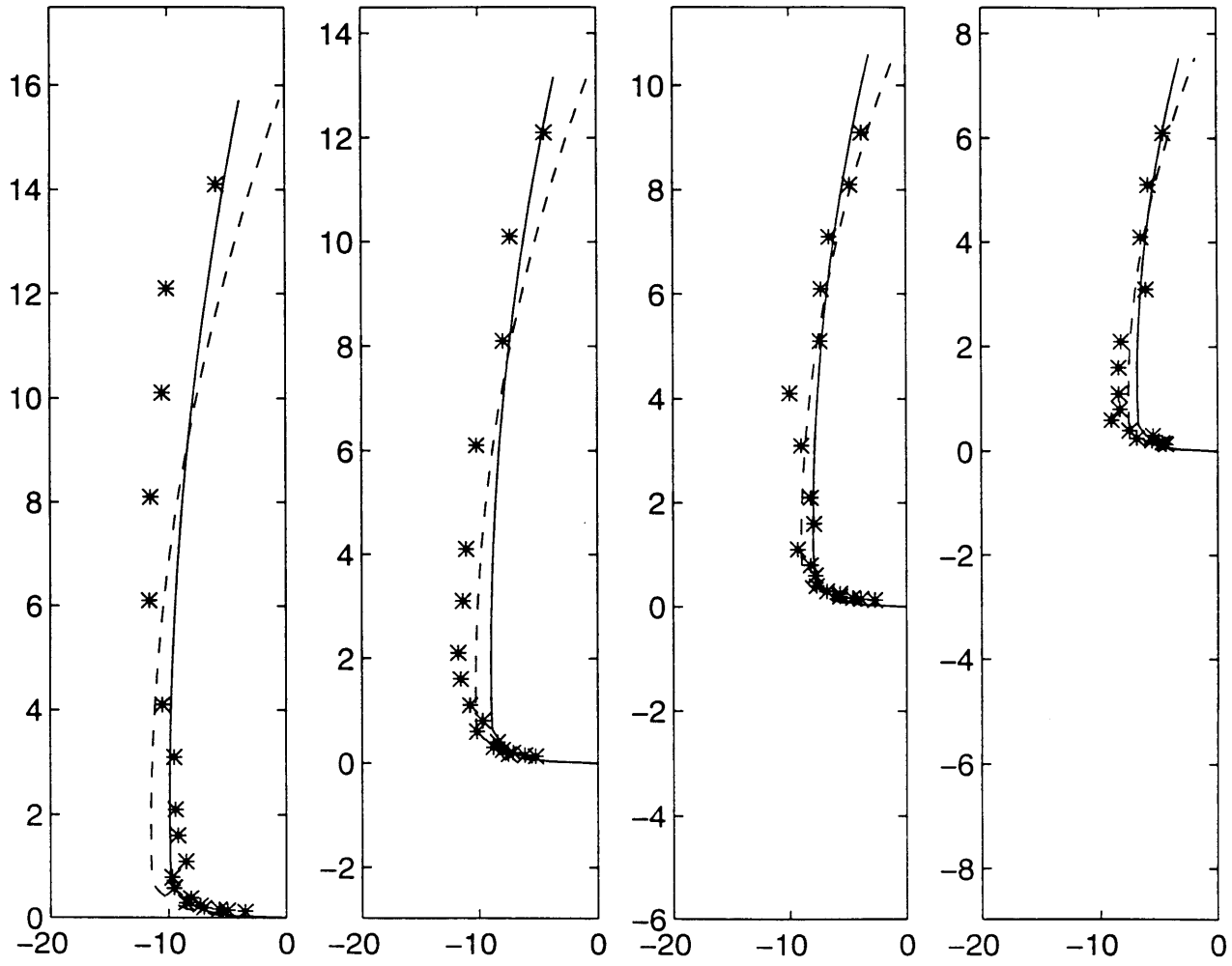

Figure 15. Sensitivity test of undertow model to variations in shear stress. The solid line (—) represents profiles generated using linear theory for the shear stress. The dashed line(---) represents the empirical relationship as presented by Stive and Wind. All other parameters used are the same as the ones used to generate figure 14.

shows results of profile variation when $\overline{U}_m$ is calculated with either Svendsen's formulation (4.24), Stive and Wind's formulation (4.23), or linear theory, (4.22). The shape factor, B_o, was estimated to be around 0.08, based on the recommendation of Svendsen [1984]. There is, it seems, little variation between the three methods. Equation (4.23) seems more effective at estimating the return flow for these sets of conditions in this particular experiment; increases in B_o would lead to satisfactory results if the use of equation (4.24) was preferred. Due to its simplicity, equation (4.23) was adopted for this particular model of the undertow. Linear theory clearly under-predicts the return flow. However, the measured return flow of -148.07cm^2/s within the transition zone (table 7) compares closely to the calculated return flow using linear theory (-150 cm^2/s).

It was also deemed important to look at how sensitive the vertical structure of the velocity was to the way wave attenuation was handled. Since our sediment transport model assumes that the wave height is linearly varying with depth, knowledge of the model's sensitivity to this propotionality constant was considered vital. So using the empirical equations for the return flow and the trough shear stress, the proportionality constant between wave height and water depth, $H = Kh$, was varied from 0.6 to 0.8. Results of this sensitivity test are shown in figure 17.

As one can see from the figure, with increasing values of K, the undertow becomes increasingly larger. Therefore, it can be inferred that an accurate rendering of wave attenuation is important in modeling the undertow. The gradient of wave heights, as well the quantitative value of the wave at any given depth, has a significant impact on both the return velocity $\overline{U}_m$ and the near surface shear, τ_{tr}. The more accurate the predictions of wave attenuation in the surf zone, the greater confidence we have in our undertow model.

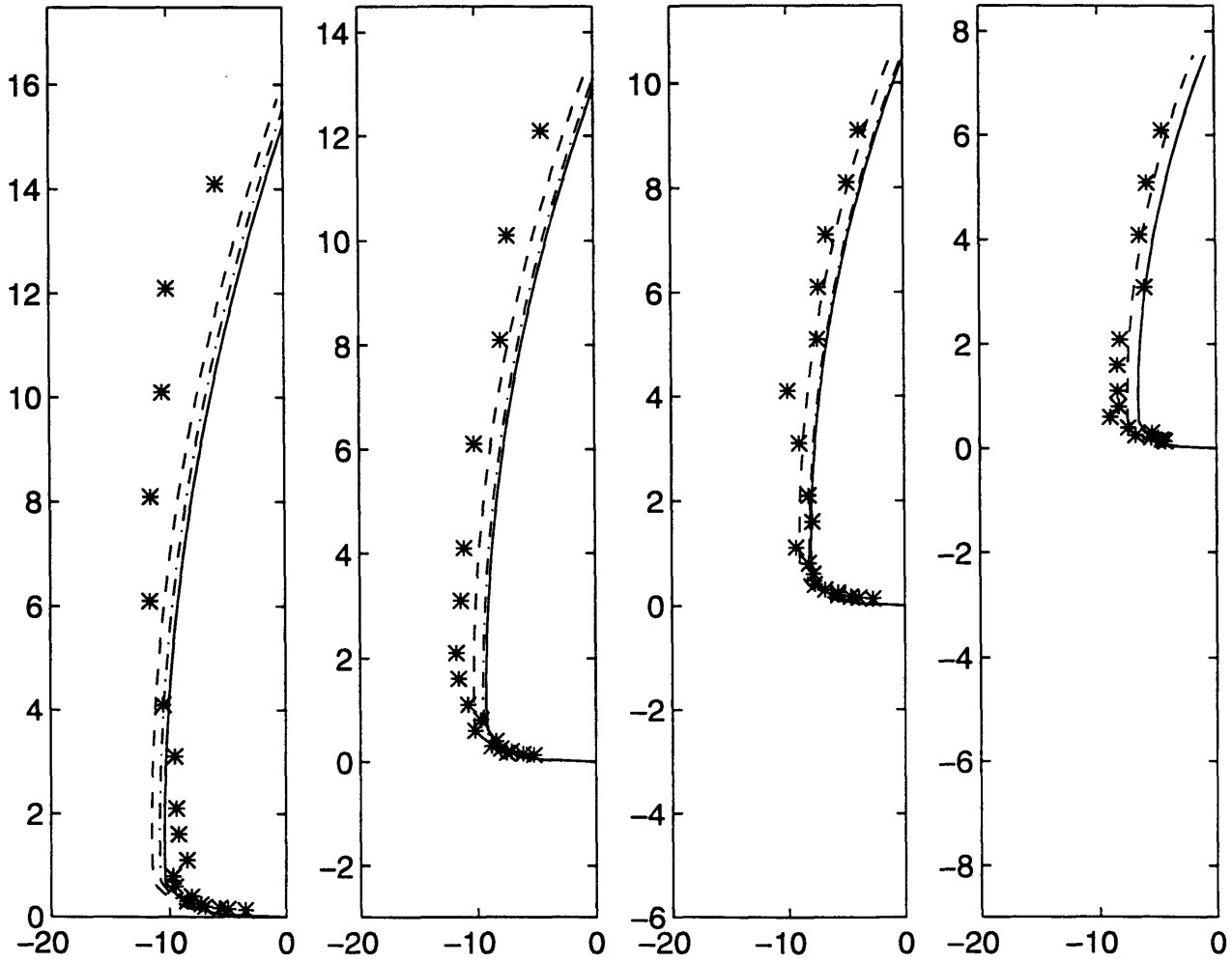

Figure 16. Sensitivity test of undertow model to variations in the mean return flow. The solid line (—) represents profiles generated with linear theory used to calculate the mean return flow. The dashed lines (---) represents profiles that used Svendsen's formulation. The dashed-dotted profile (- -) used Stive and Wind's formulation. All other parameters used are the same as the ones used to generate figure 14.

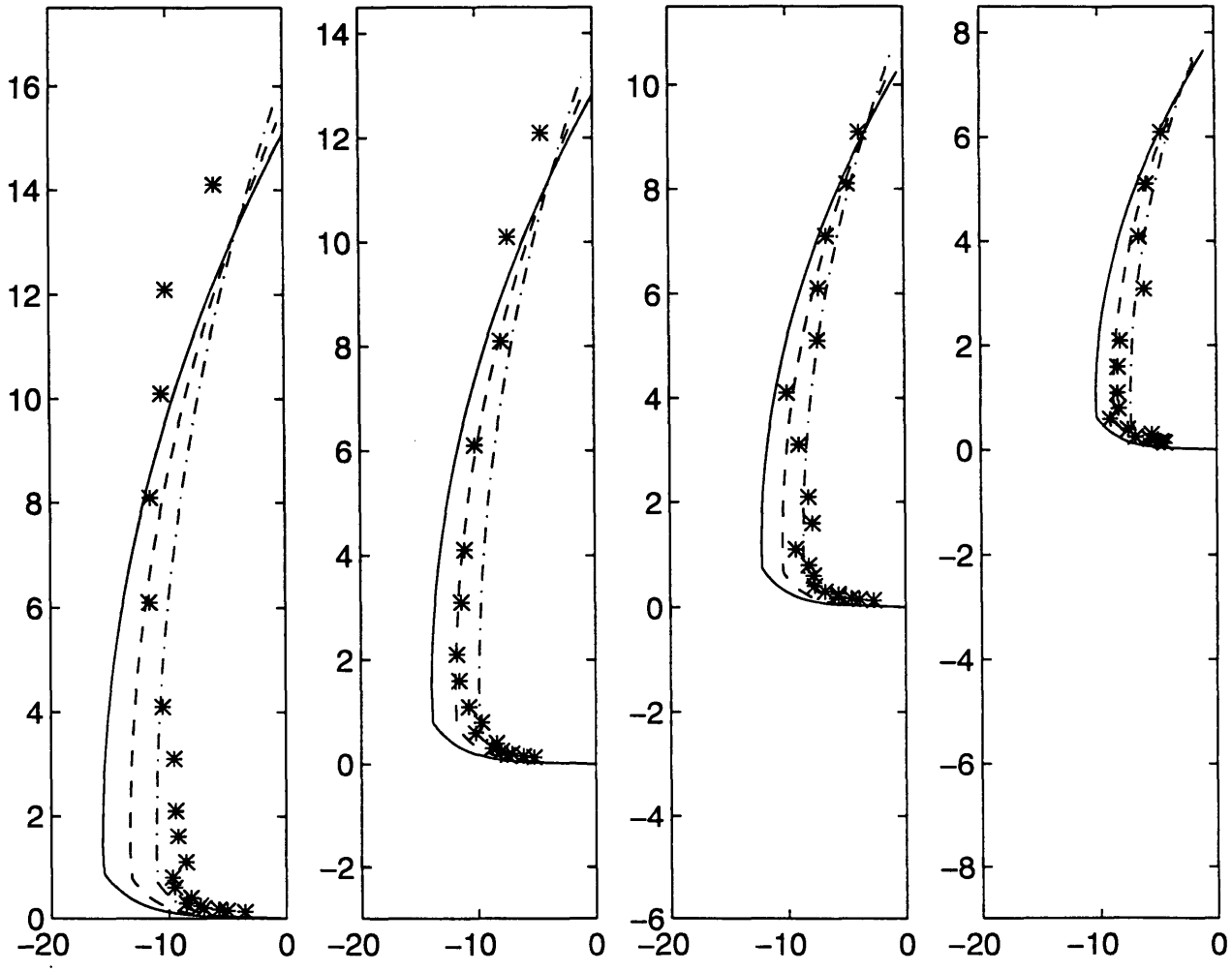

Figure 17. Sensitivity test of undertow model to variations in the way wave height is modeled. For $H = Kh$, the solid profile (—) is generated with the proportionality constant $K = 0.8$; the dashed line (---) is with $K = 0.7$; the dashed-dotted line (- -) is with $K = 0.6$. All other parameters used are similar to the ones used to generate figure 14.

4.3.2 Additional Comments and Comparisons

Another test was carried out on experimental data presented by Buhr-Hansen and Svendsen [1984]. In their test, wave heights and water depths were measured at each of the four stations presented in Table 8. In addition to the bottom slope (1/34), wave period (2.2 s), and an estimated bottom roughness of 0.1mm (smooth bottom, see Svendsen et al. [1987]) we used only known wave height to depth ratios, K, with an average value of $H = 0.73h$ within the surf zone. The undertow profiles were calculated. The solution is compared to measured results in figure 18. It seems that similar trends to those seen in the comparison with Cox and Kobayashi's data are noticed here. The shear near the surface close to the point of breaking is over-predicted resulting in discrepancies between our model and the measured data. Otherwise, the model does a fair job at predicting the undertow .

Table 8. Select measured numerical values of parameters from Buhr-Hansen and Svendsen [1984] experiments. The bed slope was 1/34 and the wave period 2.2 *s*.

X (m)	H (m)	h(m)	H/h
22.00	0.116	0.145	0.80
23.00	0.087	0.120	0.73
23.87	0.072	0.101	0.71
24.50	0.058	0.086	0.67

A little more needs to be said concerning modeling wave attenuation. As seen in figure 17, an over-prediction of the wave height gives rise to a considerably exaggerated undertow. But the problem does not stop here. A greater wave height means a greater

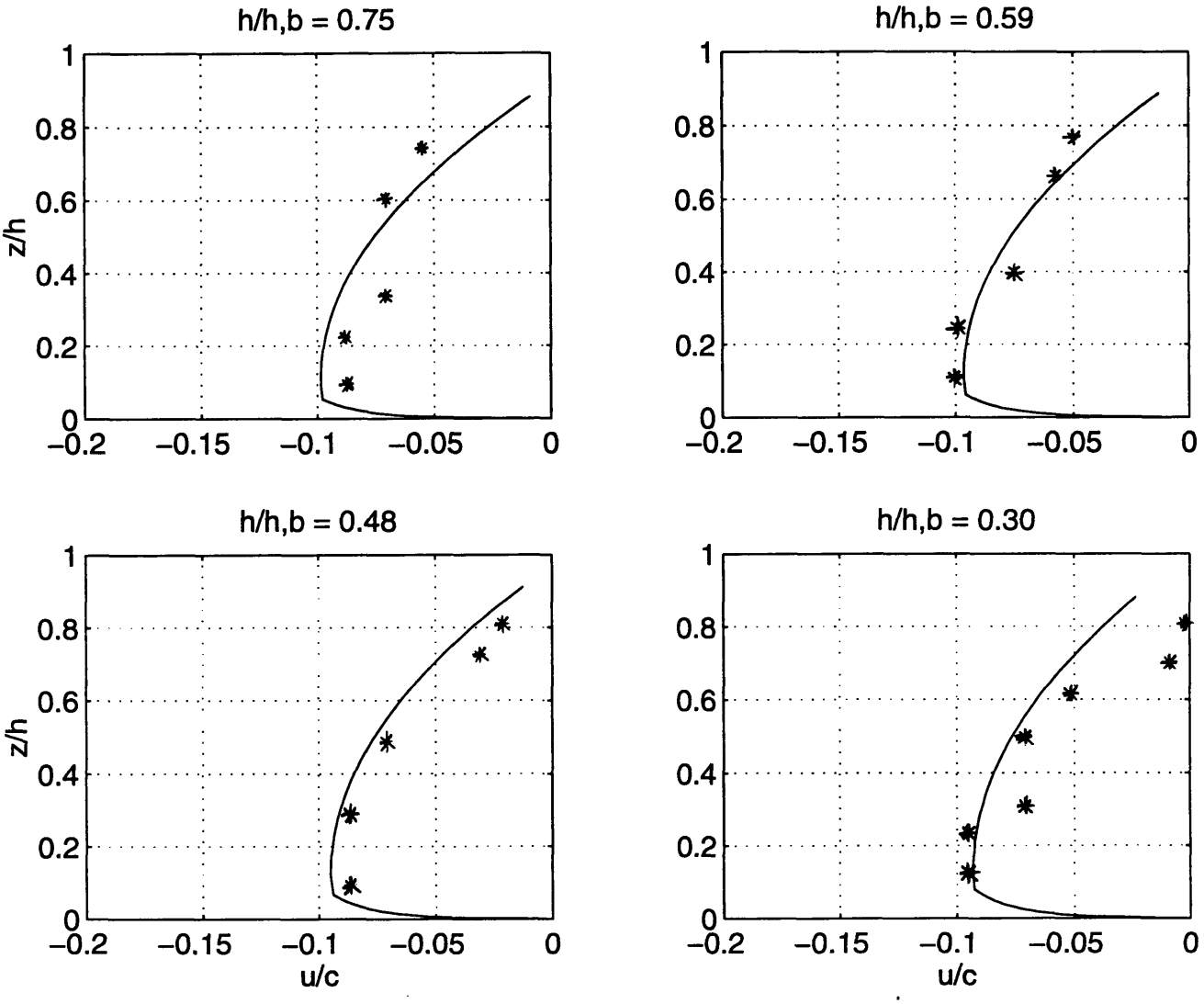

Figure 18. Comparison of undertow model to data from Buhr-Hansen and Svendsen. The bed slope was 1/34, the wave period was 2.2 s.

shear stress near the bottom which, in turn, creates more suspended sediment. Combining that fact with an over-predicted undertow current, the overall suspended load will be increased that much more. Hence, careful attention must be given to how wave attenuation is modeled. More will be written later on this subject (Chapter 5).

Our results indicate that the model is effective at predicting the undertow both inside and outside the boundary layer provided an accurate predictor of wave attenuation in the surf zone is available. It is recommended that τ_{tr} be calculated using the empirical formulation (4.26) and that $\overline{U}_m$ be calculated using Stive and Wind's formulation (4.23). The empirical formulation for the eddy viscosity outside the boundary layer (4.21) seems to do a good job within the inner surf zone and for lack of any alternative, this equation is recommended.

Chapter 5

5 Modified Model for Surf Zone Application

5.1 The Suspended Sediment Distribution

The sediment concentration profile can be described now by solving equation (4.3). Since the eddy viscosity term within the boundary layer is estimated differently from the eddy viscosity term outside the boundary layer, two solutions pertaining to the concentration distribution are necessary. Inside the boundary layer, where the boundary layer thickness is defined as $y = \delta$, and where $\nu_t = \kappa u_{*m} z$, the resulting concentration distribution is

$$C = \overline{C}_R \left(\frac{y}{Z_R} \right)^{\frac{-w_f}{0.4u_{*m}}} \quad \text{for } y < \delta \tag{5.1}$$

δ is given by (4.28); u_{*m} is the combined wave-current shear velocity and is estimated as the first harmonic shear stress (2.21), the same value used to calculate the undertow; and the reference concentration is given by equation (4.8). Outside the boundary layer, the

eddy viscosity is constant and given by equation (4.21). The solution to equation (4.3) is therefore:

$$C = C_R \left(\frac{\delta}{Z_R} \right)^{\frac{-w_f}{0.4u_{*m}}} \exp\left\{ -\frac{w_f}{\nu_t}(y-\delta) \right\} \text{ for y} > \delta \tag{5.2}$$

The integration

$$q_{ss} = \int_{Z_R}^{h} \overline{C}U dy \tag{5.3}$$

can now be done numerically. Note that U for $y < \delta$ is given by (4.27) and for $y > \delta$, U is given by equation (4.20). The transport mechanism is always offshore. The average suspended load over one wave period is obtained and then added to the bedload.

5.2 The Complete Modified Model

Following a similar methodology as used in Chapter 3, the average net transport was found at each depth in the surf zone. The slope of the bed is then adjusted until the net transport is zero.

$$q_s = \sum q_{sb,net} + \sum q_{ss,net} = 0 \tag{5.4}$$

Input values for the computer are the same as those outlined in Chapter 3. They include the angles of friction, deepwater wave height, wave period and mean sediment diameter. The waves are assumed to be periodic. The wave is shoaled to a depth in which Cnoidal theory is valid (U > 26), at which point the transport model is initiated and the slope of the bed is calculated. The bedload model is used exclusively up to the point of breaking. The wave breaks at $H_b = 0.78h_b$ and the wave height then remains at that ratio for all depths shallower. However, at the point of breaking and shoreward, it is assumed

that an undertow is present. This undertow is the offshore transport mechanism for suspended sediment, and these two coupled gives us an offshore suspended load. Clearly there is a discontinuity between the point just before the point of breaking and just after. Although this sudden appearance of an undertow is of some concern, for modeling purposes it was decided that as a first approximation this approach would suffice.

The wave characteristics at any local depth, namely $\eta(t)$, $u(t)$, and $\tau_b(t)$, were calculated depending on user input values. For any depth, these calculated characteristics remain constant regardless of bed slope. The undertow, on the other hand, does not remain constant at any given depth regardless of bed slope. This is because the near surface shear, τ_{tr}, depends on the rate of change of wave height. Since $H \propto h$, τ_{tr} must then be dependent on the rate of change of the bed slope. Therefore, input values into the undertow algorithm are the wave characteristics and an assumed bed slope.

The model, shoreward from the point of breaking, calculates both bedload, using the wave characteristics, and suspended load, using undertow characteristics. The solutions are added and averaged over one wave period. If the resultant sediment transport is onshore, the slope is increased and the undertow, net bedload transport and reference concentration are recalculated (or vice versa). This continues until the slope at any particular depth results in zero net transport.

The way the equilibrium beach profile is generated is identical to the way it was described in Chapter 3. Beginning at the depth in which the transport functions are called, the equilibrium slope is calculated as just described. Decreasing the depth by some arbitrary increment, the process is repeated until an extensive list of depths and respective

slopes are found. Slopes between two depths are averaged and the horizontal distance between them is then calculated. The profile is then plotted using this information.

5.3 Results of Model in Surf Zone

The program was run under a variety of wave conditions. It became immediately apparent that the decision to model wave energy dissipation in the surf zone, namely $H \propto h$, was inadequate. For larger wave heights or fine sediment diameters, the offshore suspended transport of the undertow dominated the onshore bedload transport at slopes of $\beta = 0$, requiring that the slope be negative for a zero net sediment transport rate. Since any increase of water depth would then increase our wave height, an obvious violation of the basic thermodynamic principles results.

5.3.1 General Results

Solutions can however be obtained for sufficiently small wave heights and wave periods. Results presented here attempt to mimic those in Chapter 3, but can not be comprehensive due to the limitations imposed by the way wave attenuation is modeled.

Figure 19 shows the variation of our complete equilibrium beach profile (EBP) with a variation of sediment diameter. For small sediment diameters, we run into the problem mentioned above: within the surf zone region, a dominant offshore suspended load makes finding a continuous beach profile impossible with the present formulation. Hence we stick to sediment diameters that result in valid results, those being 0.2 *mm*,

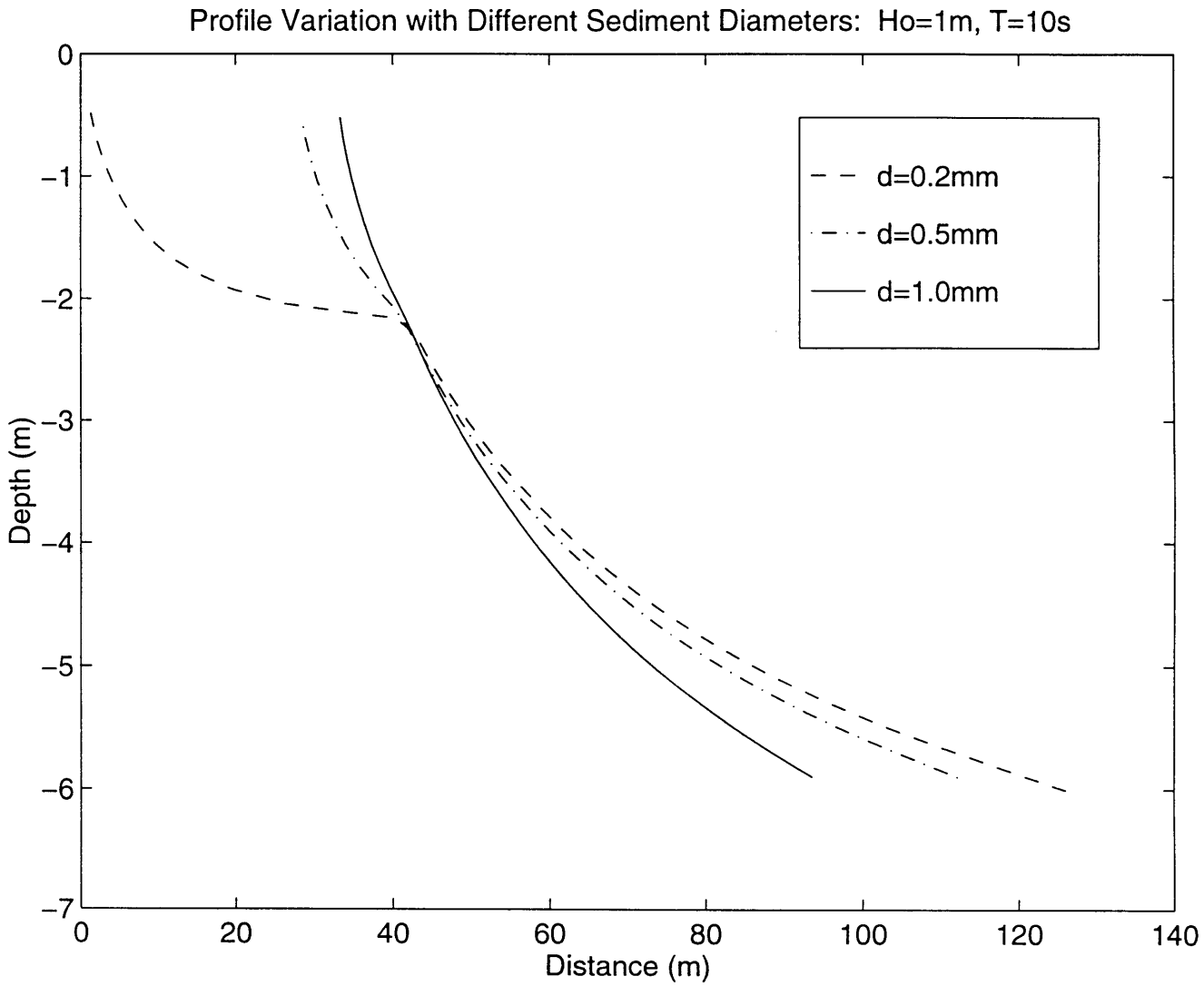

Figure 19. Equilibrium beach profile modeled for both inside and outside the surf zone. This figure looks at the variation of the model for changes in sediment diameters.

0.5 *mm*, and 1 *mm*. Unlike any other EBP, we have "hinged" the profile at the point of breaking for illustrative purposes.

Figure 19 clearly illustrates a distinct change in slope right at the point of breaking for slopes with a sediment diameter of 0.2 *mm*. This bar crest is a naturally occurring phenomenon. Figure 19 also demonstrates that with larger sediment diameters a steeper equilibrium beach slope results. As mentioned in Chapter 3, these results parallel those found in nature. Also, it is found in nature that sediments with coarser diameters are transported shorewards, while smaller sediments are transported offshore. By studying figure 19, this trend can be deduced. Examine the middle profile with $d = 0.5$ *mm* at a depth of 1.5 *m*. For smaller sediment sizes, ie. the profile with $d = 0.2$ *mm*, it is seen that the slope is gentler than the 0.5 *mm* slope at this depth. Therefore, if sediments of size 0.2 *mm* were found on a 0.5 *mm* slope, the slope would be too steep to maintain equilibrium and the 0.2 *mm* sediment will be transported offshore. By the same argument, it can be shown that coarser sediment will be transported onshore.

Changes along the shore-rise beach segment are minimal as seen in figure 19. Here, changes in the slope can be explained by examining the difference between the bottom shear stress and the critical shear stress in the bedload formulation. This difference we will define as the net resultant shear stress. Under the crest, the difference between these values is large and any minor change in the critical shear stress will not proportionally affect the net shear stress by any great amount. However, under the trough, since the absolute values are closer together, any change in the critical shear will result in a significant proportional change. So for coarser sediments, there will be a proportionally larger change in the net shear under the trough than under the crest. This will cause a net

onshore transport. For finer sediments, by the same logic, there will be an offshore transport.

However, it is within the breaker zone that we see the greatest changes. These changes are clearly related to suspended offshore transport. Once the wave breaks, an undertow current is induced. Smaller sediment diameters result in more suspended sediment and therefore a greater offshore suspended load. This essentially causes erosion, resulting in a gentler beach slope. Gentler slopes, of course, reduce the shear stress at the trough level causing less of an undertow. It is inferred from figure 19 that a significant amount of fine sediments is suspended such that even with a reduced undertow, a gentler slope is necessary for equilibrium. For coarser sediments, there is less suspended offshore transport and therefore less erosion. The slope will remain steep. Steeper slopes result in stronger undertows. But it can be inferred from figure 19 that even with a stronger undertow, the suspended load is still small such that there is minimal change in beach slope at the point of breaking. For a beach with mixed sediment, we would then expect that the fine sediments be transported offshore predominantly by the undertow current while the coarser ones would remain behind or perhaps even be transported shorewards due to bedload. Clearly, EBPs within the surf zone are very responsive to sediment diameter.

Figure 20 shows the variation of beach profiles with changing wave heights. As one can see, larger wave heights result in gentler beach slopes. Deep-water wave heights input to the computer program were 0.7 *m*, 1.0 *m*, and 1.3 *m*. Results involving wave heights larger than 1.3 *m* were not possible due to the generation of significant suspended sediment at the point of breaking. A bar crest is again seen at the point of breaking for

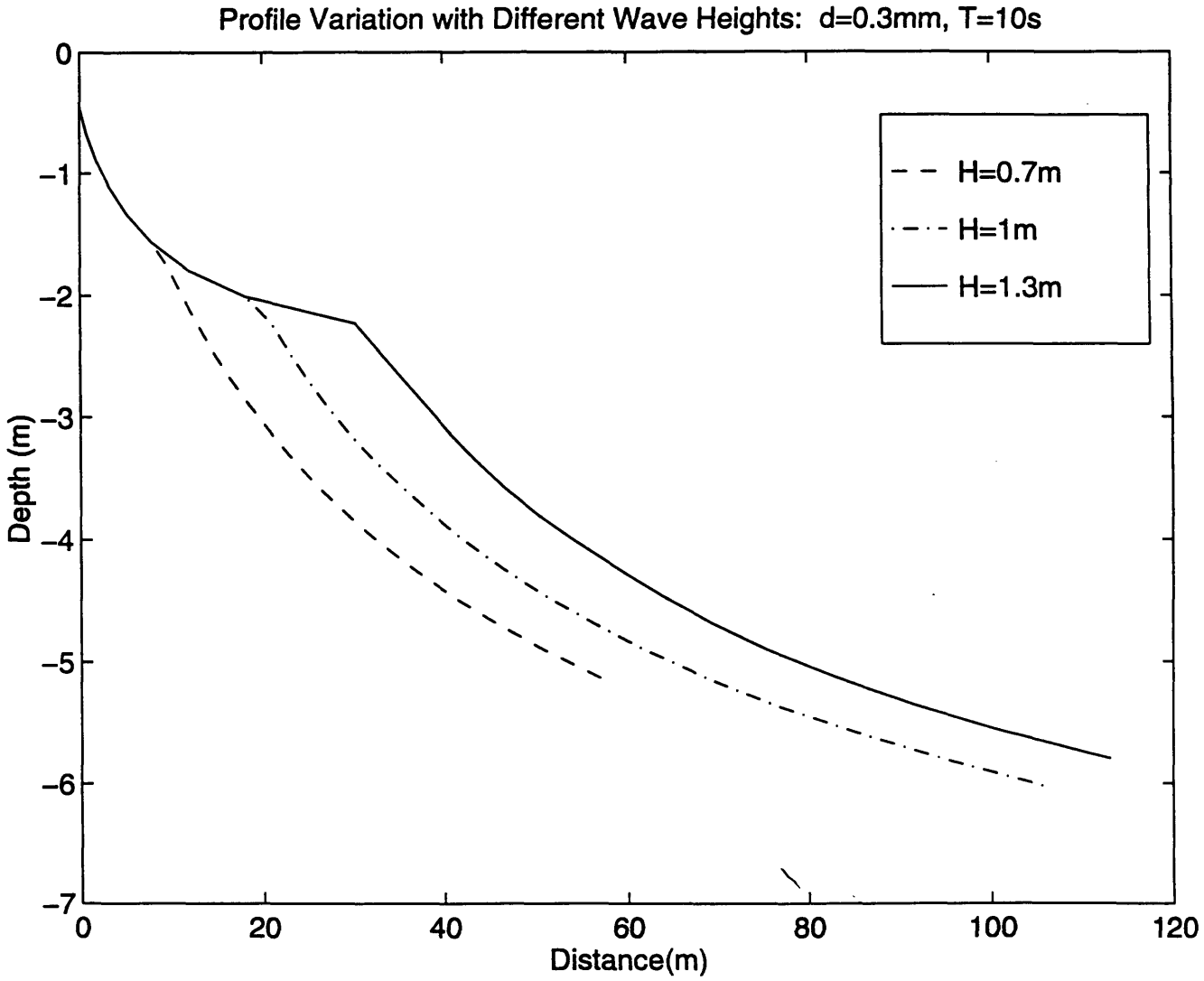

Figure 20. Equilibrium beach profile modeled for both inside and outside the surf zone. This figure looks at the variation of the model for changes in deep-water wave heights.

each wave, and it is also interesting to note that the beach profiles within the surf zone all merge into the same line. The reasons for this is that once the wave breaks we assume that the wave is proportional to water depth. Hence, at a depth of 1.5 m, an initially larger wave (ie. H_o = 1.3 m) will be the same height as an initially smaller wave (ie. H_o = 0.7 m). So at that depth, the wave climates are identical.

At first glance, figure 20 appears to indicate that smaller wave heights will cause greater erosion. However, this appearance is deceiving since we have "hinged" our profiles at the MSL. The proper interpretation is as follows. Look at the profile generated by H_o = 1.0 m at the point of breaking (the bar crest). If one were to slide the other two EBP so that the profiles more or less overlapped on the shore-rise segment, it is then easily seen that larger waves will erode the beach at that point while smaller waves will cause accretion. If one were to refer back to chapter 4, it is clear that larger wave heights create stronger undertow currents and generate larger suspended sediment concentration. So a profile generated with H_o = 1 m will be eroded by larger waves since they break in deeper water and create a stronger undertow at a deeper depth.

Dean [1994] states that beach slopes subject to steeper waves tend to have gentler slopes. Since Dean's model attempts to describe the whole beach profile, by visually examining figure 20 it is seen that the average slope of the whole profile, measured from the MSL to the deepest portion, is gentler for larger waves.

Figure 21 illustrates changes in the EBP with varying wave periods. A noticeable bar crest is seen for each profile, and it is obvious from the figure that longer waves create steeper slopes. What are the implications? The figure seems to indicate that longer

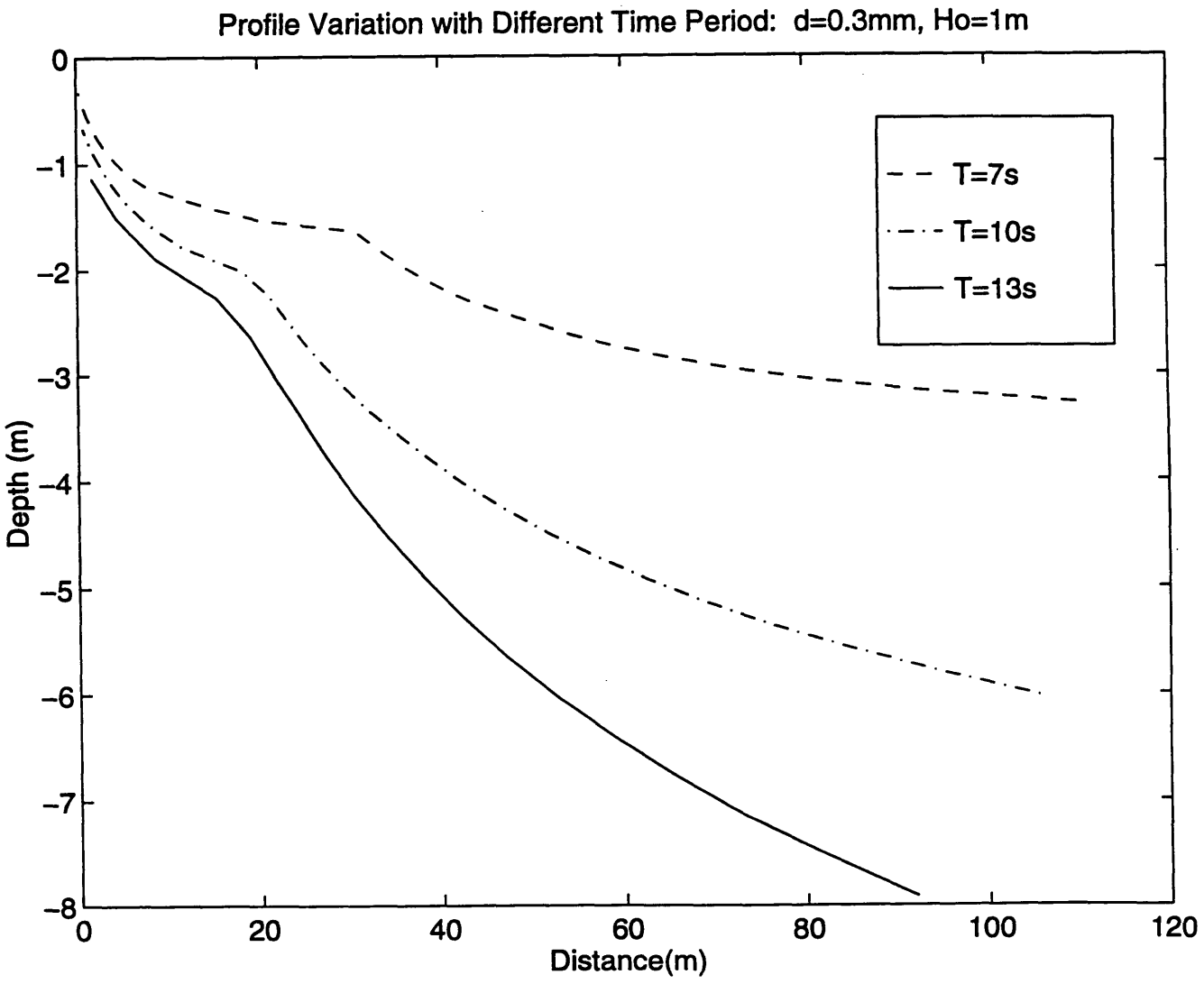

Figure 21. Equilibrium beach profile modeled for both inside and outside the surf zone. This figure looks at the variation of the model for changes in wave period.

waves create greater erosion. But again, because we have "hinged" the profile at the MSL, one must be careful in interpreting the figure.

Consider the profile that has a period of 10 *s* at a depth of 1.5 *m*. If the other two profiles were shifted so that they all match at 1.5 *m*, then it obvious that at that depth the slope for the 13 *s* profile is steeper, and for the 7 *s* profile it is gentler. It becomes now apparent that if a 13 *s* wave was run over this profile, the slope would be too gentle for equilibrium and sediment would be transported shorewards. The reverse would be true for a 7 *s* wave.

Sediment is transported shoreward for longer waves because longer waves are more nonlinear at any given depth. Greater wave nonlinearity translates into a greater shear stress under the crest than under the trough causing more onshore transport. The generated profiles seen in figure 21 simply reflect the slopes necessary to balance out this nonlinearity.

A final note concerning figure 21 is that EBP generated by this model are extremely sensitive to wave period. Any prediction of EBP using the model presented here must take extreme care in specifying the wave period.

5.3.2 Comparison with Empirical Curve-Fitting Lines

Dean suggests that equibilibrium beach profiles be of the form $y = Ah^{2/3}$ where A is a sediment scale parameter [Dean, 1991]. Dean's empirical curve-fitting methodology was predominately applied to the near-shore segment of the beach profile. In Chapter 3,

results obtained there were valid for the shore-rise segment and hence the applicability of Dean's model was suspect.

However, we now compare the complete model to Dean's curve-fitting methodology. Dean's profile has its origin at the MSL and from figure 22, it can be seen that for sediment diameters of 0.3 *mm*, the parameter *A* is to be of the order 0.3 $m^{1/3}$. We have chosen three values of *A*, 0.25, 0.30 and 0.35 and have shifted our generated profiles in the horizontal plane so that a more visual comparison with Dean's model is possible. Ideally, one should use similar wave parameters used to generate figure 10 in Chapter 3. As mentioned, such large wave heights are not possible with the present treatment of wave attenuation. Instead, the wave parameters used are identical to those in figure 20. This comparison is shown in figure 23.

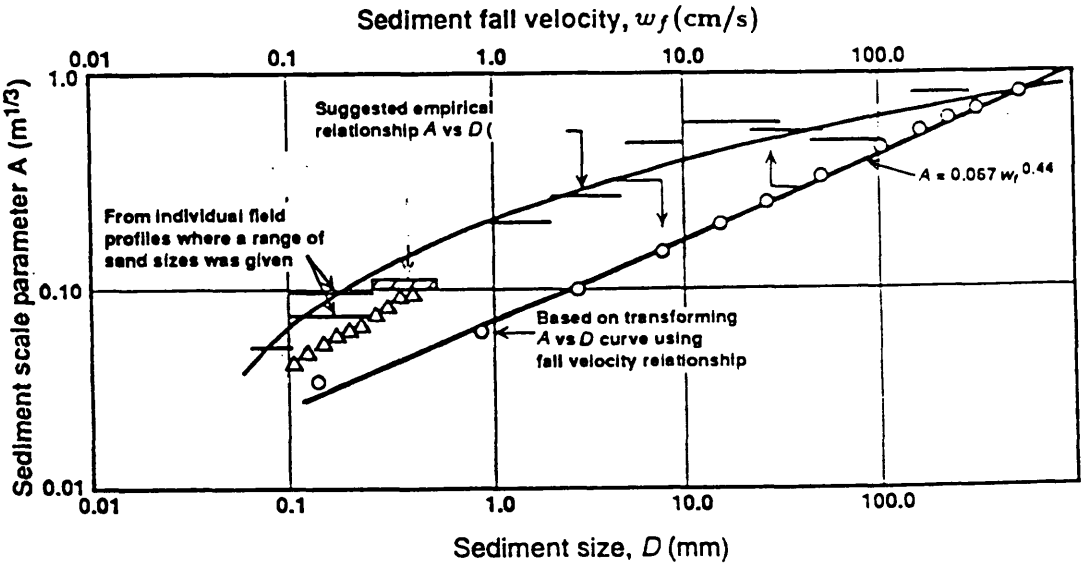

Figure 22. Variation of sediment scale parameter, *A*, with sediment size, *d*, and fall velocity, w_f. [Dean, 1991]

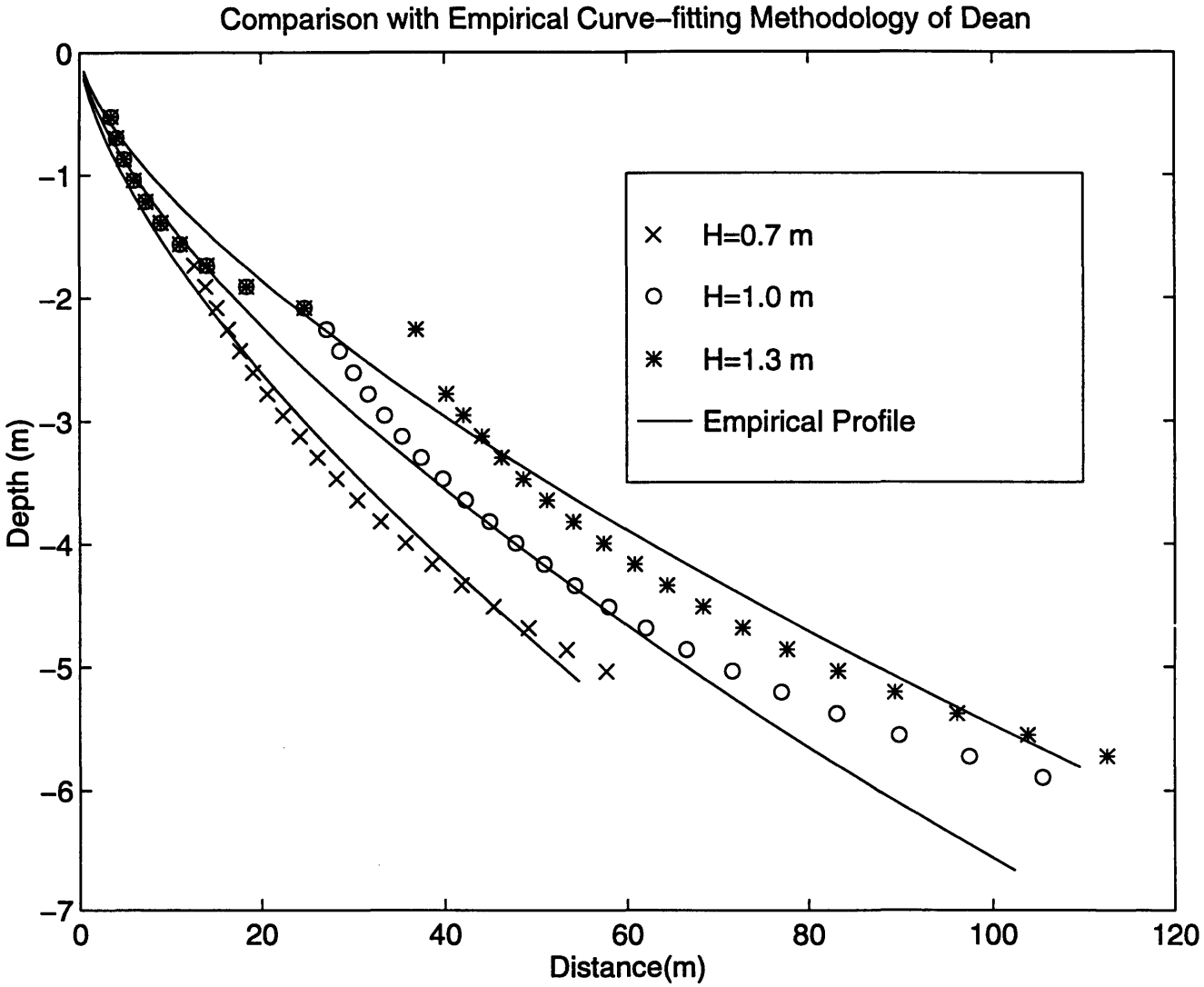

Figure 23. Comparison with Dean's Curve-Fitting methodology, $h = Ax^{2/3}$, where the three lines are generated with $A = 0.25$, 0.30 and 0.35. $A = 0.25$ is the shallowest line. The model profiles are generated assuming a sediment diameter of 0.3 *mm* and $T = 10$ *s*.

As one can see in figure 23, the comparison between Dean's empirical curve-fitting methodology and the theoretical model presented is poor in some respects, but good in others. The poor comparison is partly due to the simplicity of Dean's empirical model and partly due to the limitations of our own theoretical model. Dean's model cannot account for the bar crest, nor does is suggest any change due to variation of deepwater wave characteristics. On the other hand, our model does not take into consideration tidal fluctuations or swash-zone wave dynamics. For the good comparison, by offsetting the generated profiles' horizontal origin from the empirical model's origin as we did in figure 23, the general trend of the whole empirical EBP is captured very well by the generated EBP. Considering the inherent limitations of Dean's empirical model and the inadequacies of this model, these results are encouraging. However, it should be noted that beach forms may be dominated by larger waves than those modeled here so these results should be viewed in that context.

A comparison of our model with Inman et al. [1993] is also carried out with Inman et al. basic curve-fitting parameters for both outside and inside the surf zone. As mentioned earlier, the wave parameters used for figure 10 could not be used. Again, comparisons are made with the use of the parameters from figure 20 and is seen in figure 24. For the shore-rise beach segment, as we discussed in Chapter 3, the origin is at the MSL and the parameters for the empirical equation $h = Ax^m$ are $A = 1.16$ and $m = 0.38$. For the bar-berm, the basic data set had values of $A = 0.86$ and $m = 0.41$ where the point of origin is at a height of Z_l, which is considerably higher than the MSL, as shown by the definition sketch, figure 9. Z_l has a typical range of 3 to 4 m. Here we use $Z_l = 3.0$ m.

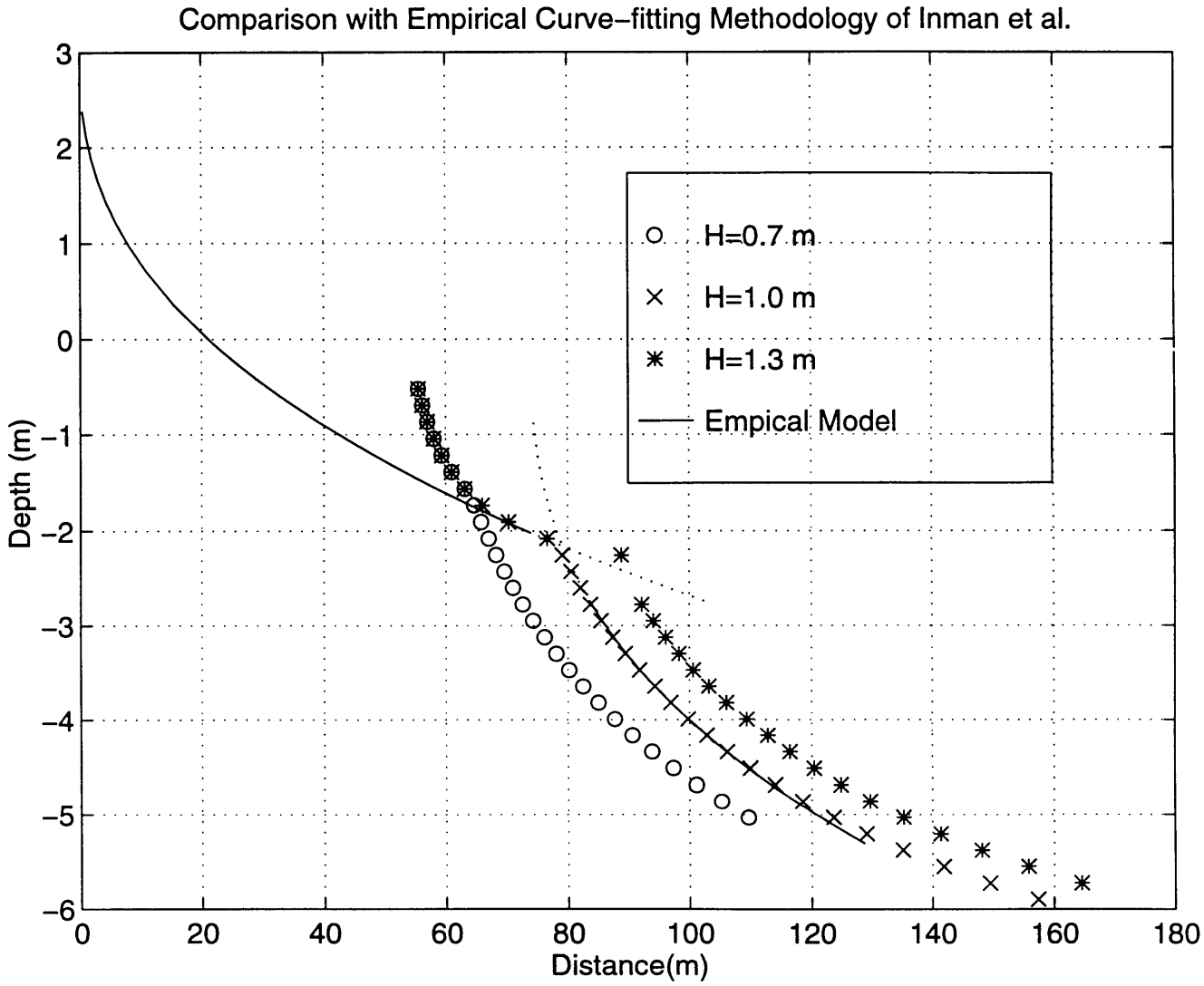

Figure 24. Comparison of Model with Inman et al. Curve-Fitting Methodology, $h = Ax^m$. The shore rise segment is generated using Inman's et al. basic data set, as is the bar-berm profiles. The origin for the bar-berm section is set at 3 *m* above the MSL. The model assumes a sediment diameter of 0.3 *mm* and $T = 10$ s. The shore-rise segment was moved along the horizontal until a visual comparison was possible with the $H_o = 1$ *m* profile.

The horizontal axis for the modeled profiles were adjusted until a visual comparison was possible. The shore-rise segment was placed to allow for a comparison with profiles generated by $H_o = 1\ m$. If one were to move the empirical shore-rise segment along the horizontal until a visual comparison was possible with the other profiles ($H_o = 0.7\ m$, $H_o = 1.3\ m$), it can be seen that there is a good comparison to these other shore-rise segments as well. It is noted here that according to Inman et al., the break-point bar was found in depths typically greater than 2 m. Wave heights greater than $H_o = 1.3\ m$

As opposed to a complete and comprehensive comparison between Inman's et al. empirical model and our model as was done for the shore-rise segment in Chapter 3, a purely visual comparison between the two models is deemed sufficient at this point for two reasons. First, as one can see from the computer generated profiles, the bar-berm appears as if it wants to curve up to the MSL with an infinite slope whereas the origin for the empirical curve-fitting methodology requires that it be a few meters above this point. This naturally creates a large discrepancy between our model and the empirical relationship. Hence, any meaningful discussion concerning the variation of the parameters A and m with varying wave conditions and how they compare to our generated profiles may be a little premature. Secondly, due to the problematic nature of creating too large of an offshore suspended load for certain conditions makes it impossible to create a wide variety of beach profiles with wave conditions and sediment diameter sizes that mimic those found on the beaches studied by Inman et al.

Regardless, it can be said that the generated profiles just shoreward of the breaking point have slopes that are comparable to the empirical profile. Closer to shore this comparison quickly breaks down. Other than that, there is fairly poor agreement between

the empirical and modeled EBP within the surf zone. However, as seen in Chapter 3, the shore-rise segment is still modeled quite well by our present model.

5.3 Model Limitations and Sensitivities

It is clear that the present model is limited. Some of the limitations of our model have already been mentioned. There is no swash zone model. The interaction between waves and a moveable bed in the swash zone region may be considerably different than what has been modeled here. Also, tidal fluctuations, which can have a range of over 3 *m*, have not be modeled. One may suggest that a beach segment subject to intermittent dry and immersed periods (i.e. at depths less than 1 *m*) should not be modeled as if it is constantly underwater. And there are problems associated with the way wave attenuation is modeled.

In addition to these limitations, the model is sensitive to certain parameters, namely those parameters that are critical in calculating the suspended load. Since the bedload transport is oscillatory, pertinent parameters have little error effect on the total net transport rate. This is due to the fact that an error affecting shoreward transport will most likely be balanced out by the same error in the seaward direction. However, for suspended sediments, the transport mechanism is in only one direction. Therefore, errors associated with the suspended concentration distribution, with the velocity distribution, or even with bedload directly affect the equilibrium beach profile.

This is illustrated by varying $\overline{C}_R$ by a factor of 0.5 to 1.5 shown in figure 25. As one can see, adjustment of this parameter causes a noticeable change in the exhibition of a bar crest as well as the overall slope of the profile within the surf zone. There is also

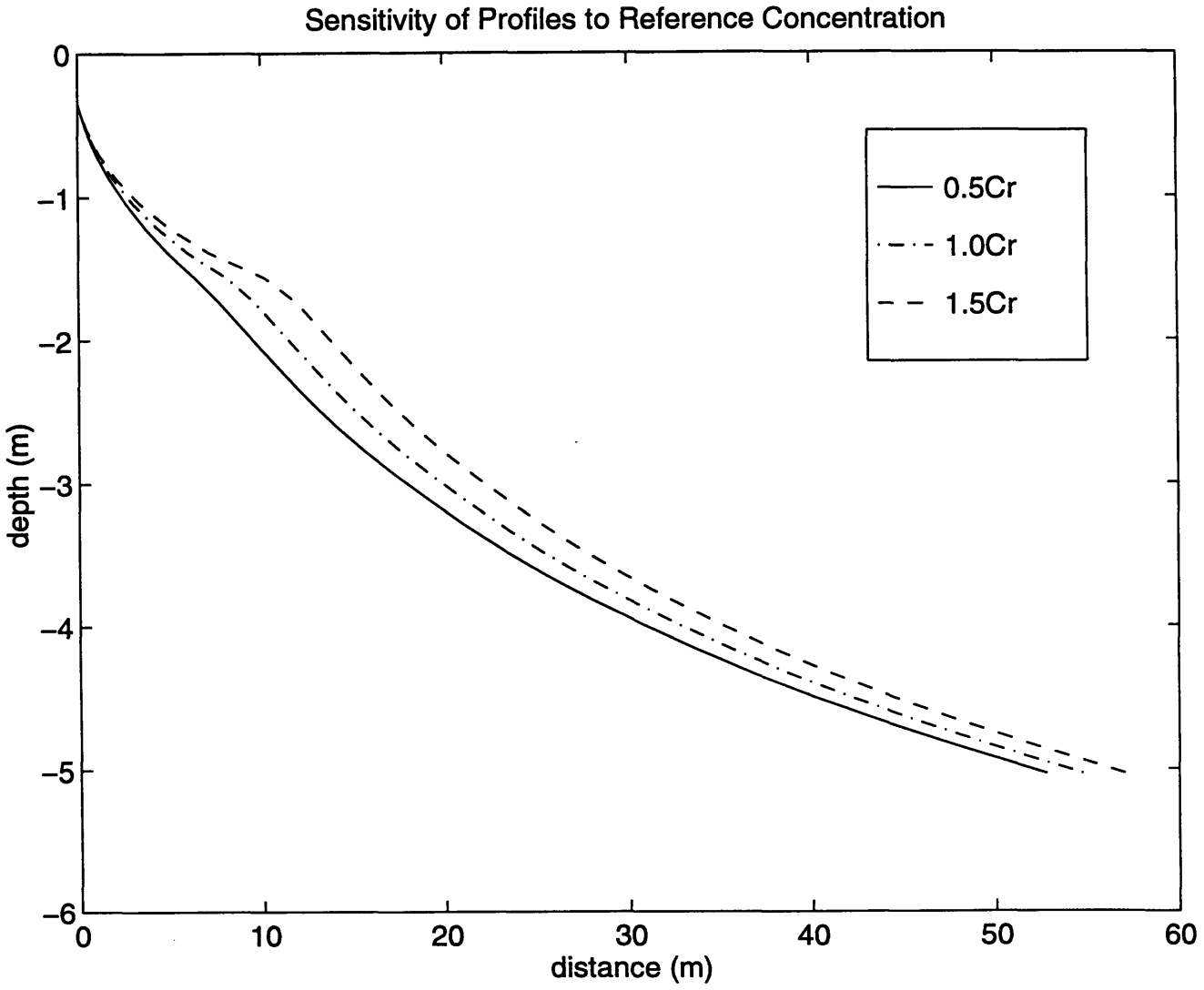

Figure 25. Sensitivity of the equilibrium beach profile to $\overline{C}_R$. Wave parameters and beach characteristics used are $H_o = 0.7\ m$, $T = 10\ s$, and $d = 0.3\ mm$.

sensitivity associated with the maximum wave-current shear velocity, u_{*1m}, used to calculate the eddy viscosity in equations (5.1) and (5.2). The sensitivity of this parameter is shown in figure 26. Again, variations in this parameter can cause noticeable changes in the profile, this even more so than the reference concentration. This is of course not surprising since $\overline{C}_R$ increases with u_{*1m}^2. Although the sensitivities associated with these two parameters are not so great to call in question the applicability of the model, care must be taken in how one specifies these parameters. With a more complete model, a thorough evaluation of these parameters is warranted.

Of course, the greatest sensitivity our EBP model is its sensitivity to wave period. As seen in figure 21, minor variations in wave period create large changes in the EBP. One must be very careful in specifying the wave period.

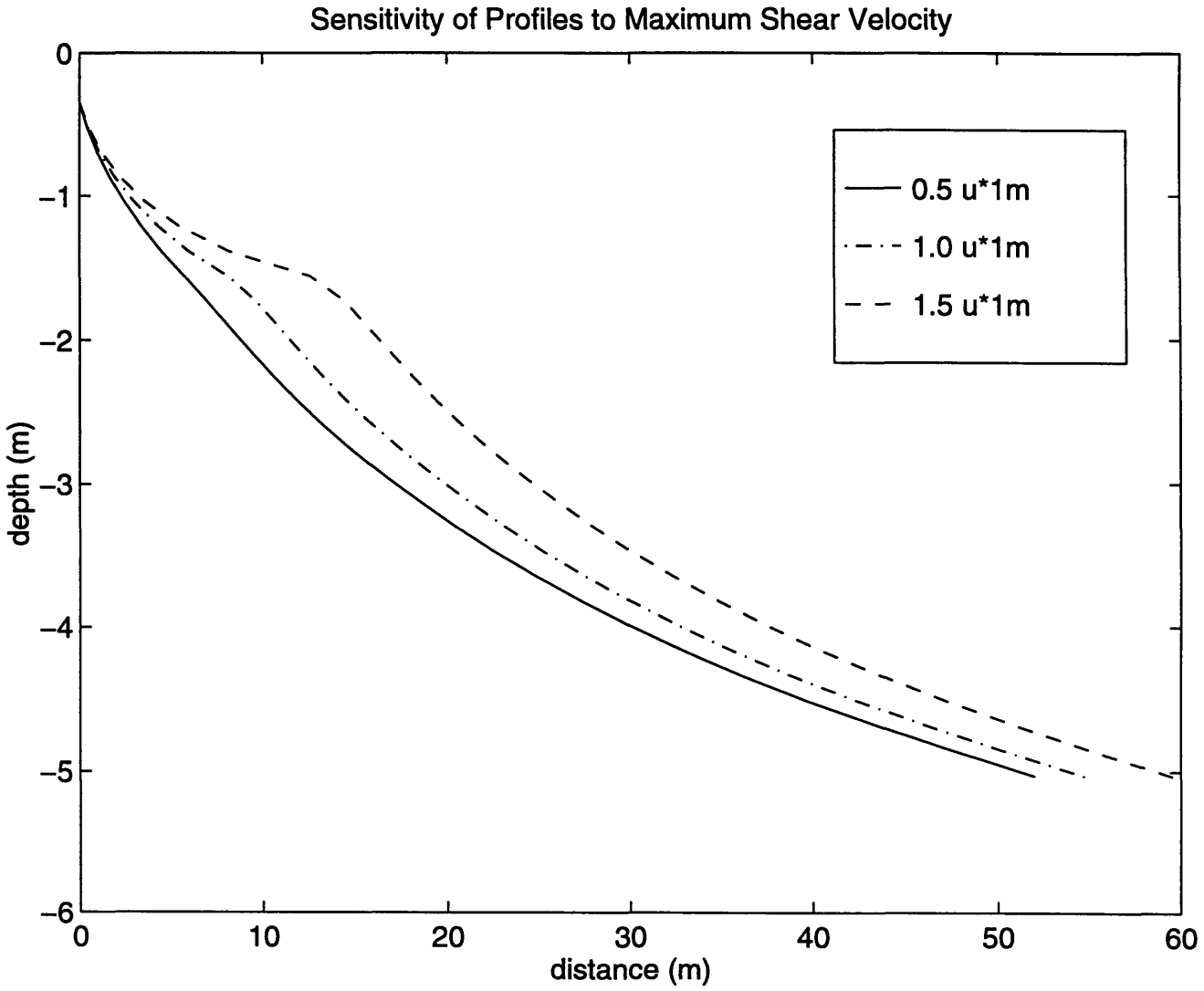

Figure 26. Sensitivity of the equilibrium beach profile to u_{*1m}. Wave parameters and beach characteristics used are $H_o = 0.7\ m$, $T = 10\ s$, and $d = 0.3\ mm$.

Chapter 6

6 Conclusion

A theoretical model describing Equilibrium Beach Profiles (EBP) is derived. Although the model attempts to describe morphology both inside and outside of the surf zone, little can be said about the quantitative accuracy of the model within the surf zone. This is mainly due to the way energy dissipation was modeled and a lack of a swash zone model. A more accurate description of wave attenuation within the surf zone is required for further development of the model. However, certain predicted qualitative beach characteristics, namely slope steepness as a function of sediment diameter parallel what is found in nature. Also, it is seen that longer waves do indeed tend to build beaches up.

While the present model formulation falls short of describing EBP within the surf zone, it does seem to effectively predict general trends of beach evolution as well as a quantitative description of the profile itself. Profiles generated compare closely to those measured by Inman et al. outside the surf zone and share certain characteristics within the surf zone.

6. 1 Modelling Energy Dissipation

It is felt that the greatest short-coming of the profile model in its present form is the way wave energy dissipation at the start of the surf zone is handled. By adopting a rather simplistic formulation, $H \propto h$, we have prevented the possibility of having a negative slope at the point of breaking, making modeling sand bars impossible. Furthermore, at the point of breaking we introduce an undertow. This discontinuity would probably be more gradual in actual field conditions. Moreover, our modeling of the undertow itself is somewhat suspect around the point of breaking. We assume a constant eddy viscosity throughout the water column, the rationale being that turbulence due to breaking is distributed throughout the entire water column. However, at the point of breaking this would probably not be the case.

Horikawa and Kuo's [1966] laboratory data relating wave height to water depth clearly demonstrates that for certain slopes, specifically slopes less that 1/30, the wave heights do not vary linearly with water depth. This is shown in figure 27. The figure shows, for four different beach slopes in which waves of differing periods and wave heights were run, how wave height varies with water depth for breaking waves. For any one particular run, at the point of breaking, the wave height and depth at which it breaks are recorded. This wave is then followed shorewards where at the subsequent shallower depths the wave height and depth are measured and plotted. Each line of Horikawa and Kuo's figure represents their predicted wave height to water depth ratio, while the symbol associated with this line represents the actual measured data. This data is compared to the ratio $H/h = 0.78$. This is also plotted on each subfigure.

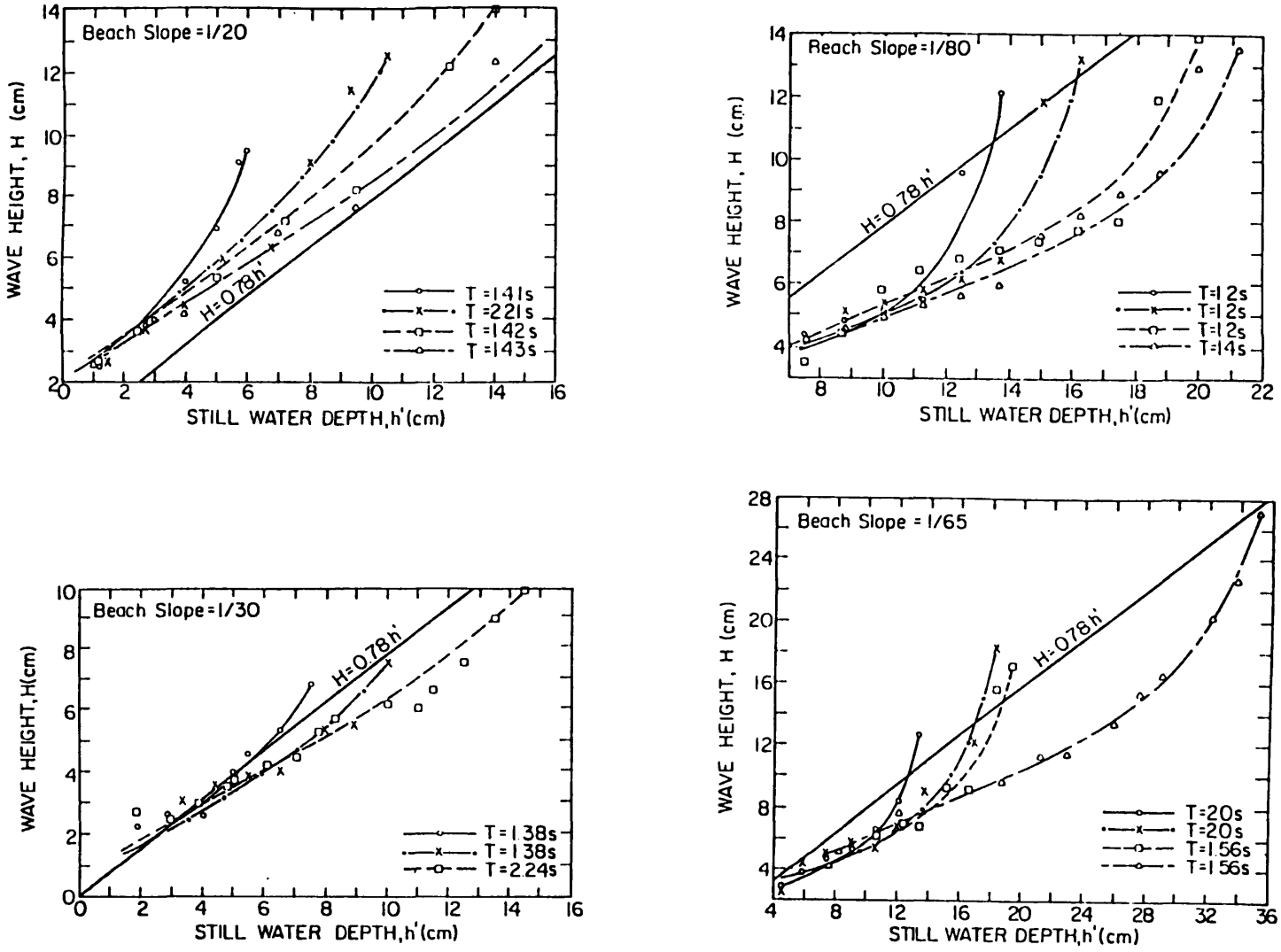

Figure 27. Comparison of breaker model and "0.78" criterion to Horikawa and Kuo's laboratory dat for the 1/20, 1/30, 1/65, and 1/80 beach slope.

Since typical beach slopes around the point of breaking are often much shallower than 1/30, using the simple formulation $H \propto h$ could introduce gross errors in the modeling of the undertow. Thus for beach slopes of around 1/80 there is a highly nonlinear relationship between water depth and wave height and the ratio itself is considerably smaller than 0.78 for most of the surf zone.

If the wave height is over-predicted, the error in offshore transport will be magnified, resulting in an inaccurate prediction of the near shore beach profile. Or if the change in H with x is under-predicted, as seen in figure 27 for the 1/80 beach just shoreward of the breaking point, the shear stress at the trough will be too small resulting in a reduced undertow and in an inaccurate prediction. A better model is necessary. However, it should be said that errors associated with predictions of the undertow are not damning. So long as the predicted wave height as well as the predicted change in wave height is reasonable, a reasonable quantitative description of the undertow is expected. But clearly, judging from the gross deviations from $H=0.78h$ as shown in some of the subfigures of figure 27, a better approximation of the wave height would greatly enhance the confidence we have in the validity of predicted profiles.

Models that attempt to predict changes in wave height within the surf zone often assume spectral waves. Since most of the sea surfaces in the field are aperiodic, to allow for this possibility would greatly enhance the flexibility of the model. There is also an additional benefit to using aperiodic waves: there is no one break-point. Using a statistics argument, only a portion of the waves are considered to be breaking at any particular depth. Since initially only a small portion of wave energy is lost due to breaking, the

undertow current due to these breaking waves will start off weak and then increase in shallow water accordingly. Hence there would be no current discontinuity between the surf zone and seaward zone; the problem of having a constant eddy viscosity at the point of breaking will also be minimized.

Minimizing errors associated with the undertow will certainly be desireable. However, as seen in section 5.3, the parameters associated with the suspended sediment concentration distribution can still introduce significant errors. Care must be taken when specifiying these parameters.

6.2 Further Refinements

Although in the formulation of the undertow the time-averaged free surface gradient was accounted for, the actual setup was never numerically calculated, let alone added to the local depth for purposes of shoaling the wave. There is a slight setup found up to the point of breaking, but once breaking occurs, there is a resulting setdown which then increases to a significant setup within the swash zone (for more detail, the reader is directed to Battjes and Janssen [1978]). Exclusion of this setup/setdown may subtly change the profile form and therefore should be included in future modifications.

A swash zone model also needs to be developed. First of all, as discussed in Chapter 3, the nonlinear nature of the wave significantly increases while the wave energy significantly decreases, such that initiation of sediment motion under the trough never occurs. This created problems when it came to predicting beach profiles in depths less than a meter or so. Even if we could predict the profile at these depths, it can be seen from the results in Chapter 5, there is a poor agreement between our model and empirical

models for beach profiles around the swash zone region. So further refinements are certainly called for.

A. References

Abramowitz, M., and I.A. Stegun, editors., 1972. "Handbook of Mathematical Functions." Dover Publications, Inc., New York.

Bagnold, R. A., 1963. "Mechanics of Marine Sedimentation," in *The Sea: Ideas and Observations*, vol. 3, Interscience, NewYork.

Bailard, J. A., 1981. "An Energetics Total Load Sediment Transport Model for a Plane Sloping Beach," *Journal of Geophysical Reasearch*, Vol.86(C11):10938-10954.

Battjes, J. A., and I.P.F.M. Janssen, 1973. "Energy Loss and Setup due to Breaking of Random Waves," Chapter 32 in *Coastal Engineering*.

Bodge, K. R., 1992. "Representing Equilibrium Beach Profiles with an Exponential Expression," *Journal of Coastal Research*, Vol 8, No. 1, pp 47-55.

Bowen, A. J., 1980. "Simple Models of Nearshore Sedimentation; Beach Profiles and Longshore Bars," in *Coastlines of Canada*, S. B. McCann, ed. Geological Survey of Canaday, Paper 80-10, p.1 – 11.

Bruun, P., 1954. "Coast Erosion and the Development of Beach Profiles," U.S. Army Beach Erosion Board Technical Memorandum No. 44.

Cox, D. T., and N. Kobayashi, 1996. "Undertow Profiles in the Bottom Boundary Layer under Breaking Waves." *Proceedings of the 24th International Conference in Coastal Engineering*, pp. 3194-3206.

Cox, D., and N. Kobayashi, 1997. "A Kinematic Undertow Model with a Logarithmic Boundary Layer," *Journal of Waterways, Port, Coastal, and Ocean Engineering*. Vol. 123, No. 6, pp.344 – 360.

Dally, W., 1992. "Random Breaking Waves: Field Verification of a Wave-by-Wave Algorithm for Engineering Applications," *Coastal Engineering*, 16, pp. 369-397.

Dally, W., and R. Dean, 1985. "Wave Height Variation across Beachs of Arbitrary Profile," *JGR*, Vol. 90, No. C6, pp. 11917 – 11927.

Dean, R. G., 1977. "Equilibrium beach profiles: U. S. Atlantic and Gulf coasts," Department of Civil Engineering, Ocean Engineering Report No. 12, University of Delaware, Newark, Delaware.

Dean, R. G., 1991. "Equilibrium Beach Profiles: Characteristics and Applications," *Journal of Coastal Research,* Vol 7, No. 1, pp 53-84.

Dean, R. G., 1994. "Cross-shore Sediment Transport Processes" in *Advances in Coastal and Ocean Engineering*, ed. Phillip L-F Lui. River Edge, N. J., World Scientific. pp. 159-220.

Dean, R. G., T. R. Healy, A. P. Dommerholt, 1993. "A 'Blindfolded' Test of Equilibrium Beach Profile Concepts with New Zealand Data," *Marine Geology*, 109; pp. 253-266.

Dean, R. G., and L. Charles, 1994. "Equilibrium Beach Profiles: Concepts and Evaluation," Florida Sea Grant College Program, UFL/COEL-94/013.

Deigaard, R., P. Justesen, and J. Fredsoe, 1991. "Modeling of the Undertow by a one-equation Turbulence Model," *Coastal Engineering*, Vol. 15, pp.431-458.

Einstein, H. A., 1950. "Bedload Function for Sediment Transportation in Open Channel Flows," *U.S. Dept. Agric. S.C.S.*, Tech Bulletin No.: 1026.

Grant, W. D., and O. S. Madsen, 1979. "Combined Wave and Current Interaction with a Rough Bottom," *Journal of Geophysical Research,* Vol. 85, No. C4, pp. 1797 - 1808.

Grant, W. D., and O. S. Madsen, 1986. "The Continental Shelf Bottom Boundary Layer," in *Annual Review of Fluid Mechanics* (M. Van Dyke, ed.) 18:265-308.

Hansen, J. B., and I. A. Svendsen, 1984. "A Theoretical and Experimental Study of the Undertow," *Proceedings of the 19th International Conference in Coastal Engineering*, pp. 2246-2262.

Inman, D. L., M. H. S. Elwany and S. A. Jenkins, 1993. "Shorerise and Bar-Berm Profiles on Ocean Beaches," *Journal of Geophysical Research,* Vol. 98, N. C10, pp.18,181 - 18, 199.

King, D. B., Jr., 1991. "The Effect of Beach Slope on Oscillatory Flow Bedload Transport," *Proceedings Coastal Sediments '91,* American Society of Civil Engineers, Vol. 1, pp. 734-744.

Longuet-Higgins, M. S., 1953. "Mass Transport in Waves." Philos. Trans. R. Soc. 345: 535-581.

Madsen, O. S., 1991. "Mechanics of Cohesionless Sediment Transport in Coastal Waters," *Proceedings Coastal Sediments '91,* American Society of Civil Engineers, Vol. 1, pp. 15 - 27.

Madsen, O. S., 1993. "Sediment Transport on the Shelf," Chapter III.6 in U.S. Army Corps of Engineers, *Coastal Engineering Manual* (to be published).

Madsen, O. S., 1994. "Spectral Wave-Current Bottom Boundary Layer Flows." *Proceedings of the 24th International Conference in Coastal Engineering*, Vol.1, pp.384-398.

Madsen, O. S., and Grant, W. D., 1976. "Quantitative Description of Sediment Transport by Waves," *Proceedings Fifteenth International Coastal Engineering Conference,* American Society of Civil Engineers, Vol. 2, pp. 1093 - 1112.

Madsen, O. S., L. D. Wright, J. D. Boon, and T.A. Chisholm, 1993. "Wind Stress, Bottom Roughness and Suspended Sediment on the Inner Shelf during an Extreme Storm Event." *Continental Shelf Research.*

Mei, C. C., 1983. "The Applied Dynamics of Ocean Surface Waves," John Wiley and Sones, New York.

Meyer-Peter, E. and Muller, R., 1948. "Formulas for Bed-Load Transport," *Report on Second Meeting of International Association for Hydraulic Research,* pp. 39 - 64.

Nairn, R. B. and H. N. Southgate, 1993. "Derterministic Profile Modeling of Nearshore Processses, Part 2. Sediment Transport and Beach Development." *Coastal Engineering*, 19, pp. 57 – 96.

Nikuradse, J., 1933. "Stromungsgesetze in rauhen Rohren," VDI Forschungsheft No. 361 (English translation NACA Technical Memorandum No. 1292).

Pechon, P., 1992. "Numerical Modelling of Wave-driven Currents and Sediment Transport in the Surf Zone." *Internal Report* EDF-LNH HF.42/92.15

Putrevu, U., and I. A. Svendsen, 1992. "Surf Zone and Wave Parameters from Experimental Data," *Coastal Engineering*, 19, pp.283-310.

Roelvink, J. A., and J. Broker, 1993. "Cross-shore Profile Models," *Coastal Engineering*, 21, pp.163-191.

Roelvink, J. A. and M. J. F. Stive, 1986. "Bar-generating Cross-shore Flow Mechanisms on a Beach." *Journal of Geophyical Reasearch*, 94(C4):4785-4800.

Shields, A., 1936. "Application of Similarity Principles and Turbulent Research to Bed-Load Movement," (translation of original in German by W. P. Ott and J. C. van Uchelen, California Institute of Technology) Mitteilugnen der Preussischen Versuchsanstalt fur Wasserbau und Schiffbau.

Southgate, H. N. and R. B. Nairn, 1993. "Derterministic Profile Modeling of Nearshore Processses, Part 1. Waves and Currents." *Coastal Engineering*, 19, pp. 27-56.

Stive, M. J. F. and H. G. Wind, 1981. "A Study of Radiation Stress and Set-up in the Nearshore Region." *Coastal Engineering*, 6, pp. 1- 25.

Stive, M. J. F. and H. G. Wind, 1986. "Cross-shore Mean Flow in the Surf Zone," *Coastal Engineering*, 10, pp. 325 – 340.

Stive, M. J. F. and J. A. Battjes, 1984. "A Model for Offshore Sediment Transport," *Proceedings of the 19th International Conference in Coastal Engineering*, pp. 1420 – 1436.

Stive, M. J. F., 1996. "A Model for Cross-shore Sediment Transport," *Proceedings of the 20th International Conference in Coastal Engineering*, pp. 1550-1564.

Svendsen, I. A., 1974. "Cnoidal Waves over a Gently Sloping Bottom." *Series Paper 6*, Institute of Hydrology and Hydraulic Engineering, Technical University of Denmark.

Svendsen, I. A., 1983. "Wave Heights and Set-up in a Surf Zone," *Coastal Engineering*, 8, pp. 303-329.

Svendsen, I. A., 1984. "Mass Flux and Undertow in Surf Zone," *Coastal Engineering*, 8, pp. 347 – 365.

Svendsen, I. A., S. A. Hemming, and J. B. Hansen, 1987. "The Interactions between the Undertow and the Boundary Layer Flow of a Beach," *JGR*, Vol.92, No. C11, pp. 11845 – 11856.

Svendsen, I. A. and U. Petrevu, 1995. "Surf Zone Hydrodynamics," *Research Report No. CACR-95-02*, Center for Applied Coastal Research.

Swart, D. H., 1991 "Beach Nourishment and Particle Size Effects," *Coastal Engineering,* 16: 61-81.

Thornton, E. B., 1983 "Transformation for Wave Height Distribution," *Journal of Geophysical Research*, Vol. 88(C10):5925-5938.

Work, P. A. and R. G. Dean, 1991. "Effects of Varying Grain Size on Equilibrium Beach Profiles," *Proceedings, ASCE Conference on Coastal Sediments '91,* pp. 890-904.

Work, P. A. and R. G. Dean, 1995. "Assessment and Prediction of Beach-Nourishment Evolution," *Journal of Waterway, Port, Coastal, and Ocean Engineering,* Vol. 121, No. 3, pp. 182 - 189.

Appendix A

B. Suspended Sediment Outside the Surfzone

Outside the surf zone it is argued that there is little suspended sediment transport due to wave action. This section addresses this argument.

The governing equation for the distribution of suspended sediment in the water column is the advective diffusive equation.

$$\frac{\partial c}{\partial t} - \frac{\partial}{\partial z}(w_f c) - \frac{\partial}{\partial z}\left(\nu_s \frac{\partial c}{\partial z}\right) = 0 \tag{A.1}$$

where w_f is the fall velocity, ν_s is the sediment diffusion coefficient and c is the volumetric concentration of suspended sediment. We assume a constant sediment size for which w_f is constant and where the sediment diffusion coefficient is approximated by the turbulent eddy viscosity. Equation (A.1) is split into two equations, one for a mean time-averaged concentration, the other a time-varying, wave-associated concentration. This is

accomplished by letting $c = \bar{c} + c_w$. The time-varying equation is the relevant equation for wave induced suspended sediment transport outside the surf zone and is

$$\frac{\partial c_w}{\partial t} - w_f \frac{\partial c_w}{\partial z} - \frac{\partial}{\partial z}\left(\nu_t \frac{\partial c_w}{\partial z} \right) = 0 \tag{A.2}$$

The boundary conditions specified for this equations are as follows: 1) no sediment is transported through the surface, or that $c \to 0$ as $z \to \infty$, and 2) a reference concentration, C_R, is specified at a reference height above the bottom, Z_R. The reference height is given as a proportionality to sediment diameter. Here we use the Madsen et al. [1993] suggested value of Z_R:

$$Z_R = 7d \tag{A.3}$$

The reference concentration, theoretically is considered to be proportional to the bedload. As discussed in Chapter 4, according to Einstein [1950], this can be expressed as

$$C_R \propto \frac{q_{sb}}{u_s Z_R} \tag{A.4}$$

where q_{sb} is the bedload and u_s is the sediment velocity. It has been shown in the Chapter 2, (2.13), that $u_s = 8(u_* - \alpha u_{*cr})$, and from equation (2.15), stated here again,

$$q_{sb} = \frac{\pm 8(|\tau_b| - \tau_{cr})}{(s-1)\rho g \cos\beta(\tan\phi_k \pm \tan\beta)}(u_* - \alpha u_{*cr}) \tag{A.5}$$

we derive an expresion for C_R.

$$C_R = \frac{\gamma(|\tau_b(t)| - \tau_{cr})}{Z_R \rho g (s-1)(\tan\varphi_k \pm \tan\beta)} \tag{A.6}$$

where γ is a proportionality constant and $\tau_b(t)$ is found from (2.40). The empirical resuspension constants, γ', for flat beds taken from Wikramanayake and Madsen [1992] was found to be 2 x 10^{-4} with a reference concentration defined as:

$$C_R = \gamma' C_b \left(\frac{\tau_b(t)}{\tau_{cr}} - 1 \right) \tag{A.7}$$

where C_b is the volume concentration of sediment in the bed, generally taken as 0.65. By equating (A.6) and (A.7) and solving for γ when $\beta = 0$, it can be shown that $\gamma \cong 10^{-2}$, for a sediment diameter of 0.2 *mm*. For simplicity and consistency, we use $\gamma = 10^{-2}$ for all cases.

Equation (A.2) can be solved exactly once the eddy diffusivity is specified. However, before a lengthy analytical analysis was carried out, an approximate evaluation of the relative importance of this transport mechanism compared to bedload transport was deemed prudent. If the importance of suspended load compared to bedload was shown to be insignificant, a lengthy analysis would not be necessary. Hence, some simplifications are made: it is assumed that the sediment concentration will be a function of z only at each instance of time. Therefore, equation (A.2) can be rewritten as

$$\frac{\partial}{\partial z}\left[w_f c_w + \left(\nu_t \frac{\partial c_w}{\partial z} \right) \right] = 0 \tag{A.8}$$

Integrating with respect to z we obtain

$$w_f c_w + \nu_t \frac{\partial c_w}{\partial z} = K \tag{A.9}$$

where K is some arbitrary constant which, since we assume a zero net flux of sediment in the vertical, is set to 0. Since we are looking at wave action alone, we assume that the sediment eddy viscosity is that of the turbulent eddy viscosity:

$$\nu_t = k u_{*1m} z \tag{A.10}$$

for $z \le \delta_{cw}$. The solution to (A.9) is then

$$c_w(t) = C_R(t)\left(\frac{z}{Z_R}\right)^{-\frac{w_f}{\kappa u_{*1m}}} \tag{A.11}$$

u_{*1m} is found from (2.40) where $u_b(t)$ is equal to (2.41). C_R is calculated using equation (A.6); the sediment fall velocity, w_f, is estimated using the Madsen Grant [1976] graph relating fall velocity versus sediment-fluid parameter S_* (figure 11); and Z_R is found using (A.3).

Transport due to wave action is restricted to below the boundary layer, δ. The boundary layer thickness is found from equation (4.28). Therefore, the velocity profile can be expressed using a logarithmic solution:

$$u(t) = u_{*b}(t)\frac{1}{\kappa}\ln\frac{z}{z_o} \tag{A.12}$$

where $u_{*b}(t)$ is found from (2.40). Therefore, the total suspended load within the wave boundary layer is

$$q_{ss}(t) = \int_{z_R}^{\delta} c_w u dz \tag{A.13}$$

This expression can be solved analytically

$$q_{ss} = \left(\frac{C_R(t)u_{*b}(t)}{\kappa}\right)\frac{1}{(y+1)}\left\{\frac{\ln(Z_R/z_o)}{Z_R^{\,y}}\left(\delta^{y+1} - Z_R^{\,y+1}\right) + Z_R\left[\left(\frac{\delta}{Z_R}\right)^{y+1}\ln\left(\frac{\delta}{Z_R}\right) - \frac{1}{(y+1)}\left(\left(\frac{\delta}{Z_R}\right)^{y+1} - 1\right)\right]\right\} \tag{A.14}$$

where y is $-w_f/\kappa u_{*1m}$. A net suspended sediment transport rate is found much like the net bedload transport rate is. Using Cnoidal theory outlined in Chapter 2, the time varying shear stress is found (2.40). Using this value at each phase in the wave period, the reference concentration is calculated (A.6) and then the suspended load (A.14) is subsequently calculated. The average transport rate is then calculated over one wave period.

This analysis does not take into consideration phase shifts between actual suspension of the particles and the transport mechanism. It is assumed that the instantaneous velocity is responsible for both the amount of sediment in the water column and its transport rate. Therefore, at times where we have the greatest wave orbital velocities, we also have the greatest sediment concentration distribution. This is considered to lead to a conservatively high estimate of the wave-induced suspended sediment transport. The amount of net suspended transport relative to the net bedload transport for $\beta = 0$ is shown to be small in table A1. Right around the point of breaking, q_{ss} is approximately 5% of q_{sb}.

Table A1. Comparison of Wave Induced Suspended Transport and Bedload transport at varying depths. The wave and sediment characteristics used to calculate these values were $Ho = 1\ m$, $T = 10\ s$, $d = 0.1\ mm$.

Transport Mechanism	Depths (m)			
	2.1	3.1	4.0	5.7
Qsb	1.1	0.65	0.24	0.05
Qss	0.07	0.03	0.006	~0

To further illustrate this point, figure A1 is included to visually demonstrate how the profile model changes when the time-varying wave-induced suspended transport is added. Hence, since the amount is relatively negligible for the most conservative case, it was decided to not include this wave-induced suspended sediment transport into the profile model outside the surf zone.

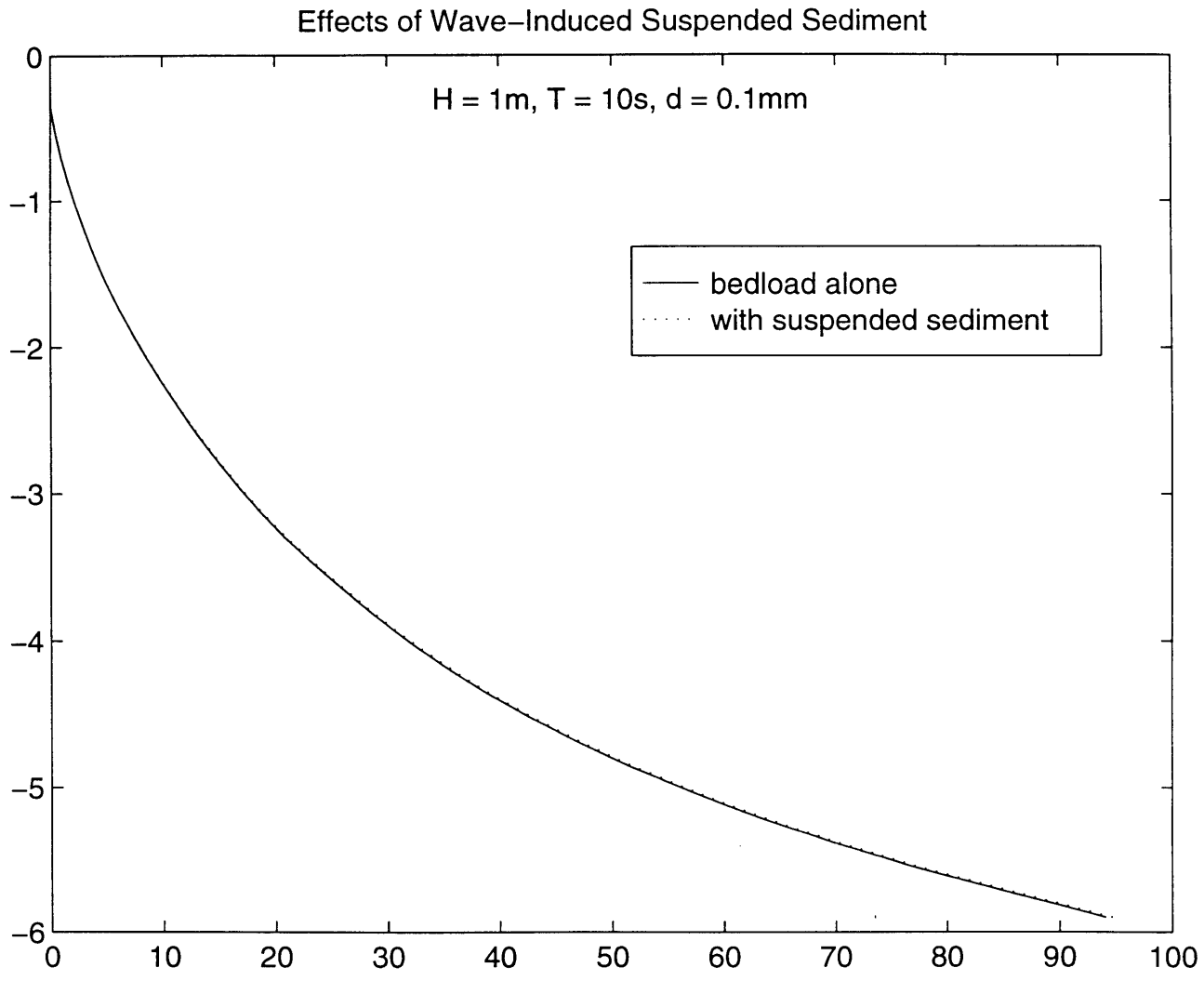

Figure A1. Comparison between wave-induced suspended load with bedload and bedload alone.